

Spring 2004

Dynamically variable focal length microlens by microfluidic and electroactive polymer approaches

Jackie Ching-Lung Chen

Follow this and additional works at: <https://digitalcommons.latech.edu/dissertations>

Recommended Citation

Chen, Jackie Ching-Lung, "" (2004). *Dissertation*. 627.
<https://digitalcommons.latech.edu/dissertations/627>

This Dissertation is brought to you for free and open access by the Graduate School at Louisiana Tech Digital Commons. It has been accepted for inclusion in Doctoral Dissertations by an authorized administrator of Louisiana Tech Digital Commons. For more information, please contact digitalcommons@latech.edu.

**DYNAMICALLY VARIABLE FOCAL LENGTH MICROLENS BY
MICROFLUIDIC AND ELECTROACTIVE
POLYMER APPROACHES**

by

Jackie Ching-Lung Chen, B.A.Sc, M.S

A Dissertation Presented in Partial Fulfillment
of the Requirement for the Degree of
Doctor of Philosophy in Engineering

**COLLEGE OF ENGINEERING AND SCIENCE
LOUISIANA TECH UNIVERSITY**

May 2004

UMI Number: 3126268

INFORMATION TO USERS

The quality of this reproduction is dependent upon the quality of the copy submitted. Broken or indistinct print, colored or poor quality illustrations and photographs, print bleed-through, substandard margins, and improper alignment can adversely affect reproduction.

In the unlikely event that the author did not send a complete manuscript and there are missing pages, these will be noted. Also, if unauthorized copyright material had to be removed, a note will indicate the deletion.

UMI[®]

UMI Microform 3126268

Copyright 2004 by ProQuest Information and Learning Company.

All rights reserved. This microform edition is protected against unauthorized copying under Title 17, United States Code.

ProQuest Information and Learning Company
300 North Zeeb Road
P.O. Box 1346
Ann Arbor, MI 48106-1346

LOUISIANA TECH UNIVERSITY

THE GRADUATE SCHOOL

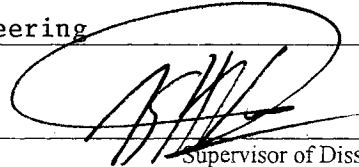
May 7, 2004

Date

We hereby recommend that the dissertation prepared under our supervision
by Jackie Ching-Lung Chen

entitled Dynamically Variable Focal Length Microlens by
Microfluidic and Electro-active Polymer Approaches

be accepted in partial fulfillment of the requirements for the Degree of
Doctor of Philosophy in Engineering



Supervisor of Dissertation Research

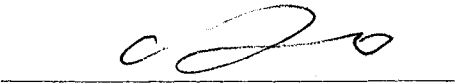
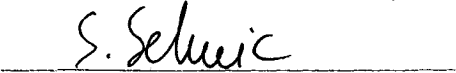
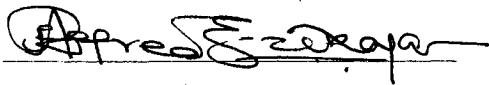
Ray Z. Sterling

Head of Department

PRO in Engineering

Department

Recommendation concurred in:



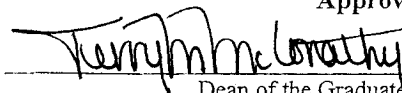
Advisory Committee

Approved:



Director of Graduate Studies

Approved:



Dean of the Graduate School



Dean of the College

ABSTRACT

This research is on a development of a variable focusing microlens system. The studies of modern researchers have thrown new light on this subject, which has aroused intense interest in making tunable focusing microlenses. The most well-known methods are liquid crystal and electrowetting. Both methods require electrodes immersed in the electrolyte solution, causing severe optical distortion, and require complicated fabrication processes. Few attempts have thus far been developed to make variable focusing lens using other approaches.

However, two novel actuation mechanisms have been developed in this work for generating significant forces to change the physical dimensions of an elastic polymeric lens structure to control the focal length. The two proposed actuation mechanisms are: 1) the microfluidic and 2) the Electro-Active Polymer (EAP) actuations. By pneumatically regulating the pressure of the microfluidic chamber, the elastic lens can be deformed, causing the changes in the focal length. EAP is another method to transfer electrical energy to mechanical deformation. This energy transformation causes the deflection on the lens and induces its focal plane to be shifted.

For the microfluidic lens system, a novel PDMS to PDMS casting process to fabricate 3D convex elastic microlens diaphragm is developed. This new fabrication technique has a potential for producing low-cost elastic microlens arrays. Microlenses, with a diameter of 600~1400 μm , are fabricated using this fabrication technique. The curvature changes of the microlens were from 1210 μm to 3238 μm . With this wide

range of curvature changes, one can control the back focal length from 3.82 mm to 10.64 mm, and the numerical aperture from 0.09 to 0.24. The numerical aperture of this optical device can then reach 0.24, about 4 times that of a conventional planar diaphragm (NA=0.05).

Moreover, a new “two-step copolymerization” technique has been developed to fabricate an elastic silicone-based gradient refractive index (GRIN) lens. This is a flat lens with a gradient refractive index distribution within the lens structure. Moreover, this GRIN lens is elastic, so it is deformable with high elongation under mechanical stresses. Finally, this lens is made by a dielectric material, and can be integrated easily into an EAP actuator, generating enough mechanical force to cause the deflection on the GRIN lens and induce a shift in focal length. The characteristics of GRIN lenses and EAP actuation have been studied in this work. It appears that this is the first reported work proposing a dynamically tunable focusing GRIN lens with an EAP actuation. Further research needs to be carrying out for optimizing the proposed approach for its desired application.

APPROVAL FOR SCHOLARLY DISSEMINATION

The author grants to the Prescott Memorial Library of Louisiana Tech University the right to reproduce, by appropriate methods, upon request, any or all portions of this Dissertation. It is understood that "proper request" consists of the agreement, on the part of the requesting party, that said reproduction is for his personal use and that subsequent reproduction will not occur without written approval of the author of this Dissertation. Further, any portions of the Dissertation used in books, papers, and other works must be appropriately referenced to this Dissertation.

Finally, the author of this Dissertation reserves the right to publish freely, in the literature, at any time, any or all portions of this Dissertation.


Author 
Date May 17 2004

TABLE OF CONTENTS

LIST OF TABLES	ix
LIST OF FIGURES	x
ACKNOWLEDGMENT.....	xiv
CHAPTER 1 INTRODUCTION	1
1.1 Overview of Variable Focusing Lens	1
1.2 Variety of Variable Focusing Microlenses	2
1.3 Objective	5
1.4 Methodology.....	7
1.4.1 Microfluidic Actuation.....	8
1.4.2 Electro-Active Polymer Actuation.....	8
1.5 Outline of Dissertation.....	9
CHAPTER 2 MULTI-FOCAL LENS SYSTEM DESIGN.....	11
2.1 Design Overview	11
2.2 3-D Flexible Polydimethyl-Siloxane (PDMS) Microlens.....	13
2.3 Gradient Refractive Index (GRIN) Lens.....	15
2.3.1 Axial Gradient.....	17
2.3.2 Transverse Gradient.....	18
2.3.3 Radial Gradient	18
2.3.4 Spherical Gradient	19
2.3.5 Current Available Gradient Index Lens Fabrication.....	19
2.3.6 Novel Method of Fabricating an Elastic GRIN Lens.....	23
2.4 Micro-Fluidic Actuation System.....	25
2.5 Electro-Active Polymer (EAP) Actuation System.....	26
2.5.1 Out-of-Plane EAP Actuator	28
2.5.2 In-Plane EAP Actuator	29
CHAPTER 3 VARIABLE FOCUSING MICROLENS WITH MICROFLUIDIC CHIP	31
3.1 Basic Design Concept	31
3.2 Fabrication Processes.....	33
3.2.1 Fabrication of Photoresist-Reflow Microlens.....	34

3.2.2	Casting Method for Elastic PDMS Microlens	37
3.2.3	Microfluidic Chip Fabrication	38
3.3	Characteristics for 3D PDMS Microlens	39
CHAPTER 4	DEVELOPMENT OF ELASTIC POLYMER GRADIENT-INDEX LENS	42
4.1	Background and Related Research	42
4.2	Optical Properties for Thin Gradient-Index Lens	45
4.3	Material Design Principle	48
4.3.1	Diffusion Mechanism.....	51
4.3.2	Polymer Chemistry	53
4.4	Material Preparation.....	55
4.4.1	Possible Silicone Combinations.....	55
4.4.2	Polymer Matrix	59
4.4.3	Photo-Sensitive Macromer.....	61
4.5	Fabrication Procedures.....	63
4.5.1	Silicone Compositions	63
4.5.2	Lithography Exposure Steps	65
CHAPTER 5	SMART MATERIALS: ELECTRO-ACTIVE POLYMER (EAP)	67
5.1	Introduction to EAP	67
5.2	Actuation Principle	70
5.2.1	Dielectric Properties.....	71
5.2.2	Maxwell Stress.....	73
5.3	Variety of Compliant Electrodes	75
5.3.1	Carbon Black Dust Electrodes	76
5.3.2	Grease Electrodes.....	76
5.3.3	Conducting Silicone Rubber Electrodes	77
5.4	Actuator Fabrication	78
5.4.1	SU-8 Electrode Pattern Design	78
5.4.2	SU-8 Electrode Master.....	79
5.4.3	Silicone Film Spinning	81
5.4.4	Conducting Film Squeegee-Coating Processing.....	83
CHAPTER 6	RESULTS AND DISCUSSION	85
6.1	3D Microfluidic PDMS Lens.....	85
6.2	Silicone-Based GRIN Lens.....	90
6.3	Silicone EAP Actuators	93
6.3.1	Deflection Testing Setup.....	94
6.3.2	RC Circuit and a DC-to-HV DC Converter Setup.....	95
6.3.3	Deflection Results of EAP Actuator	97

CHAPTER 7 CONCLUSIONS AND FUTURE WORK	104
7.1 Conclusions.....	104
7.2 Future Work.....	107
REFERENCES	108
APPENDIX A Mathematic Calculations for Back Focal Length and Number Apertures	111
APPENDIX B Published Papers	115

LSIT OF TABLES

Table 2.1	Possible fabrication techniques for making microlenses	13
Table 2.2	Methods for GRIN glass fabrication with approximate maximum gradient depth and Δn	20
Table 2.3	Methods for GRIN plastic fabrication with approximate values for maximum gradient depth and Δn	21
Table 2.4	Electrical and mechanical performance for all types of actuators	27
Table 3.1	Comparison of surface roughness for photoresist microlens, PDMS master and final PDMS microlens	40
Table 4.1	Basic material information for matrix and macromers	56
Table 4.2	Physical appearance after mixing macromer and matrix	57
Table 4.3	Molecular weight and refractive index of matrix and macromer	59
Table 4.4	Material composition for making GRIN lenses	63
Table 5.1	Relationship for thickness and spin speed for SU-8 50	80
Table 6.1	Optical properties of a 1400 μm diameter of microlens with different pumped-in volume	88
Table 6.2 (a)	Comparison of EAP thickness and electrode size at an applied voltage of 13V and carbon grease was used as the electrode material	98
Table 6.2 (b)	Comparison of EAP thickness and electrode size at an applied voltage of 13V and conducting silicone rubber was used as the electrode material	98

LIST OF FIGURES

Figure 1.1	Schematic cross section of the fluid lens principle	3
Figure 1.2	Schematic cross section of electrowetting microlens	4
Figure 1.3	Concept map for the methodology.....	7
Figure 2.1	Sketch of photoresist reflow process	14
Figure 2.2	Profile of conventional lens	15
Figure 2.3	Profile of a GRIN lens	17
Figure 2.4	Axial gradient-index lens.....	17
Figure 2.5	Transverse gradient-index lens	18
Figure 2.6	Radial gradient-index lens	19
Figure 2.7	Cartoon schematic illustrating the proposed diffusion mechanism	23
Figure 2.8	Overall microfluidic system and its components.....	26
Figure 2.9	Circular EAP with out-of-plane deflection	28
Figure 2.10	Deformation distribution (a) top view, (b) bottom view.....	29
Figure 2.11	In-plane movement with circular EAP	30
Figure 3.1	Fabrication sequence for array of polymer microlenses	34
Figure 3.2	SEM images of 1400um diameter photoresist microlens (a) single spherical lens (b) an array of microlenses (c) closer view on the edge of photoresist microlens.....	36
Figure 3.3	SEM photographs for (a) PDMS concave master, and (b) final PDMS film with convex lens.....	37

Figure 3.4	Schematic cross section for microfluidic chip structure	38
Figure 3.5	A prototype of variable focal lens with microfluidic chip	39
Figure 3.6	Surface profile for photoresist microlens.....	40
Figure 3.7	The relationship of applied force and film displacement.....	41
Figure 4.1	Illustration of optical parameters for radial gradient-index lens	45
Figure 4.2	Material design for GRIN lens.....	50
Figure 4.3	Schematic illustrating the proposed mechanism of diffusion	52
Figure 4.4	Polymer structures	53
Figure 4.5	Absorption spectrum for various concentration of Darocur 1173	65
Figure 4.6	Photography of mask	66
Figure 5.1	Functional element of dielectric elastomers	69
Figure 5.2	Sketch for electric field in (a) vacuum, the dipoles orientations for dielectric material (b) between two electrodes, and (c) outside the electrodes	72
Figure 5.3 (a)	The mask layout of 4" wafer.....	79
Figure 5.3 (b)	Three sizes of the electrodes.....	79
Figure 5.4	(a) Photography for three electrode sizes made by SU-8 photoresist, and (b) SEM micrograph for three sizes of electrode mold.....	81
Figure 5.5	Photograph of PDMS electrode patterns on PDMS after peeling-off from the SU-8 master mold	83
Figure 5.6	Schematic illustration of the squeegee-coating process.....	84
Figure 5.7	Photograph of compliant electrode	84
Figure 6.1	Experimental setup for contact angle measurement	85

Figure 6.2	Photo for the curvature changes of PDMS film lens with different volume of pumped-in fluid	86
Figure 6.3(a)	Linear relationship between pumped-in volume and contact angle.....	87
Figure 6.3(b)	Relationship between contact angle and curvature.....	87
Figure 6.4	Relationship between back focal length and pumped-in volume	88
Figure 6.5	2D ANSYS simulation of microlens (a) for deformation, (b) for stress distribution	89
Figure 6.6	3D ANSYS simulation of microlens (a) for stress on bottom surface (b) for stress on top surface	90
Figure 6.7	Optical setup for diverging GRIN lens	91
Figure 6.8	Optical setup for converging GRIN lens	91
Figure 6.9	Images obtained from CCD camera through a diverging GRIN lens	92
Figure 6.10	Images obtained from CCD camera through a converging GRIN lens.....	92
Figure 6.11	Sketch for three different heights of SU-8 electrode molds with a same thickness of PDMS.....	93
Figure 6.12	Experimental setup for measuring the deflection of EAP actuator.....	95
Figure 6.13	RC circuits in (a) charging mode, and (b) discharging mode	96
Figure 6.14	Linear relationship between input and output voltages from a DC-DC converter	97
Figure 6.15	Deflection measurements with different EAP thicknesses (carbon grease).....	100
Figure 6.16	Deflection measurements with different EAP thicknesses (conducting silicone rubber).....	101

- Figure 6.17 Deflection measurements obtained on the same electrode size (small) with different thicknesses and electrode materials. This plot is for charging mode.....103
- Figure 6.18 Deflection measurements for 20 μ m thick PDMS and small-size electrode with two different electrode materials.....103

ACKNOWLEDGMENT

In following my graduate research path toward completion of the doctorate, I have learned many lessons from academic coursework, research projects and student life at Louisiana Tech University. Not all the lessons were wanted or appreciated at the time of occurrence; however, they have come to serve make me wiser and deepen my appreciation for my past, present, and future. This rewarding experience not only enhances my professional knowledge, but also enhances my approach to problem solving.

I would like to express my thanks and appreciation to Mr. Ji Fang, for his immense support and encouragement during the course of this research. His knowledge and experience has been a guiding influence, and I am deeply grateful for his competent guidance over the many stumbling stones I encountered. I owe an equal debt of gratitude to Dr. Kody Varahramyam, my dissertation chair, for planning and supporting my research work at IfM (Institute for Micromanufacturing).

I am also appreciative and thankful for the support of the members of my committee, Dr. Alfred Gunasekaran, Dr. Cheng Luo, and Dr. Sandra Selmic. Without their support, this dissertation could not have been written. They have modeled a lesson I will gladly carry forward into my professional career. Moreover, I would like to thank all IfM staff for always finding time for my process requests over other ongoing work.

I would also like to express appreciation to my parents, my sister, and my friend, Renee Chien. Over the past four years, they has been witness to the many ups and downs

of my own dissertation process, and no one could ask for more support than they have given me.

CHAPTER 1

INTRODUCTION

1.1 Overview of Variable Focusing Lens

This dissertation concerns the theoretical design description and device fabrication of two dynamic variable focal lens systems by two different actuation approaches: microfluidic and Electro-Active Polymer (EAP) actuations. These two actuation methods can change the shape or refractive index profile of the lens and its focal length according to image viewing distance. With the ability to vary the focal length, these optical devices can may have improved good image for different viewing distance and provide image correction for large viewing angle. This variable focal length lens is a useful component for optical communication, biomedical instruments, and other diverse micro-optical system applications. For example, in medical instrumentation, a microlens is ideal for advanced bioanalytical instruments, and microscale microscopes have potential in genomics and proteomics, as well as high-throughput clinical applications. Moreover, various kinds of optical devices such as cameras, microscopes and optical pick-ups need lens and focusing mechanisms to obtain clear images or optical signals.

Most commercial optical devices have conventional lens and mirrors with no inherent focusing function, made of glass or plastic has a fixed focal length. They must focus by moving the optical element or the object. For this reason, many moving parts

such as combdrives, slides, and motors are used for conventional optical devices. Systems with many moving parts require more complicated driving mechanism and more working space. However, complex system architecture assumedly reduces the reliability.

To eliminate all the abovementioned drawbacks, the lens with a variable focal length should work like a human eye's crystalline lens, which is deformed by muscles. The lens made of only solid material cannot realize the focal plane shift without any movement of lens. For the purpose of focal plane shift by the lens itself, the structure of the lens must be flexible and deformable under mechanical stress. In this dissertation, a new design concept with two different actuation approaches is proposed to fabricate a lens which has the focusing function itself without optical element movement.

1.2 Variety of Variable Focusing Microlenses

Single microlenses and microlens arrays have been developed in the past for applications in photolithography, imaging, optical communications, and more recently, for lab-on-a-chip systems as the multiplex focusing components [1]. Dynamically tunable lenses have also been reported as an initial effort to extend the current capabilities and applications of such microlenses. These tunable lenses eliminate the need for optical alignment or scanning. Liquid crystal immersed microlenses [2] and variable focal length liquid lenses controlled by electrowetting [3, 4, 5] have been proposed to fulfill these needs. The liquid crystal microlenses, however, suffer from aberrations due to non-uniformities in the electric field, and the operation of electrowetting-based microlenses requires high driving voltages and is accompanied by liquid evaporation.

Recently, a novel variable-focus lens system with no mechanical moving parts has been developed and demonstrated by Stein Kuiper and his colleagues at Philips Research

Laboratory. The shape of the lens is adjusted by applying an electric field across the hydrophobic coating such that it becomes less hydrophobic—a process called ‘electrowetting’, that results from an electrically induced change in surface-tension. As the surface tension changes, the aqueous solution begins to wet the sidewalls of the tube, altering the radius of curvature of the meniscus between the two fluids and, hence, the focal length of the lens. By increasing the applied electric field, the surface of the initially convex lens can be made completely flat (no lens effect) or even concave. Figure 1.1 shows the schematic cross-section and the results of its design. When a voltage is applied, charges accumulate in the glass wall electrode, and opposite charges collect near the solid/liquid interface in the conducting liquid. The resulting electrostatic force lowers the solid/liquid interfacial tension and with that, the contact angle θ and thereby the focal distance of the lens. In (C) to (E) in Figure 1.1, ones are shown the shapes of a 6-mm diameter lens changes at different applied voltages [5]

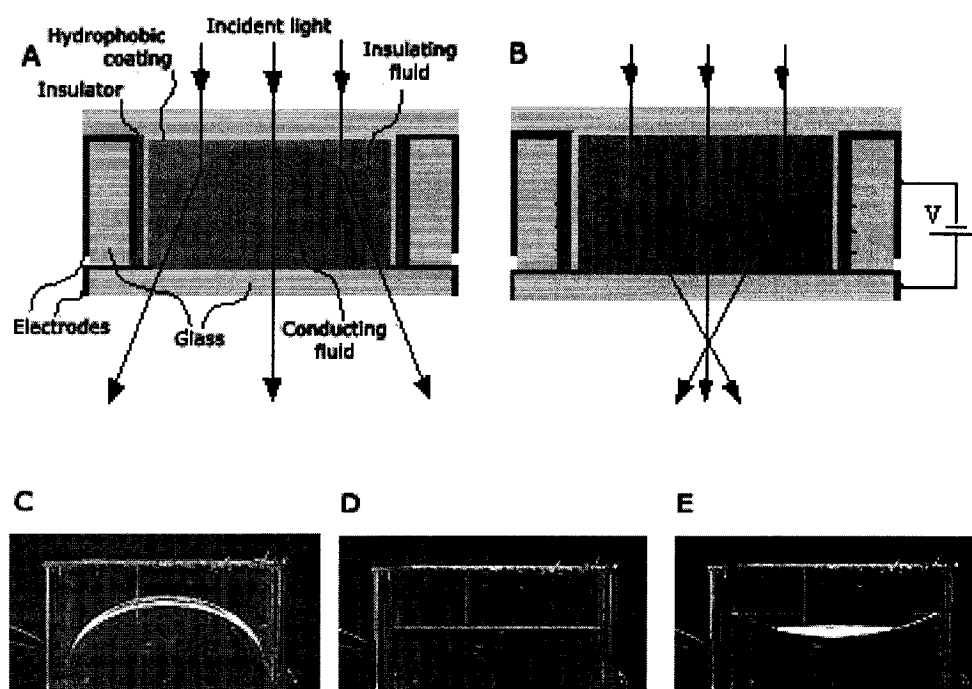


Figure 1.1 Schematic cross section of the fluid lens principle

Another tunable electrowetting liquid microlens was demonstrated in Bell Laboratories, Lucent Technologies [6]. The microlens consists of a droplet of a transparent conductive liquid placed on a dielectric substrate with a low surface energy coating. By varying the voltage applied to a set of electrodes positioned underneath of the dielectric substrate, both the position and curvature of the microlens can be reversibly changed. Figure 1.2 shows the cross-section design of Lucent's tunable microlens.

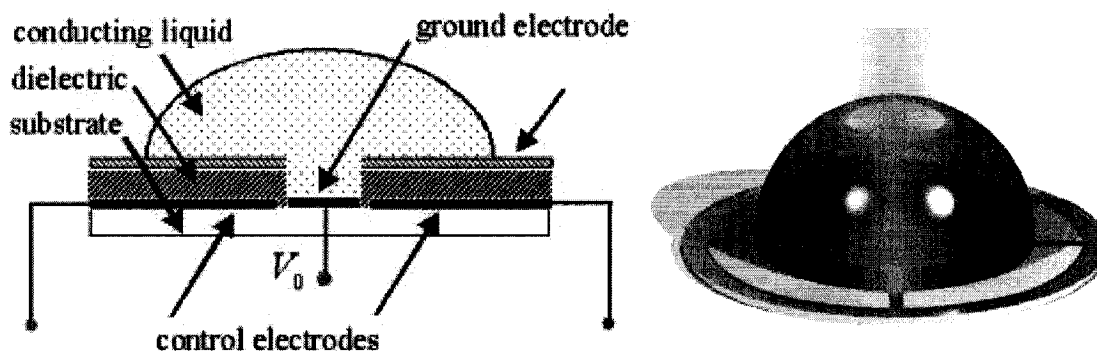


Figure 1.2 Schematic cross section of electrowetting microlens

As seen in the examples above, the liquid lens proposed by Philips Research provides an exciting result of changing a liquid lens's curvature by adjusting applied voltage. However, the design of the electrodes and chamber sealing issues greatly the complexity of device fabrication. The other liquid lens design, demonstrated by Lucent Technologies, provides a simple electrode design positioned underneath the dielectric substrate. The electrodes are of indium tin oxide (ITO). Although ITO is a transparent conducting material, it still causes some optical distortion when light passes through the conducting liquid and ITO electrodes. Therefore, an alternative variable focusing lens of much simpler design is needed. In this dissertation, two variable focusing lens systems have been presented.

1.3 Objective

This dissertation is proposed to design and fabricate novel polymeric lenses with two different variable focal length actuating mechanisms. More specifically, it is to design and fabricate a new optical lens with the ability of fine tuning focal length. The function of the new elastic polymeric lenses' designs with variable focal length is a necessary attribute in many applications of optical systems. It is desirable to implement the systems without mechanical moving parts. This research work is broken into two parts: an elastic polymeric lens and a multi-focal actuation system. It is necessary to have an elastic polymeric lens which can be deformed under an applied force and return to its original dimension when the stress is released. Further, control of the focal length can be achieved by changing the radius of the curvature of the lens or the gradient index distribution within the lens structure. By using microfluidic and electro-active polymer (EAP) actuators, two complete optical systems with multi-focal actuator have been developed.

Many different actuating approaches have been studied. This multifocal actuator is an independent subsystem, indispensable for a complete optical device with elastic polymeric lenses. The design concept is to use appropriate energy transformation techniques to generate exactly specified forces. The function of the multifocal microactuator is based on conventional force-producing principles to control the lens curvature or the gradient refractive index distribution. Based on the force-producing principles which cause the changes in focal length, there are several restrictions on mechanical, electrical, and material properties of lens structure: the lens must be soft and

flexible, or it should have dielectric properties in an electric field, and have gradient refractive index distribution within the lens structure.

Material selection for a lens becomes very important to fulfill the necessary requirements. Two lens designs have been proposed: a 3D convex elastic microlens and a Gradient Refractive Index (GRIN) lens, each lens having its own actuation system. The 3D convex lens must be flexible, such that it can be integrated with a microfluidic chamber to simultaneously control the focal length. The focal length of 3D lens is dynamically adjusted by pneumatically controlling the pressure within the microfluidic chamber. Furthermore, GRIN lenses offer an alternative to the conventional 3D lenses. Perhaps the best known lenses are made of gradient-index glasses or gradient-index polymers. The commercial GRIN lens made of glass or plastic has a fixed focal length. All these gradient-index materials create a rigid, non-deformable lens structure; therefore, they were eliminated in the preliminary material design stage. Only a few gradient-index polymers have high elongation and dielectric properties. Selecting proper polymers for an elastic GRIN lens is critical to the overall variable focal length system. Because materials for GRIN lens must meet all the above three requirements to be integrated in EAP actuators, the GRIN lens is a very important optical component in EAP driven actuator, and it becomes crucial to the success in this research project. For the reasons stated, it is necessary to understand the gradient-index lens with their optical properties. A summary of all 3D elastic lens and gradient-index lens designs and their fabrication methods, together with microfluidic and EAP actuator systems is presented in Chapter 2. The design concept for fabricating variable focusing lenses will be discussed in detail in this chapter.

1.4 Methodology

The total concept map for the methodology is given in Figure 1.3. The goal is to design and fabricate a dynamically tunable focusing lens, as the final system level of the project. Top-down design is the most effective methodology for the design of complex integrated lens with an actuator. To simplify the task of top-down design, the concept map helps to understand design principles and their fabrication difficulties. However, bottom-up verification requires a connection to the physical design. For optical Micro-Electro-Mechanical Systems (MEMS) devices in this project, the components in the physical design are 3D elastic polymeric lens and GRIN lens. There are two independent design approaches for making a tunable focal length microlens. Microfluidic actuation and EAP actuation are two different mechanisms which can be used as multi-focal driving actuators. Exploiting this simple optical device involves materials design and processing, as well as design for actuators and lenses.

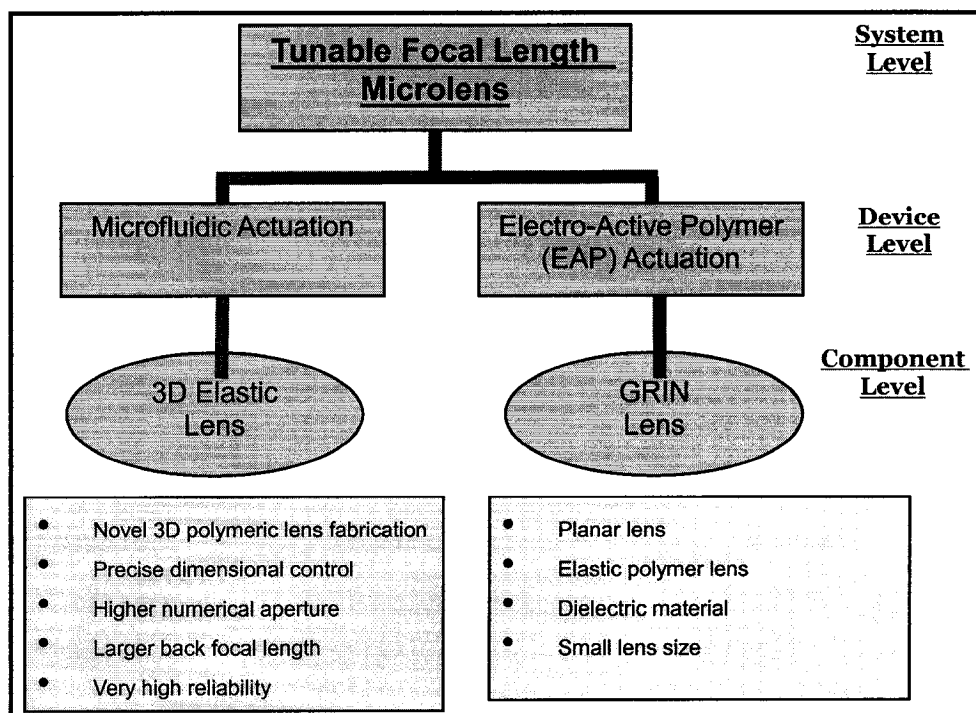


Figure 1.3 Concept map for the methodology

1.4.1 Microfluidic Actuation

Fluidic devices are well suited for producing forces or movement in a simple actuation structure. When used in microsystem, fluidic drives can take over a wide range of tasks. They are particularly suited for MEMS devices because they have high power density despite their sub-millimeter dimensions. Various types of fluidic components are being used in medicine for microdosing systems, suction catheters, as well as in environmental protection for chemical analysis. In this project, a 3D convex elastic lens is integrated with a microfluidic actuator to simultaneously control the focal length of the 3D convex lens. The focal length of the 3D convex lens is dynamically adjusted by pneumatically controlling the pressure within the microfluidic actuating system. A focal length tuning ranging from hundreds of microns to several millimeters can be achieved.

1.4.2 Electro-Active Polymer Actuation

An electro-active polymer (EAP) elastomer actuator is basically a compliant capacitor. The EAP is a dielectric medium consisting of incompressible, yet highly deformable, elastomeric material. The electrodes are designed to be able to comply with the deformations of the elastomer. As with any capacitors, when an electric field is applied to the electrodes, positive charges appear on one electrode, and negative charges on the other. This effect gives rise to Coulomb force between opposite charges, generating a pressure known as the Maxwell Stress.

The Maxwell stress forces the electrodes to move closer, thereby squeezing the elastomer. As the elastomer is thinned, it elongates in the directions perpendicular to the applied force. By using the deformation, EAP is used as a micro-actuator to change the

dimension of lens and to control its focal length. A GRIN lens is integrated in the EAP actuation mechanism as a complete dynamic focusing microlens system.

1.5 Outline of Dissertation

The objective of this project is to develop and characterize a dynamically tunable focal length microlens that can change its focal length with a driven actuator. This research is to systematically characterize the design of flexible polymeric lens and examine the actuation system for various focal lengths. This research is accomplished through design concepts, computer modeling, fabrication, and optical testing. In total, this dissertation develops design techniques, fabrication, and characterization of polymeric lenses.

To provide a basic understanding of the principle of the optical lenses and actuation systems, an introduction to the material design and optical properties of elastomer lenses and two designs of driven actuators is covered in Chapter 2. There are two approaches for using different driving force to adjust the focal length of the lens. Both variable focal length microlenses using fluidic and electrical actuation are discussed, and both actuation mechanisms are characterized with their performance evaluated.

Chapter 3 demonstrates the design and fabrication of tunable liquid-filled microlens integrated with microfluidic actuator. The characteristics of the 3D PDMS convex lens are measured. The lens surface and mechanical properties of PDMS film are presented in Chapter 3.

Chapter 4 focuses on material design and processing for gradient-index lens fabrication with a description of the polymer synthesis. The optical principle of GRIN

lens, the basic material design of silicones by two-step copolymerization method, and its polymeric structure have been examined.

To investigate an efficient electrical actuator with the GRIN lens, Chapter 5 addresses the elastic nature of the EAP material. This chapter is devoted to the description of material properties, including EAP material and compliant electrode materials. The principle behind the dielectric properties is outlined, and the fabrication procedure for actuators developed from silicone elastomer is depicted.

In Chapter 6, the deflection of the 3D microfluidic convex lens is measured. With a complete relation equation between uniform pressure and deflection, the variation of the focal length is presented. Moreover, the experimental results for the optical measurements of GRIN lens, made by two-step copolymerization method are shown. Measurements of the voltage vs. deformation curves for varying thickness of EAP film is also presented, along with comparisons to the different compliant electrode materials used in the applications.

Chapter 7 provides a summary of results, comparison of these two approaches, and recommendations for future research.

CHAPTER 2

MULTI-FOCAL LENS SYSTEM DESIGN

2.1 Design Overview

The purpose of this research is intended as a development of variable focusing lens system. The studies of modern researchers have thrown new light on this subject, arousing immense interest in making tunable focusing microlenses. Most well-known methods are liquid crystal and electrowetting. Both methods require electrodes immersed in the electrolyte solution, and this requirement causes severe optical distortion. The fabrication processes for both methods are also very complicated. Only a few attempts have so far been made to make variable focusing lens by using other approaches. Liquid-filled microlenses provide an alternative method to control the focal length of the lens by changing the curvature of the lens. As a beginning for this project at the preliminary design stage, the very first question to be discussed is suitable actuation mechanism may be used in this case. This new actuation mechanism must take advantages of other existing approaches which have been already used.

Two novel actuation mechanisms are proposed for generating significant forces to change the physical dimensions of lens structure and to control the focal length. These two actuation mechanisms are microfluidic chip and Electro-Active Polymer (EAP). By pneumatically regulating the pressure of the microfluidic chamber, the elastic lens can be

deformed causing the changes on the focal length. EAP is another method to transfer electrical energy to mechanical deformation. This energy transformation causes the deflection on the lens and induces the focal length shifted.

After the actuation systems have been decided, the second task is to design a lens which can be integrated into the actuation systems. The lens, as mentioned above, must be elastic, so it can be deformed under stress and returned to its original shape when the stress is released. Two types of polymeric lenses with high elongation under stress are proposed and designed. A 3D polymeric lens, coupled with microfluidic chip, can provide a wider range of focal length and a higher numerical aperture. In addition to the 3D convex polymer lens, a novel process has been developed to fabricate a Gradient Refractive Index (GRIN) lens by two-step polymerization method. Later sections of this chapter present the optical characteristics for these two types of lenses in detail.

It will be useful first to make a distinction between the lens components and actuation mechanisms. Designs for lens components and actuation mechanisms can be separated, but they are closely dependant on each other. Chapter 2 offers the key to an understanding of each component's functionalities. This chapter is split into two parts: the first section concentrating on describing the optical design for 3D microlens and GRIN lenses in detail. Some of the optical properties of the lenses are examined, and the optical principle of the lenses discussed. The second section presents the performance of microfluidic and EAP actuation mechanisms.

2.2 3-D Flexible Polydimethyl-Siloxane (PDMS) Microlens

A new concept has been developed to fabricate a flexible PDMS microlens, based on a continuation of fabrication process on a well-developed photoresist reflow technique. Numerous manufacturing attempts have been made by researchers to demonstrate the microlenses for many years. Many methods have been examined for the production of microlenses; these include chemical process methods, physical method, and optical methods [7]. Table 2.1 summarizes the process techniques for both methods.

Table 2.1 Possible fabrication techniques for making microlenses

Chemical Method	Physical Method	Optical Method
Reactive ion etching [8]	Hot embossing [11]	Optical interference [13]
Ion etching [9]	Photoresist reflow [12]	
Deep proton irradiation [10]	Mechanical milling [12]	

The polymer microlens examined in this research is produced using the photoresist reflow method and mold casting technique. A mold casting method to fabricate polymer microlens has never been examined. This method provides a novel way to fabricate microlenses with low cost and precise dimension control for mass production. This new process development has been claimed as an invention for a patent. This method is now discussed in detail.

The photoresist reflow method was suggested by Popovic in 1988 [14]. The reflow photoresist method involves the melting of islands of photoresist. When the islands are melted, the liquid photoresist surfaces are pulled into a shape which minimizes the energy of the system. The shape of the microlens can be well approximated by a spherical surface. The critical angle, θ_c , is the angle at which the photoresist meets the solid substrate, as illustrated in Figure 2. Three surface tensions become involved in this

process. They are as follows:

1. S_{LS} : Surface tension between the substrate and the liquid,
2. S_{LV} : Surface tension between the liquid and the vapor,
3. S_{SV} : Surface tension between the vapor and the substrate.

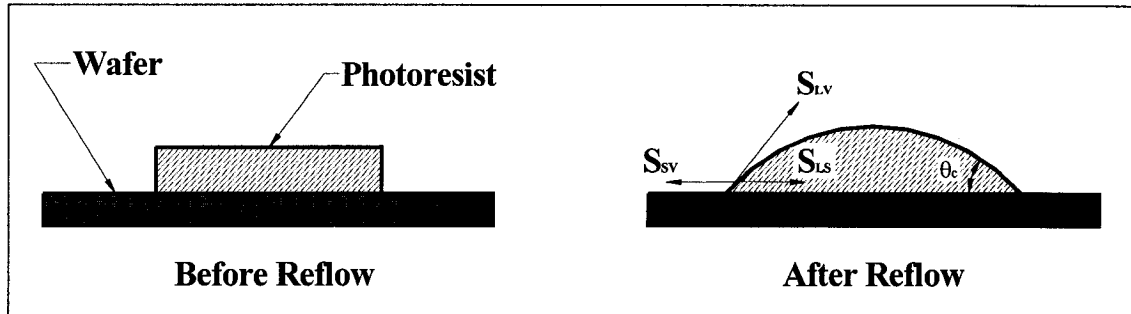


Figure 2.1 Sketch of photoresist reflow process

These three surface tensions have to reach the static equilibrium and the convex shape. The magnitude of the critical angle, θ_c , is governed by the surface tensions of the liquid resist, the surrounding air, and the substrate properties. The reproducibility of fabrication of same critical angle of microlens is achieved at constant material properties and ambient conditions.

After melting photoresist structure to form spherical lens shape, this microlens is used as a mother lens. The next step is to transfer the photoresist microstructure to PDMS master by casting method. This PDMS master consists of concave microlens, which is the negative from the original reflowed photoresist lens. By spin-coating a PDMS thin film on the PDMS master, a convex PDMS microlens can be fabricated. This technique of making a PDMS microlens from a PDMS master mold is innovated. There are no reports in the literature of making elastic polymeric microlenses by using the same material for both master mold and final lens structure. The details of fabricating 3D PDMS microlens array are presented in Chapter 3.

2.3 Gradient Refractive Index (GRIN) Lens

To understand the nature of gradient-index (GRIN) lenses, one should consider the way a conventional lens works. A conventional glass lens can bend light only at its surfaces. At the interface between air and glass, rays of light will change direction according to the abrupt change in the index of refraction. By carefully controlling the shape and smoothness of the lens surfaces, these rays can be brought to a focus and form an image.

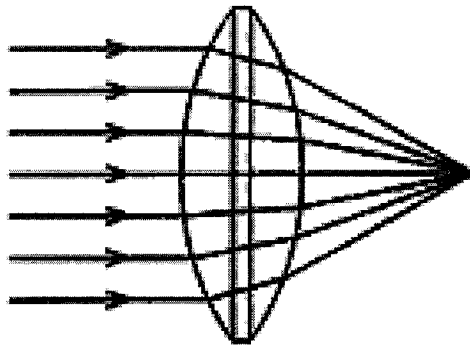


Figure 2.2 Profile of conventional lens

The shape and smoothness are two most important factors which may affect the image quality. Many techniques have been investigated for obtaining a lower surface roughness and a better surface curvature controlling in conventional lens industry. With improper lens surface profile and lens material impurity, chromatic aberration, spherical aberration, and astigmatism account as serious problems in image quality and image detecting ability. In the device-design stage, engineers have to study these three main aberrations on the optical components to design a good optical lens. In production lines, technicians have to assemble all optical components in a systematic way to avoid the image distortion and to obtain a “perfect” image. The high cost of lens fabrication and assembly and the low reliability of the device have goaded researchers to find alternative

ways to replace the conventional lens. Gradient Refractive Index (GRIN) lenses have thus gained attention by several research groups.

Because of these considerations, optical designers are becoming interested in utilizing gradient-index optics to replace the conventional lens. GRIN lenses offer an alternative to the often painstaking craft of polishing curvatures onto glass lenses. When exploring this area, the results show that Gradient-index (GRIN) profiles are a part of daily life, and variations of refractive index are part of living creatures. Exner in 1889 discovered that insect eyes are composed of rods which act as lenses due to their varying index of refraction [15]. The human eye as well has a radial gradient-index profile [16]. Gradient-index lenses are useful for optical communications and in imaging systems because they do not rely on shape for their optical properties; a completely flat piece of GRIN material can act as a lens. In addition, rods or fibers with this characteristic can be used to image an object at one end to a detector at the other. These properties simplify both the design and alignment of optical systems and allow them to be smaller than they conventionally would be.

As the diagram (Figure 2.3) indicates, by gradually varying the index of refraction within the lens material, light rays can be smoothly and continually redirected towards a point of focus. The internal structure of this index "gradient" can dramatically reduce the need for tightly-controlled surface curvatures and results in a compact and simple lens geometry. In other words, controlling light ray direction by changing the index of refraction and having all optical characteristics of conventional lens without strict requirements of surface curvature, GRIN lens can be expected to become an important role in the photonic industry in near future.

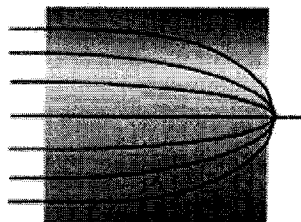


Figure 2.3 Profile of a GRIN lens

In the current commercial GRIN lens market, GRIN lens designs can be classified into four (4) main groups: axial gradient, transverse gradient, radial gradient, and spherical gradient.

2.3.1 Axial Gradient

Axial symmetric gradients are studied and manufactured more commonly. This type of lens has a gradient profile in which the refractive index varies along the direction of light propagation, or optical axis. This type of lens has the same refractive index plane, called an “isindex surface,” perpendicular to the lens axis, as shown in Figure 2.4 [17]. This index gradient provides additional degrees of freedom in lens design for aberration control. Axial gradient lenses can correct spherical aberration from a spherical lens. This ability helps to increase the tolerance budget on optical aberration, the reason why this type of lens has attracted more and more attention from optical design engineers.

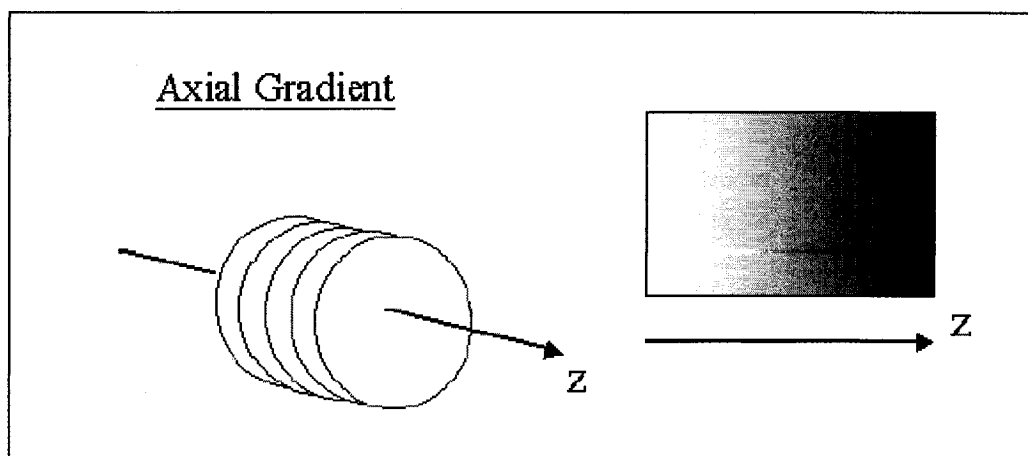


Figure 2.4 Axial gradient-index lens

2.3.2 Transverse Gradient

The second type of gradient-index lens is transverse gradient. A gradient profile's refractive index varies perpendicular to the direction of light propagation, or optical axis, shown in Figure 2.5 [17]. This type of lens has the same refractive index plane, called an "isindex surface," parallel to the lens axis. The principle of this lens is very similar to the axial gradient lens.

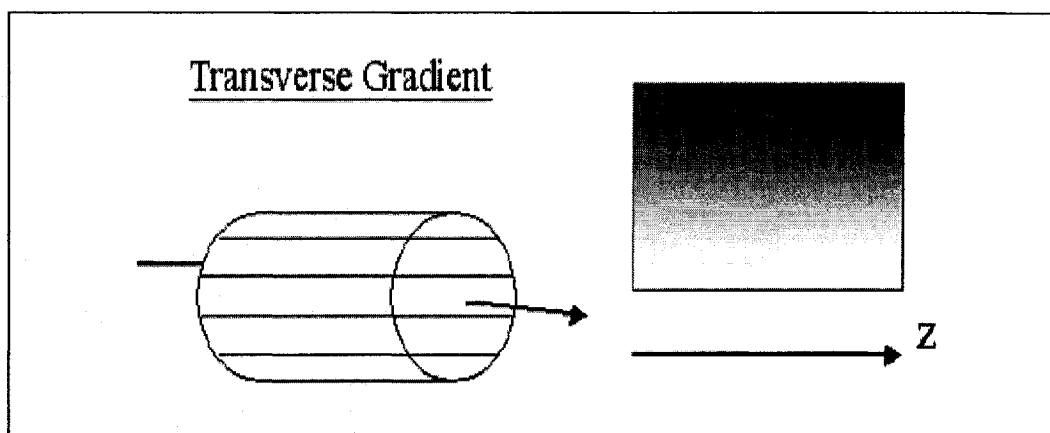


Figure 2.5 Transverse gradient-index lens

2.3.3 Radial Gradient

The third type is the radial gradient. The axial gradient provides aberration control; the radially-symmetric gradient can provide optical power. A gradient index profile's refractive index varies in a direction perpendicular to the optical axis, shown in Figure 2.6 [17]. Radial gradient lenses can focus light even when the lens surfaces are flat, in which case, they are called Wood lenses. The isindex surface is a cylindrical shape parallel to the lens axis.

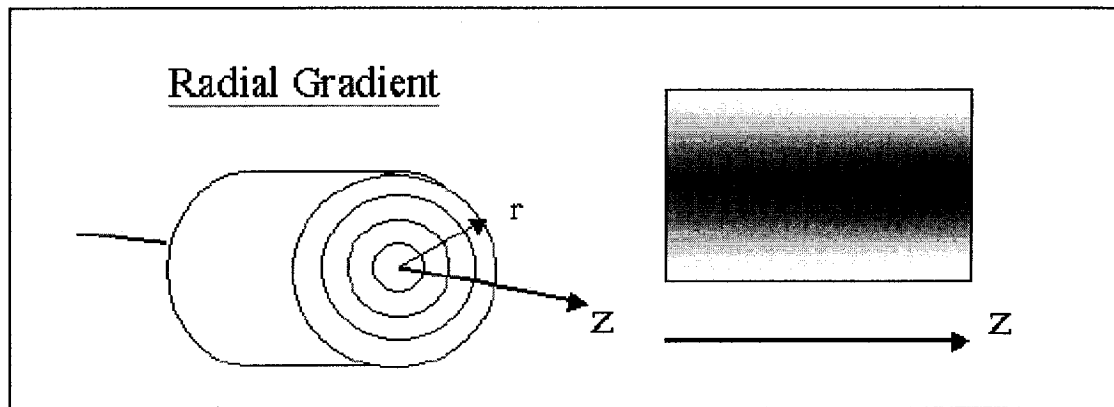


Figure 2.6 Radial gradient-index lens

2.3.4 Spherical Gradient

The vast majority of gradient-index lens designs have some degree of symmetry. The earliest gradient-index designs a spherically symmetric lens, the Maxwell fisheye lens. It provides perfect point-to-point imaging within the lens. This lens is also called a Luneberg lens, for Luneberg proposed as a spherical lens which can image an external object.

2.3.5 Current Available Gradient Index Lens Fabrication

Glass and polymers are the two well-known materials applied in the optical field. Glasses have excellent transparency and low optical attenuation, but brittleness and high process cost are their disadvantages. Polymers, on the other hand, have higher optical loss but excellent mechanical properties, light weight, good flexibility, easy processing, and low cost. As a result, the development of GRIN lens, based on both materials, has grown rapidly in recent years. Several methods have been used to prepare GRIN lens. The following sections introduce the fabrication method for glass and polymer GRIN lens in detail.

There are a variety of ways to fabricate gradient-index materials. Perhaps best known are gradient-index glasses. The different fabrication methods have different index gradient sizes and depths, summarized in Table 2.2 [18].

Table 2.2 Methods for GRIN glass fabrication with approximate maximum gradient depth and Δn

Method	Spatial Extent (mm)	Δn (max)
Ion Exchange	10	0.04
Neutron Irradiation	0.1	0.02
Chemical Vapor Deposition	0.1	0.01
Polymerization Techniques	100	0.01
Ion Stuffing	50	0.04
Crystal Growing	20	0.05

Neutron irradiation is a method in which a boron-rich glass is bombarded with neutrons to create a change in the boron atoms and a consequent change in the refractive index. Via masking, a three-dimensional index variation can be achieved. However, heavy neutron doses are required, and there are doubts about the stability and radiation hazards of the material produced.

Chemical vapor deposition (CVD) is primarily used to fabricate fiber optics with radial index gradients. A glass or quartz tube has gases passed through it, causing glass to form inside the tube, from the tube edge inward. By varying the gas compositions, an index-gradient can be created.

For ion exchange, a base glass is immersed in a molten salt bath. Cations from the bath exchange with the alkali ions in the salt (composing the glass), a proven technology with decades of study and is used for commercial products. Furthermore, designs for manufacturing methods are becoming more available. However, this technology requires high-temperature ovens to melt the salt bath, and is therefore energy intensive.

Ion stuffing uses special glass which its phase separates when heated. One phase of the glass is soluble in acid and can be dissolved out to leave a glass sponge. When the sample is exposed to a bath containing suitable ions or molecules, these diffuse in, creating an index gradient.

With the crystal growing method, a seed crystal is used to pull a larger crystal from a bath containing a mixture of chemicals. As the crystal is pulled, the amount of one chemical in the bath decreases, causing the crystal to take more of a second chemical, creating a change in refractive index. This process is potentially useful for working with infrared optics.

These methods are all useful for various applications. But as has been seen, most glass-based GRIN materials possess a relative small Δn , typically less than 0.04. Moreover, the GRIN lens structure is rigid. It can not be coupled with an actuation system for changing its focal length. Therefore, glass-based GRIN materials are not suitable for this research.

As with the gradient-index glasses, there are several ways to make gradient-index plastics. The different fabrication methods have different index gradient sizes and depths, summarized in Table 2.3. Because polymers have refractive indices ranging from 1.4 to 1.6, it is expected that a large range of maximum Δn can be achieved, and this result is indeed the case.

Table 2.3 Methods for GRIN plastic fabrication with approximate values for maximum gradient depth and Δn .

Diffusion Method	Spatial Extent (mm)	Δn (max)
Photocopolymerization	3	0.05
Interfacial-Gel	10	0.02
Vapor Phase Transfer	5	0.03
Curved Mold	35	0.02
Immersion	40	0.1

Photo-copolymerization, activated by ultraviolet light, is typically made with two or more monomers mixed together in a glass tube. The tube is rotated, at a high speed in RPM and illuminated by UV light. Only a portion of the tube is illuminated by the light, and the light is moved upward at a constant rate, approximately 1 mm/sec. The variation in the rate at which the monomers polymerize as the light travels upward leads to variation in refractive index.

Interfacial-gel copolymerization typically uses a hollow tube made of one of the two polymers being used for the diffusion. The tube is filled with a mixture of both monomers. The tube is heated, and the polymerization proceeds from the inside tube wall. The differing rates of polymerization of the two materials lead to an index gradient.

The vapor phase transfer method places a partially polymerized rod in an inert atmosphere. The vapor of the diffusant monomer is introduced, which diffuses into the rod. After diffusion is complete, the rod is heated to complete the copolymerization.

The curved mold method is a geometrical approach to creating large-radius gradient-index polymers. A partially polymerized gel is made in a mold with a curved top. A second liquid monomer is added, covering the gel. The monomer diffuses into the gel; the whole of it is then heated to complete polymerization. An effective gradient-index variation is achieved through the varying composition of the sample. This effect can also be thought of as a variation of the immersion method, described next.

For immersion copolymerization, the first monomer is partially polymerized, and the gel immersed in a liquid second monomer. After diffusion, or during diffusion, it is fully polymerized. Both radial-symmetric and axial index-gradients can be created.

2.3.6 Novel Method of Fabricating an Elastic GRIN Lens

A new fabrication technique, developed by Calhoun Vision, is capable of easy pattern formation for gradient-index polymer lens [19]. A guest macromer with higher or lower refractive indices is diffused into the first polymer matrix made by PDMS, and then the diffusion profile is fixed by final polymerization. The gradient-index profiles can be selectively formed in the ultraviolet (UV) irradiated regions by using the difference in diffusion rate. The proposed approach to modulate the refractive power of GRIN lens composed of a first cross-linked silicone polymer matrix (PDMS), a guest macromer, and a photoinitiator. The application of the appropriate wavelength of light onto the central optical portion of the lens polymerizes the macromer in the exposed region, thereby producing a difference in the chemical potential between the irradiated and nonirradiated regions. To reestablish thermodynamic equilibrium, the unreacted macromer and photoinitiator diffuse into the irradiated region. As a consequence of the diffusion process and the material properties of the host silicone matrix, a gradient refractive index distribution is formed within the lens. Figure 2.7 shows the schematic process flow [19].

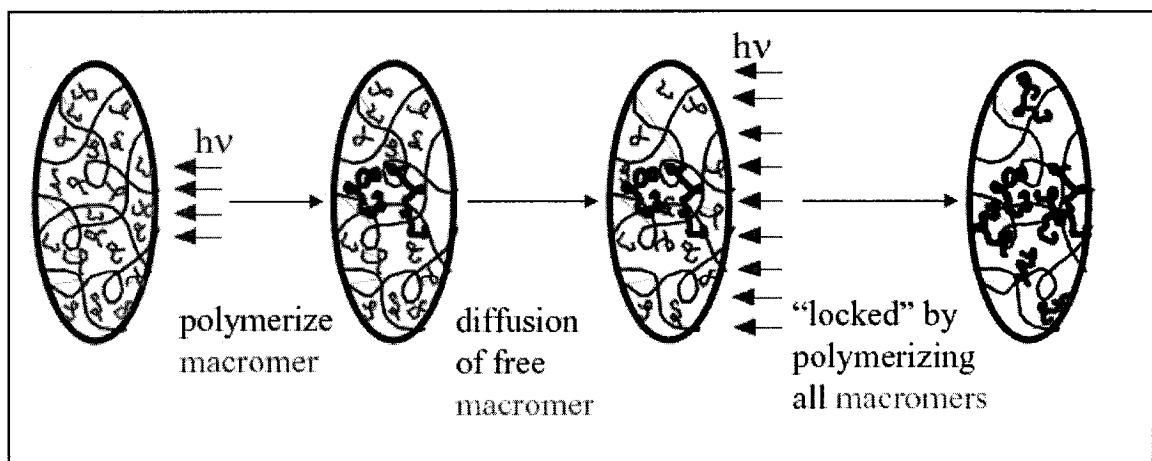


Figure 2.7 Cartoon schematic illustrating the proposed diffusion mechanism

The novel GRIN planar lens comprises a first polymer matrix and a macromer dispersed therein. The first polymer matrix forms the optical element framework and is generally responsible for many of its material properties. The macromer is a compound that is capable of photo polymerization. The macromer is capable of photo-induced polymerization and may be monomers, so long as:

1. It is compatible with the formation of the first polymer matrix;
2. It remains capable of photo-induced polymerization after the formation of the first polymer matrix; and
3. It is freely diffusible within the first polymer matrix.

Because of the requirement that the monomers must be diffusible within the first polymer matrix, the monomers generally tend to be smaller (have lower molecular weights) than the monomers which form the first polymer matrix. In addition to the monomers, the macromer may include other components such as initiators and sensitizers that facilitate the formation of the second polymer matrix. In the current material research based on our previous work on variable focal length lens and EAP actuation, the first polymer matrix is set to poly-dimethylsiloxane (PDMS). Based on the properties of PDMS matrix, material for the macromer, photo-initiators, and sensitizers have been searched for finding proper materials and fulfill the above three requirements.

Another important reason for using this approach is due to the cross-linked silicone polymer matrix which is made by PDMS with gradient refractive index distribution; its dielectric property makes integrating with the EAP actuation mechanism easy. Therefore, the whole device can be made of GRIN PDMS lens with two compliant electrodes. It can fulfill the functions of gradient refractive index distribution, and variable focal length.

2.4 Micro-Fluidic Actuation System

A new polymer microlens with the variable focusing properties is proposed in this section. The microlens consists of a thin diaphragm with 3D convex lens, chamber, and microchannel made of Polydimethyl-Siloxane (PDMS). Figure 2.8 shows the overall microfluidic actuation design and its components. The microfluidic system provides simultaneous control by adjusting the fluid pressure within the microfluidic system. According to “*Micro/Nano R&D Magazine*”, the US microfluidics market was ~\$128 million in 2002, and expected to grow to ~710 million by 2008. Microfluidics has a great market potential as an actuation system. The novel fabrication approach has been developed to cast a 3D PDMS microlens film by the PDMS mold. This film with a microlens acts as a diaphragm. The flexible PDMS microlens and diaphragm then are integrated on a microfluidic chip. Varying the pressure in chamber, which produces the focal plane shift, can change the curvature and back focus length of the lens. The new fabrication method provides the easy fabrication, reproduction, and precise dimension control. The variable focal length of microlens is critical to increase the efficiency of the light detection in optical or biophotonic applications. In this study, the fabrication processing, mechanical and optical property testing, and simulation results are presented in detail in Chapter 3.

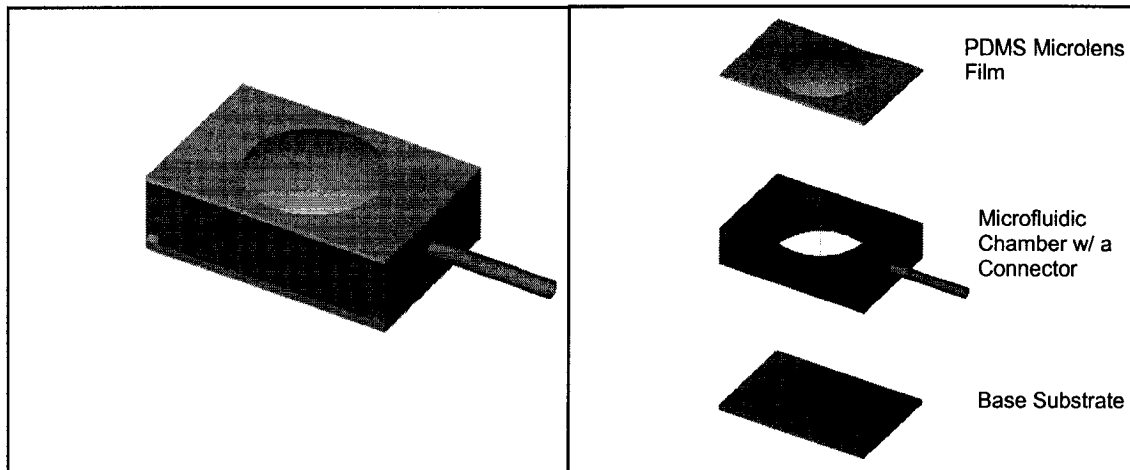


Figure 2.8 Overall microfluidic system and its components

2.5 Electro-Active Polymer (EAP) Actuation System

Limiting factors to microfluidic actuation, introduced in the previous section, are the slow actuation response time, complicated fabrication process, and lack of precise focal tuning control. Electro-Active Polymer (EAP) has attracted much attention to be used as another alternative actuation for tuning focal length of the PDMS lens. The advantages of EAP are the following:

1. Operating in room condition for long period of time
2. Having Rapid response time (mSec levels)
3. Holding strain under DC activation
4. Inducing relatively large actuation forces

EAP has unique characteristics that determine its applicability to transducer applications. Table 2.4 highlights aspects of its unique performance, operations, materials, and manufacturing characteristics. The data in Table 2.4 attempt to identify the fundamental material performance of each technology [20].

Table 2.4 Electrical and mechanical performance for all types of actuators

Actuator Type (specific example)	Maximum Strain (%)	Maximum Pressure (MPa)	Specific Elastic Energy Density (J/g)	Elastic Energy Density (J/cm ³)	Maximum Efficiency (%)	Relative Speed (full cycle)
Dielectric Elastomer (Acrylic) (Silicone)	380 63	7.2 3.0	3.4 0.75	3.4 0.75	60–80 90	Medium Fast
Electrostrictor Polymer (P(VDF-TrFE))	4.3	43	0.49	0.92	~80 est.	Fast
Electrostatic Devices (Integrated Force Array)	50	0.03	0.0015	0.0015	> 90	Fast
Electromagnetic (Voice Coil)	50	0.10	0.003	0.025	> 90	Fast
Piezoelectric Ceramic (PZT) Single Crystal (PZN-PT)	0.2 1.7	110 131	0.013 0.13	0.10 1.0	90 90	Fast Fast
Polymer(PVDF)	0.1	4.8	0.0013	0.0024	~80 est.	Fast
Shape Memory Alloy (TiNi)	> 5	> 200	> 15	> 100	< 10	Slow
Shape Memory Polymer	100	4	2	2	< 10	Slow
Thermal (Expansion)	1	78	0.15	0.4	< 10	Slow
Electrochemo-mechanical Conducting Polymer (Polyaniline)	10	450	23	23	< 5% est.	Slow
Mechano-chemical Polymer/Gels (polyelectrolyte)	> 40	0.3	0.06	0.06	30	Slow
Magnetostrictive (Terfenol-D)	0.2	70	0.0027	0.025	60	Fast
Natural Muscle Peaks in nature Human Skeletal	100 >40	0.80 0.35	0.04 0.07	0.04 0.07	- -	Slow-Fast Medium

By applying DC voltage on two compliant electrodes, the polymer shrinks in thickness and expands in area. With these characteristics, circular electrodes are designed and examined. With different DC voltages, electrostatic force causes the polymer to be deformed. Depending on the fabrication processes, the polymer film would be bent and produce an out-of-plane or in-plane deflections. These two actuation configurations are described in following sections.

2.5.1 Out-of-Plane EAP Actuator

The EAP diaphragm actuators can take advantage of the large strain capability of dielectric EAPs to produce large out-of-plane deflections and correspondingly large axial displacement. This large deflection makes a concomitant decrease in the radius of curvature of the lens. The best films allow for out-of-plane deflection equal to 50% of the diaphragm diameter [20]. Figure 2.9 shows a PDMS diaphragm actuator undergoing out-of-plane deformation in which the diaphragm changes shape from flat to hemispherical. The small number of moving parts will allow for high reliability and quiet operation.

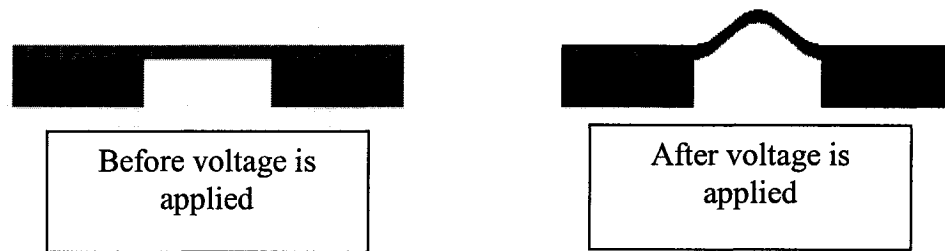


Figure 2.9 Circular EAP with out-of-plane deflection

Figure 2.10 also indicates the simulation result on the deformation profile by Convector. The simulation results show that an out-of-plane deflection is induced when the boundary conditions between the surfaces of substrate and diaphragm are fixed in all directions.

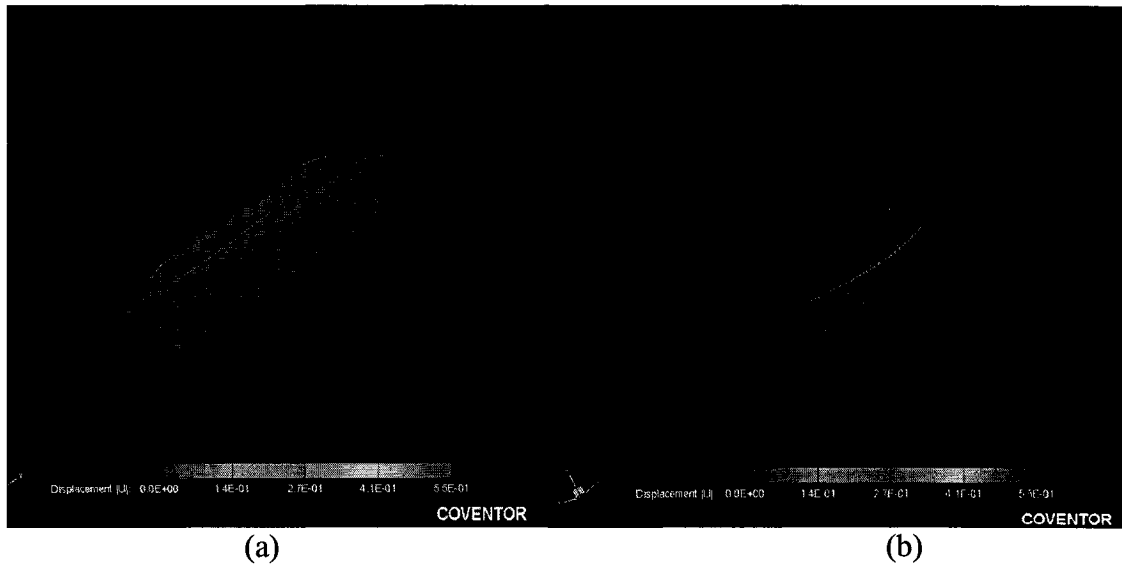


Figure 2.10 Deformation distribution (a) top view, (b) bottom view.

2.5.2 In-Plane EAP Actuator

The second EAP diaphragm actuators can produce large in-plane area expansion and cause the lens area to be squeezed in area and thicken in the thickness. A thin PDMS film is stretched uniformly across a circular hole in a rigid frame. Carbon grease is applied to small hollow circles at the center of film and on top and bottom of film as compliant electrodes. When a voltage is applied to the electrodes, the film between the electrodes expands in area, and contracts in thickness. This expansion in area and contraction in thickness on the hollow electrode areas can cause the center portion to be squeezed in area and thicken in the thickness. By controlling the applied voltage, the area and thickness of lens can be measured with an optical microscope, a video camera, video digitizing hardware, and digital measurement software. So the lens's in-plane area changes can be determined when a given voltage is applied. By coupling with axial GRIN lens, the focal length varies when the refractive index distribution is changed by the lens's area and thickness. By changing refractive index distribution along the distance from center axis, the focal length can be controlled accurately. Figure 2.11 shows the

in-plane actuator mechanism and illustrates the refractive index distribution changed when the GRIN lens structure changes.

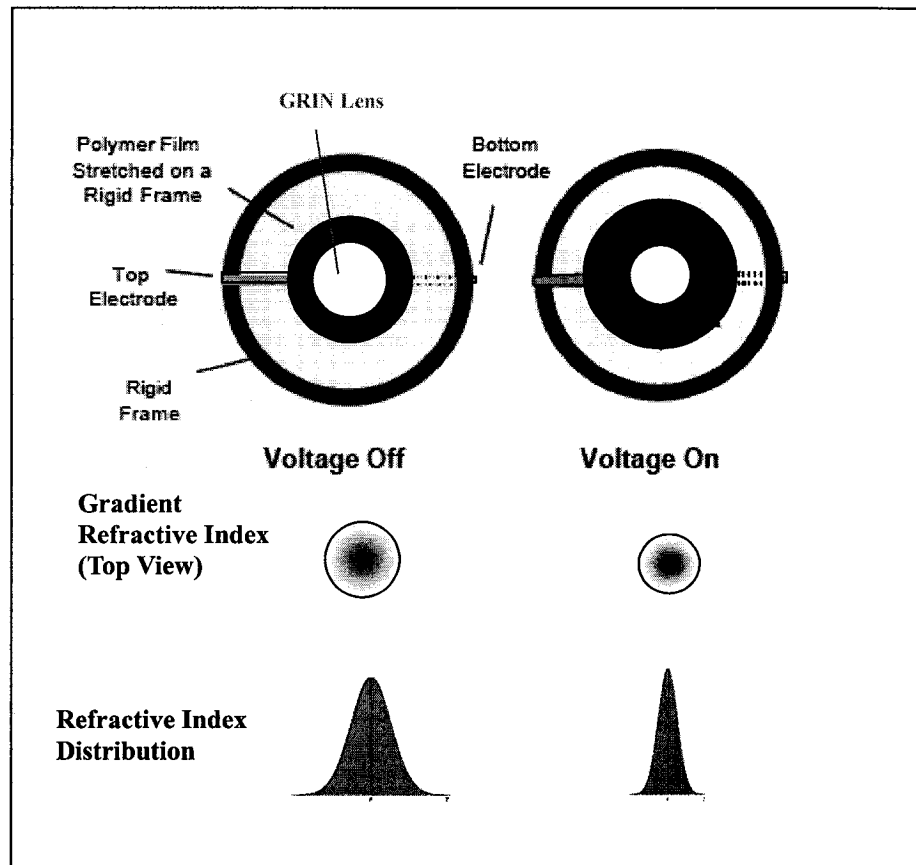


Figure 2.11 In-plane movement with circular EAP

CHAPTER 3

VARIABLE FOCUSING MICROLENS WITH MICROFLUIDIC CHIP

3.1 Basic Design Concept

The study of the variable focusing microlens has been an area of activity for many years. Variable focal length is a necessary attribute in many optical applications if the object being imaged is not in a fixed position. Several recent publications have recognized that the potential for variable microlens impacts significantly the field of optical applications [21][22]. The variation of focal length can be provided by a focalizing mechanism to cause the focal plane shift. The different approaches using liquid crystal [23][24] and electrowetting method [3][25] have been investigated by some researchers, but the liquid crystal lens is limited to the small lens, and the electrowetting liquid concept lens requires a high-voltage source. Both methods required electrodes, which are immersed in the electrolyte solution, causing severe optical distortion. A variable focusing liquid-filled lens with a pressure-driven mechanism was also demonstrated [26]. However, the numerical aperture of this lens is limited because the lens was made by a planar glass diaphragm.

A new concept has been developed to fabricate a flexible polydimethyl-siloxane (PDMS) microlens with microfluidic chip. The microlens is a 3D convex polymer lens on

a thin diaphragm. The diaphragm is integrated on a microfluidic chamber to simultaneously control the focal length of microlens. The microchamber on the microfluidic chip is filled with working fluid. Changing the fluid pressure causes the change of the curvature of the polymer lens inducing focal plane shift. Together with the deflection of PDMS diaphragm, a microlens, attached on the diaphragm can provide with much higher numerical aperture than a planar glass or polymeric membrane. Moreover, the 3D convex lens provides a focal point when the diaphragm is at an initial position. This design of microlens, working much as a human eye's crystalline lens, provides more flexibility on back focal length and higher numerical aperture than previous research showed on liquid-filled variable focal lens. The numerical aperture of the new PDMS microlens can be achieved to 0.24, about four times of conventional planar glass diaphragm ($NA \approx 0.05$) [26]. The higher numerical aperture microlens, integrated on a microfluidic chip will perform a high-resolution and high signal-to-noise detection in optical MEMS applications. The high numerical aperture of a microlens is critical to increase the efficiency of the detection ability. This design has the advantages to be used as a micro optical component with high numerical aperture, variable focal length, and low optical distortion. These attributes make this design attractive to the optical pickup in many applications, such as optical switch, camera, microscope, and optical signal processing.

In addition, a novel batch process of making polymer lens arrays has been developed. It is a cast method to fabricate convex PDMS microlenses on a thin diaphragm by using a cured PDMS concave microlens master mold. This method can produce highly

dimensional accuracy, high optical quality, and a high production rate with low cost. The design, fabrication, and characterization are presented in this chapter.

3.2 Fabrication Processes

The conventional lens has a fixed focal length. However, a variable focus lens should work like a human eye's crystalline lens that can be deformed by muscles. The variable focal length microlens was successfully designed and fabricated which included two parts: a microlens diaphragm and a microfluidic chip. The PDMS thin film with convex lens is a passive diaphragm while the microfluidic chip acts as an actuating part. PDMS is selected as the lens material because it features a good optical property with large elongation and bio-compatible.

The new design and fabrication technology of microstructure for optical elements with the diversification of optical devices and system are been strongly demanded. One of keys to processing is 3D microlens fabrication. It was observed in the preceding chapter that various fabrication processes of microlens have been reported, such as reactive ion etching (RIE), ion diffusion, deep proton irradiation, and physical methods such as hot embossing, injection molding, micromachining, and photoresist reflow. The microlens materials are varied depending on the fabrication methods, which include polymethyl methacrylate (PMMA), photosensitive glass, photopolymers, and UV curable resins [14]. However, each microlens produced from these methods has a rigid structure with a unique focal length. Most of fabrication processes are complicated and require specific facilities for producing microlenses. A novel PDMS casting fabrication processing has been developed to fabricate a elastic three-dimensional Polymer microlens. The processing schematic is shown in Figure 3.1.

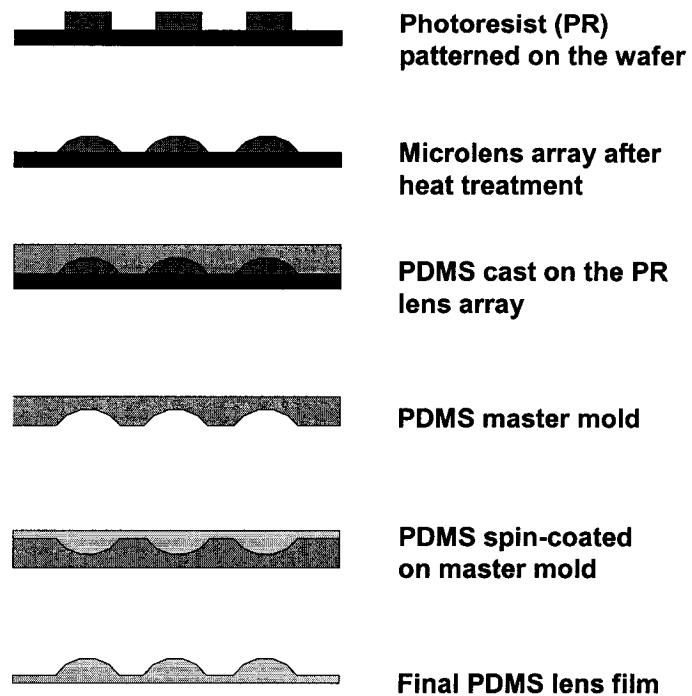


Figure 3.1 Fabrication sequence for array of polymer microlenses

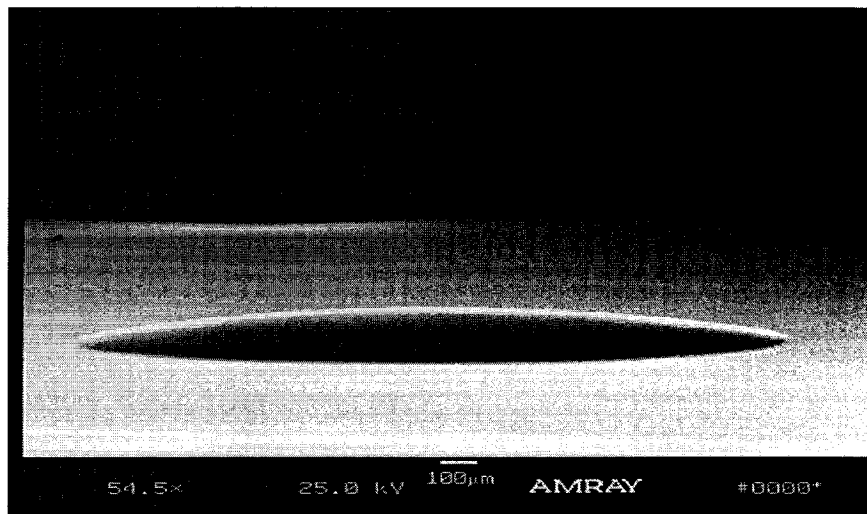
3.2.1 Fabrication of Photoresist Reflow Microlens

To fabricate the microlens by molding, a mother lens of the same shape as the final PDMS lens is needed, and the photoresist reflow method is used to make it. The first step is to generate photoresist pattern by conventional photolithography. Second, the photoresist pattern is thermally treated for reflowing into lens shape. The photoresist reflow method, suggested by Prpovic in 1988, is to melt photoresist structure to form small lenses shape due to the surface tension of the liquid resist [14]. The method of creating a smooth profile hemispherical polymeric mound has been used in applications such as three-dimensional inductors and fiber optics devices and for microfluidic applications. In this work, the same method is used in the fabrication of microlenses.

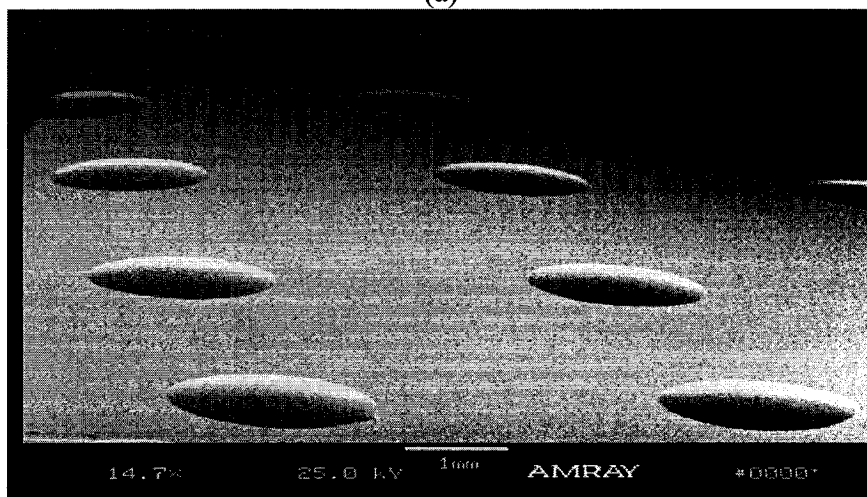
Depending on the final thickness desired, Clariant® AZ 100XT photoresist was spin-on coated with different spinning speeds on 4-inch diameter silicon wafers. The

sample was soft baked from 70°C to 110°C on a hot plate for 30 minutes or longer, depending on the final thickness of the photoresist layer. After the soft curing, the sample was taken out from the hot plate and naturally cooled down to room temperature overnight. Before UV exposure, the sample was dipped in DI water for one hour to let the photoresist absorb moisture. Conventional UV lithography was carried out to create patterned circular photoresist mesas, and the sample was developed in MF300 developer (Shipley).

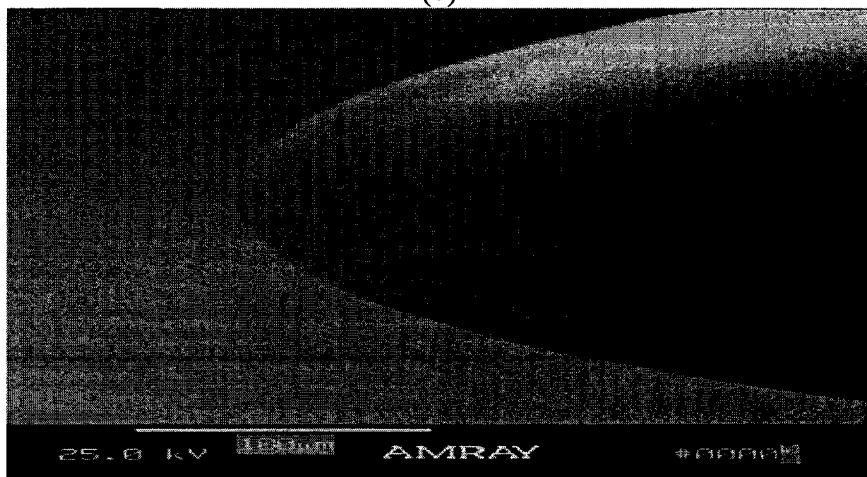
Next, the photoresist layer in the sample was thermally reflowed on a hot plate to convert photoresist mesa structures into the deformed photoresist mounds. To create the uniformly deformed photoresist mound, the sample was exposed to acetone vapor before the thermal reflow process, as suggested by Fletcher et al. [27]. The hot plate was preheated to 50°C before acetone exposure was started. The sample was placed on a 4-inch petri dish, which is in turn placed in an acetone-contained 6-inch petri dish with a spacer. Another 6-inch petri dish was placed on top of the bottom 6-inch petri dish right after the acetone was poured in so that the evaporated acetone vapor was kept inside the petri dishes and the photoresist mesa was exposed to the evaporated acetone vapor. The wafer was immediately placed on another hot plate with temperature of 95°C, and was kept at that temperature for 10 minutes. At this point, the polymeric mesa was uniformly deformed. Acetone vapor and moisture absorbed inside the polymeric mesa were removed. The final hard curing of the mesa from 120°C to 150°C on the hot plate stabilized the mesa from further reflow in subsequent fabrication processes. SEM photomicrographs of photoresist microlens with a diameter of 1400 μ m and its array after thermal reflow process are shown in Figure 3.2.



(a)



(b)



(c)

Figure 3.2 SEM images of 1400μm diameter photoresist microlens (a) single spherical lens (b) an array of microlenses (c) closer view on the edge of photoresist microlens

3.2.2 Casting Method for Elastic PDMS Microlens

After completing the photoresist mother lens, the next step is the transfer of photoresist microstructure to PDMS master by casting method. PDMS is chosen as a master material because it provides high dimensional accuracy and easy fabrication. Dow Corning Sylgard 186 silicone is used as the master material. After the PDMS master is dried in a vacuum oven for 2 hours at 5 mtorr of pressure with 75°C, the mold is peeled off from the mother lens wafer. The PDMS master consists of a concave microlens array. Figure 3(a) shows the SEM images of the master. The diameter of the concave surface is 1400 μm .

The final step is spin coating PDMS on the PDMS master. Depending on the spinning speed, a thick or thin film with a unique dimension of microlens can be obtained; then, PDMS film is dried for 2 hours at 5 mtorr of pressure at 75°C. Finally, the lens film is peeled out from the PDMS master. Before the new PDMS layer does not crosslink with the cured PDMS master mold on the interface during curing process, it is easy to peel-off the film from the master mold. The SEM pictures at Figure 3.3 show a PDMS mold and PDMS microlens film with a microlens (1400 μm at diameter and 85 μm height at the center of lens).

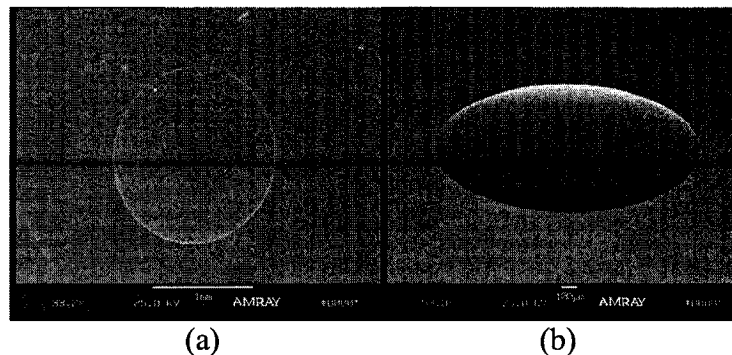


Figure 3.3 SEM photographs for (a) PDMS concave master, and (b) final PDMS film with convex lens

3.2.3 Microfluidic Chip Fabrication

The microfluidic chip includes a silicone chamber and a PDMS chamber block with an inlet channel. Figure 3.4 shows the cross-section view of the microfluidic chip structure. It is necessary to have a silicon wafer between PDMS microlens film and PDMS chamber block for the silicon wafer provides smooth and rigid surface for bonding with both PDMS microlens film and PDMS chamber block. A through hole on a silicon wafer with a diameter of 1400 μm is formed by Inductively Coupled Plasma (ICP) dry etching. A chamber mold is designed and built to create a circular chamber with an inlet channel. PDMS prepolymer mixture is then cast to form the body of a 1400 μm chamber and a channel. The PDMS mixture is subsequently cured in an oven for 2 hours at 75°C. The cured PDMS chamber is peeled off from the mold.

Finally, both the lens film and PDMS chamber block are bonded to the silicon substrate by using a high strength epoxy to avoid any leakage (Devcon All Purpose Epoxy). The overall dimension of the prototype, as shown in Figure 3.5, is about 5mm x 4.5mm x 2.5mm (L x W x H).

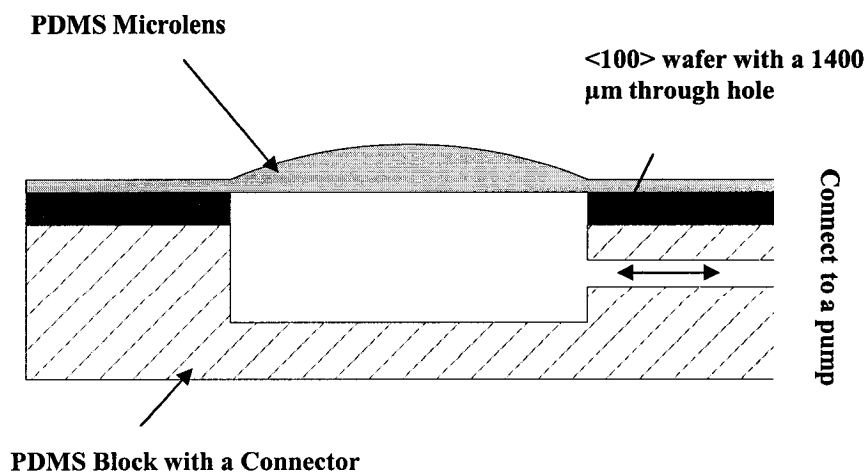


Figure 3.4 Schematic cross section for microfluidic chip structure

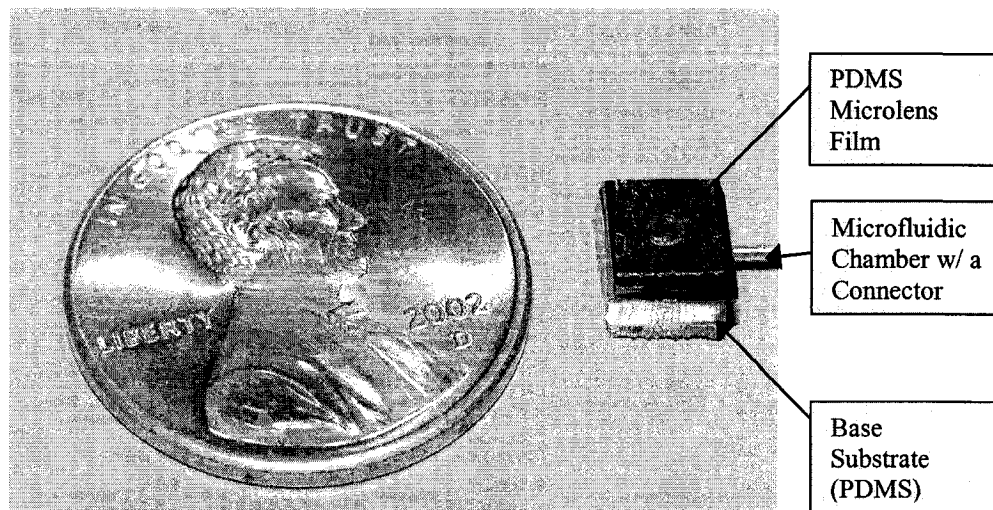


Figure 3.5 A prototype of variable focal lens with microfluidic chip

3.3 Characteristics for 3D PDMS Microlens

PDMS microlenses, diameter range from $600\mu\text{m}$ to $1400\mu\text{m}$, are successfully fabricated. In this chapter, a microlens with $1400\mu\text{m}$ diameter has been used for characterization. The surface profile, the mechanical and optical properties of PDMS microlens, has been characterized. In addition, the simulation with finite element analysis (FEA) has been examined.

The surface profile of melted photoresist microlens is measured using Tencor Alpha Step 500 System. This equipment uses a stylus with a $2\mu\text{m}$ chisel head as a probe and scans the sample surface. Figure 3.6 shows the surface profile of photoresist lens. The height of photoresist mother lens is $85\mu\text{m}$ at the center point and the diameter is $1400\mu\text{m}$, shown in Figure 3.6.

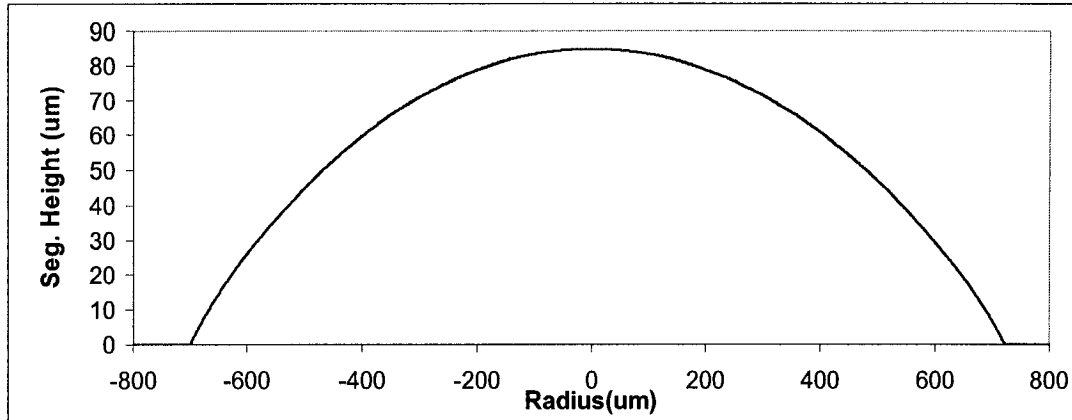


Figure 3.6 Surface profile for photoresist microlens

The surface roughness of mother lens and PDMS master mold are very important parameters which may affect the optical properties of final lens. An atomic force microscope (Quesant Instruments scanning probe microscope, AFM) examines the surface roughness. AFM provides true 3D topographic images, which also yield surface roughness data on the nanometer scale. In the analysis, AFM measures surface roughness on an area of 10umX10um of sample's surface. Table 3.1 indicates the comparison of average surface roughness for photoresist microlens, PDMS master mold, and 3D PDMS microlens. The results indicate that surface roughness is changed after each processing step of PDMS coating and peel-off process. However, the surface roughness for the PDMS master and final PDMS microlens film does not show any significant change. The roughness for both master mold and final PDMS microlens film is about 17~18.6 nm, which is still in an acceptable range for optical lens requirements.

Table 3.1 Comparison of surface roughness for photoresist microlens, PDMS master and final PDMS microlens

	Photoresist microlens	PDMS master	Final PDMS microlens
Average Roughness	8.61 nm	17.2 nm	18.6 nm

The mechanical properties of PDMS film are examined by applying a load at the center of the PDMS film. The corresponding deflections with various loadings are measured. Figure 3.7 shows a linear relationship between applied load and deformation at the center of the film. The maximum loading force for 100 μm thick PDMS film is about 20g. The PDMS film can be ruptured if the applied force is larger than this value.

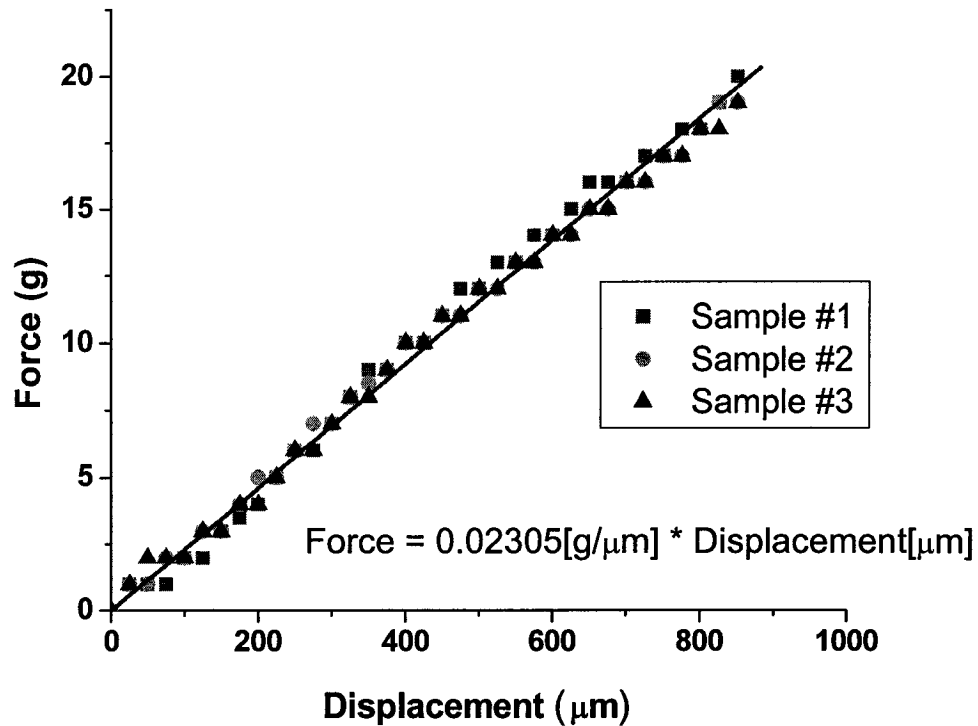


Figure 3.7 The relationship of applied force and film displacement

The optical characterization of microfluidic lens with variable focal length is studied further in Chapter 6. The back focal length is characterized by measuring the changes in the lens's contact angle. A study of the relationship between pump-in volume, contact angle, and focal length is examined and the results are discussed in Chapter 6. Moreover, a simulation on the deflection of 3D PDMS microlens film is used to compare the experimental results. A complete optical experimental results and simulation analysis are presented in Chapter 6.

CHAPTER 4

DEVELOPMENT OF ELASTIC POLYMER

GRADIENT-INDEX LENS

4.1 Background and Related Research

A gradient refractive-index (GRIN) lens is an optical medium with a parabolic refractive distribution. For a converge GRIN lens, the refractive index is highest on the circular lens' axis and decreases toward the periphery with the square of the radial distance from the optical axis. The refractive index, $n=c/v$, is the ratio of the speed of light in a vacuum (c) to the speed of light in the material medium (v). The refractive index at any distance r from the optical axis is given by

$$n(r) = n_0 \left(1 - A \cdot \frac{r^2}{2} \right) \quad (4.1)$$

where $n(r)$ is the refractive index at any distance r , n_0 is the refractive index of the optical axis, A is the positive gradient constant, and r is the radial distance from the optical axis. GRIN elements with imaging and light-focusing properties have been used widely in image-transmission system and optical communication systems such as copy machines, facsimile lens arrays and optical circuit networks. In the current commercial GRIN market, the manufacturing techniques provide only lenses with a fixed focal length because the lens structure is rigid. A tunable focal length of GRIN lens may enhance the

ability of image capture and quality by changing the focal length to detect the images with various distances.

The objective of this chapter is to fabricate a polymer GRIN lens and integrate it with a proper actuation to change the shape of GRIN lens and to control the focal length. In this project, GRIN lenses with high focal length tuning ability are for the first time, to be designed to eliminate the need for 3D lens fabrication and provide higher optical performance. This design can be widely used in many optical systems, and has very high market potential.

To design a tunable focal length lens, there are three requirements for the material design of a gradient index lens. First, the ability to dynamically tune the microlens with an integrated actuator is the most important goal in the overall project. The lens must be deformable under an external force. The lens is elastic with high elongation when a force is applied. Second, the GRIN lens is integrated in an electro-active polymer (EAP) driving mechanism, so the lens must be a dielectric material. The mechanical driving force of the dielectric elastomer derives from Coulomb charge attraction. Both electrical and mechanical phenomenon of electro-active polymer (EAP) actuation mechanism will be described in Chapter 5. Finally, a proper material design is needed to develop a gradient refractive distribution inside the lens structure. Glasses and polymer are the two well-known materials applied in the GRIN lens field [29]. The former have excellent transparency and low optical attenuation, but brittleness and a high process cost are their disadvantages. Therefore, glasses cannot be deformed under an applied force and provide only one fixed focal length. The latter have higher optical loss but excellent mechanical properties, light weight, good flexibility, easy processing and low cost. To fulfill the

above three requirements, glasses materials are eliminated, and polymers are the only possible materials in this application.

Before selecting a proper polymeric material for GRIN lens structure, it is necessary to understand all the recent GRIN lens development in current academic research and industrial technology. The development of GRIN polymers has grown rapidly in recent years. Indeed, several methods have been used to prepare GRIN polymeric optical lens: two-step copolymerization [30,31], the extrusion method [32], interfacial-gel copolymerization [33], and photopolymerization [34]. In the two-step copolymerization method, a lower-refractive-index monomer diffuses into a crosslinking matrix to form a GRIN distribution, but this method is restricted by the lens geometry. In the extrusion method, the GRIN profile is formed mainly by the diffusion or volatilization of a monomer; however, the long processing time required strictly limits the diameter of the GRIN lens. In the case of the interfacial-gel copolymerization method, polymerization in the interfacial-gel phase is faster than in the monomer mixture solution, and a GRIN polymer is gradually formed from the periphery toward the center of the lens owing to the difference between the monomer reactivity and the molecular size of the monomer pairs. However, this method also generates many voids and bubbles as a result of the gel effect of polymerization. To avoid the drawbacks of these methods, a new method for preparing a GRIN lens is proposed in this chapter. This novel method is very similar to two-step copolymerization. It uses the advantages of two-step copolymerization, but it creates a larger lens size by modifying the molecular sizes of monomers for a higher diffusion rate.

To investigate this new technique on fabricating GRIN lens, it becomes essential to consider the synthesis mechanism of polymers for designing polymeric GRIN lenses. Silicones, such as polydimethylsiloxane (PDMS), are considered in this study and seem to be a good candidate for application in both GRIN lens and EAP actuator. Silicones have thousands of different compositions and the most important thing is that it is a dielectric material. This aspect makes PDMS very attractive for fabricating an adjusting focal GRIN lens with EAP technology. The scope of this chapter is to explore the optical principle of GRIN lens, the basic material design of silicones by two-step copolymerization method, and its polymeric structure.

4.2 Optical Properties for Thin Gradient-Index Lens

The first step in the design of a GRIN lens is to determine the index of refraction necessary for a radial-gradient lens to produce an extended focus, with an infinite object distance. The design constrained the line focus to be offset from the back surface. The index profile is derived with geometrical optics. As seen in Figure 4.1, the GRIN lens has a radial gradient-index distribution with planar surfaces, whose back focal length is proportional to incident ray height away from the optical axis [35].

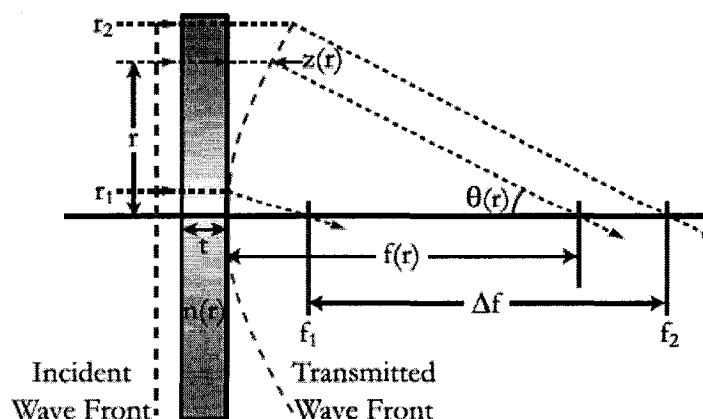


Figure 4.1 Illustration of optical parameters for radial gradient-index lens

Higher incident ray indicates a larger value of r . From the optical geometry in Figure 4.1, it is easy to find out that the back focal length increases when r increases. D. J. Fischer et al reported an investigation of a Gradient-Index Axicon [35]. This investigation indicated the incident light is assumed to be collimated and collinear with the optical axis. For this design, a simple focal behavior is desired, and the back focal length is chosen to be

$$f(r) = f_1 + \frac{r - r_1}{r_2 - r_1} \Delta f \quad (4.2)$$

where r is the radial ray position at the front surface ≥ 0 and is always positive ($r \geq 0$), r_1 and r_2 is the minimum and the maximum incident ray height allowed, f_1, f_2 is the back focal length for a ray entering at the ray height r_1, r_2 , Δf is $f_2 - f_1$ and is equal to the focal region length, and $n(r)$ is the refractive index, as a function of radius.

Assuming a thin sample, equivalently a weak gradient, the index variation experienced by any ray is small, and there is negligible beam displacement in the material. The radial ray position at the emerging wave front is then considered equal to the input position. The wave front displacement $z(r)$ from the back surface describes the emergent wave front. The slope of the wave-front normal is then given by $-dz/dr$. Because the geometrical ray angle is equal to slope of the wave front normal, the wave front is described by the ray angle $\theta(r)$ by

$$\tan(\theta) = -\frac{dz}{dr} \approx -\frac{r}{f(r)} \quad (4.3)$$

Where $z(r) \ll f(r)$, and the wave front offset from the back surface is assumed to be much smaller than the back focal distance. With the focal-length expression and the

identity

$$\int \frac{x}{a+bx} dx = \frac{x}{b} - \frac{a}{b^2} \ln(a+bx) \quad (4.4)$$

The wave front is determined to be

$$z(r) = \frac{r_2 - r_1}{\Delta f} r - \left(f_1 - \frac{r_1}{r_2 - r_1} \Delta f \right) \left(\frac{r_2 - r_1}{\Delta f} \right)^2 \ln \left[f_1 + \frac{\Delta f}{r_2 - r_1} (r - r_1) \right] \Bigg|_{r_1}^r \quad (4.5)$$

The weak gradient assumption allows the determination of the index of refraction by the optical path argument:

$$\begin{aligned} n(0)t &= n(r)t + z(r) \\ n(r) &= n(0) - \frac{z(r)}{t} \end{aligned} \quad (4.6)$$

where $n(0)$, the index of refraction at the center of lens.

With Eq(4.5) for $z(r)$ and simplifying, the index profile for this GRIN lens is

$$n(r) = n_0 - \frac{r_2 - r_1}{t(\Delta f)^2} \left\{ (r - r_1) \Delta f - [(r_2 - r_1) f_1 - r_1 \Delta f] \ln \left[1 + \frac{r - r_1}{r_2 - r_1} \frac{\Delta f}{f_1} \right] \right\} \quad (4.7)$$

where n_0 is equal to $n(0)$. Assuming no central obscuration, $r_1=0$, the index expression reduces to the form

$$n(r) = n_0 - \frac{r_2}{t(\Delta f)^2} \left\{ r \Delta f - r_2 f_1 \ln \left[1 + \frac{r}{r_2} \frac{\Delta f}{f_1} \right] \right\} \quad (4.8)$$

One can confirm this index equation by inspecting two limiting case: $\Delta f \rightarrow 0$, and $f_1 \rightarrow 0$ where $r_1=0$. In the first case, by using L'Hospital's Rule, the design is reduced to that of a unifocal lens. As expected, the index equation reduces to the quadratic radial-gradient form for a lens with back focal length f_1 ,

$$\lim_{\Delta f \rightarrow 0} n(r) = n_0 - \frac{r^2}{2tf_1} \quad (4.9)$$

In the second case, again found by use of L'Hospital's Rule, the focus begins at the back surface. The index equation reduces to a linear form, as expected,

$$\lim_{f_1 \rightarrow 0} n(r, r_1 = 0) = n_0 - \frac{r_2}{t\Delta f} r \quad (4.10)$$

Insight into the role of the GRIN profile is gained by writing equation (4.8) in a series expansion,

$$n(r) = n_0 - \frac{1}{2tf_1} r^2 + \frac{\Delta f}{3r_2 tf_1^2} r^3 - \frac{(\Delta f)^2}{4r_2^2 tf_1^3} r^4 + \dots \quad (4.11)$$

The first term is the index of refraction at the center of the GRIN lens. The second term describes the paraxial base power of the lens. This focusing power provides the offset of the focal region from the back surface. The remaining terms are factors of Δf and are sources of aberration. Similar to theory of using an aberrated-lens system, this aberration can be viewed as providing the linear focal shift.

4.3 Material Design Principle

While the GRIN plastics and their fabrication methods have been studied, no investigations of manufacturing a flexible GRIN lens have been done. Most GRIN plastic provides only a rigid plastic lens structure and a unifocal length. Rigid lens structures cannot provide the change of the focal length. Therefore, it is necessary to create a new material design which can produce a flexible and dielectric polymeric lens. Silicone-based materials have been attractive candidates for making elastic GRIN lenses with a good dielectric property. Therefore, the research focuses on the development of the

silicone-base polymeric GRIN lens. Silicone-base polymers provide many special characteristics which can meet both optical and mechanical requirements.

Primarily, the silicone-based lens is elastic and deformable under stresses. Moreover, silicone-base polymer, such as polydimethyl-siloxane (PDMS), is a dielectric material which can be integrated with the actuation system. Finally, silicone-base polymers with different curing system have been studied. Two-step curing can induce a gradient refractive index distribution. The most well known methods for silicone curing mechanisms are addition cure (Platinum cure), peroxide-activated cure, and UV cure. In the later sections of this chapter, a novel two-step polymerization has been designed for fabricating GRIN lenses. This new method uses two different silicone materials with different curing systems: addition cure and UV cure.

A flexible GRIN silicone lens comprises with a cross-linked silicone polymer matrix, a homogeneously embedded photosensitive macromer, and a photoinitiator, shown in Figure 4.2 [19]. Herein, the polymer matrix forms the basic optical element framework and is generally responsible for many of its material, mechanical, and optical properties. The macromer is a low-molecular-weight polymer linked to a photo sensitive group. The photo-initiator is an organic molecule that undergoes dissociation into reactive radicals that begin the polymerization process on exposure to a specific wavelength of light.

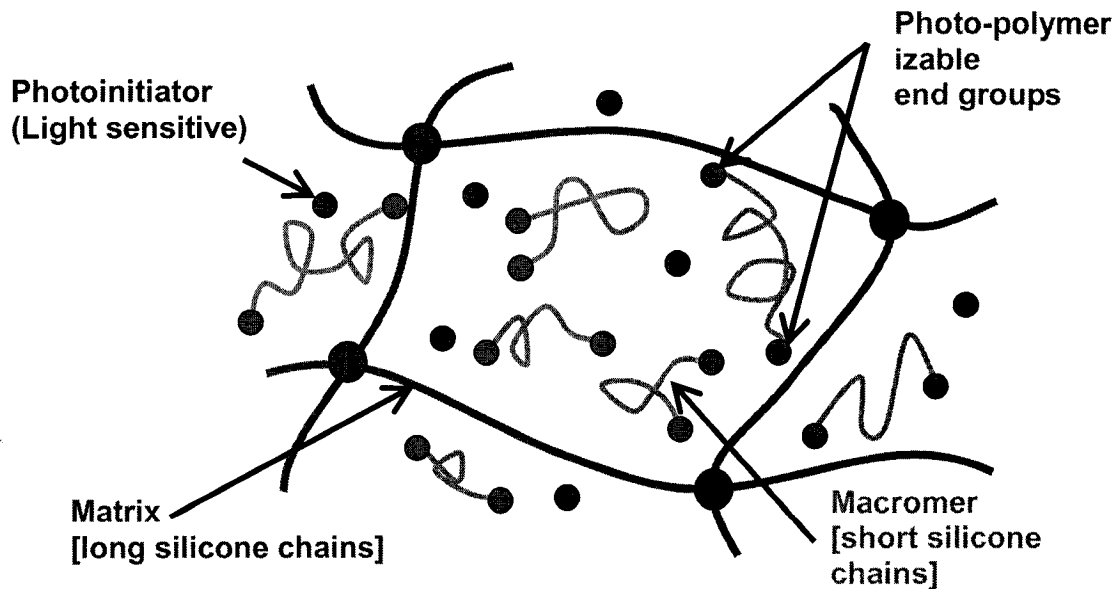


Figure 4.2 Material design for GRIN lens

After the polymer matrix is formed, the refractive power of the lens may be selectively adjusted by exposing the lens to an ultraviolet (UV) light. On UV irradiation, polymerization of the photosensitive polymer occurs. The application of ultraviolet light to a portion of the lens optic results in disassociation of the photoinitiator to form reactive radicals that initiate polymerization of the photosensitive macromers within the irradiated region of the silicone matrix. Polymerization itself does not result in changes in lens power; it does, however, create a concentration gradient within the lens resulting in the migration of non-irradiated macromers into the region now devoid of macromer as a result of polymerization. The resulting chemical potential causes migration of unpolymerized macromers and photo initiators down a diffusion gradient into the irradiated area of the lens to form a gradient-index distribution. Once the desired power change is achieved, irradiation of the entire lens to polymerize all remaining macromer "locks in" the adjustment so that no further power changes can occur.

4.3.1 Diffusion Mechanism

The polymeric GRIN lens comprises a photosensitive macromer dispersed in a polymer matrix. The polymer matrix forms the optical element framework. The photosensitive macromer may be a single compound or a combination of compounds that is capable of photo-polymerization. As a general rule, the polymer matrix and the photosensitive macromer are selected such that the components that comprise the photosensitive macromer are capable of diffusion within the polymer matrix. Thus, a loose polymer matrix will tend to be paired with larger photosensitive macromer components, and a tight polymer matrix will tend to be paired with smaller macromer components. Figure 4.2 shows the illustration of matrix and photosensitive macromer, as a two-step polymerization system. The GRIN copolymer is examined for the fabrication of a 2mm in diameter GRIN lens.

Upon exposure to an appropriate UV light, photosensitive macromer typically forms a second polymer matrix in the exposed region of the optical element. The presence of the second polymer matrix changes the material characteristics of this portion of the optical element to modulate its refraction capabilities. In general, the formation of the second polymer matrix changes the refractive index of the affected portion of the optical element. After exposure, the photosensitive macromer in the unexposed region will migrate into the exposed region over time. The amount of photosensitive macromer migration into the exposed region is time dependent and may be precisely controlled by diffusion time. If enough diffusion time is permitted, the photosensitive macromer components will re-equilibrate and redistribute the refractive index profile throughout optical element of the first polymer matrix, including the exposed region. When the

region is re-exposed to the energy source, the photosensitive macromer that has since migrated into the region, which may be less than if the photosensitive macromer is allowed to re-equilibrate, polymerizes to further increase the formation of the second polymer matrix. After the diffusion step is finished, the entire optical element is exposed to the UV-light to "lock in" the desired lens property by polymerizing the remaining photosensitive macromer components that are outside the exposed region before the components can migrate into the exposed region. Because freely diffusible photosensitive macromer components are no longer available, subsequent exposure of the optical element to UV light cannot further change its power. Figure 4.3 shows the sequence of macromer diffusion steps.

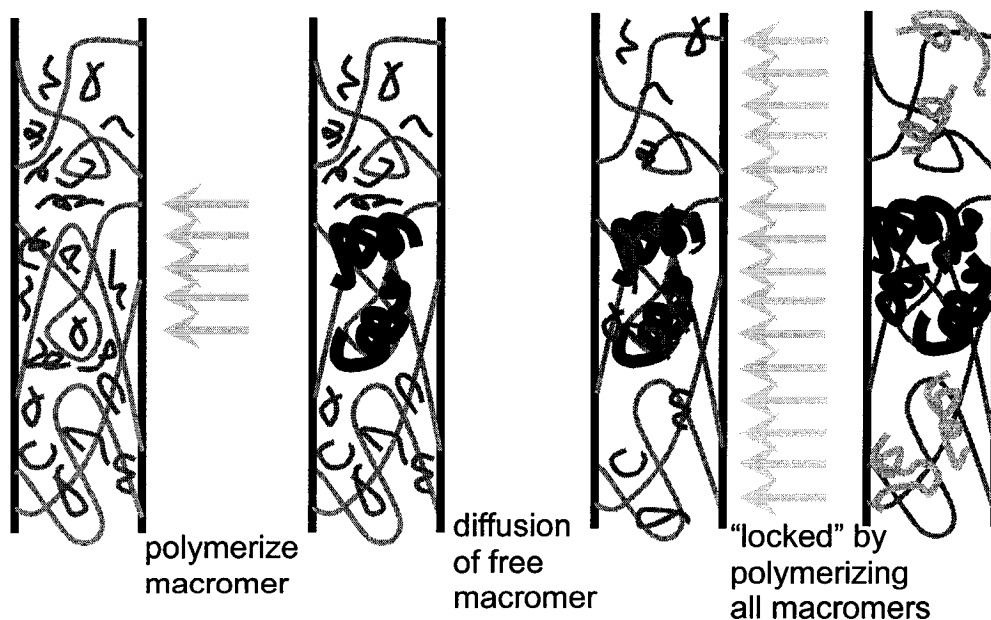


Figure 4.3 Schematic illustrating the proposed mechanism of diffusion.

4.3.2 Polymer Chemistry

Both matrix and macromer are macromolecules, long molecule chains made of a number of smaller molecules, monomers, bonded covalently. Therefore, it is necessary to apply the most fundamental concept of polymer chemistry. A polymer is often the name given a group of very long polymer chains. These two basic polymers types are homopolymers and copolymers. Homopolymers contain only one type of monomer unit, while copolymers are composed of two or more monomer units.

Polymers are also commonly classified according to their structure, elasticity, response to heating, and chemical components. The structures (see Figure 4.4) are linear, branched, and networked. These classifications describe the amount of branching and interconnections of the polymer chains.

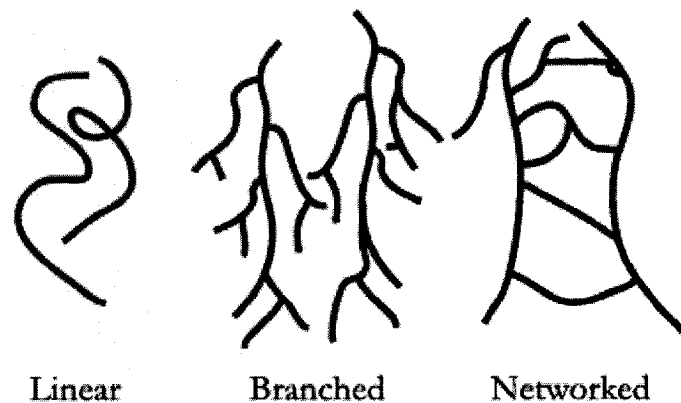


Figure 4.4 Polymer structures.

The elasticity categories are elastomers, plastics, and fibers. Elastomers can be greatly stretched and then returned to their original dimensions. In contrast, fibers are the least elastic; plastics are somewhere in between. The polymer used for GRIN lens which is integrated with electro-active polymer actuator must be an elastomer, so that the lens can be deformed by a force applied in order to change the focal length.

The heat-response categories are thermoplastics and thermosets. Thermoplastic polymers soften when heated without their chemical structure being altered. The polymer chains first soften allowing the separate polymer chains to slide past each other. Then the Van Der Waals bonding is broken and chains separate completely, allowing the material to flow. Thermosets are rigid polymers due to a high-degree of crosslinking, creating a dense molecular network. Heat does not cause these polymers to change shape until the stress is so great that the covalent bonds of the polymer chains degrade, and the polymer is caused to decompose.

Polymers can be synthesized several ways. Step-growth polymerization, or condensation polymerization, is a reaction between an organic base and an organic acid which produces a polymer and a smaller molecule, such as water, that is condensed out. Addition polymerization is the addition of single monomer molecules to a growing chain. This process has the three steps of initiation, propagation, and termination.

Initiation for a typical monomer occurs when one of its carbon-carbon double bond ($C=C$) is broken. This effect creates an active site with a strong affinity to react with other monomer molecules. The two types of active sites are ionic and free-radical. A free-radical site can be activated by ultra-violet light exposure or by heat application. The creation and polymerization by free-radical sites can be promoted using an initiator, such as benzoyl peroxide (BPO). Initiation begins when the molecule breaks due to heat, providing two phenyl rings with open bonding sites. These rings bond to a monomer, breaking the $C=C$ bond and creating a free-radical site.

The initiated monomer then leads to propagation, as it has an activated site and can bond to another monomer. This ability creates a subsequent bonding site, propagating the

polymerization. If the monomer only has a single double bond, the polymer chain will be linear. If there is more than one double bond, then the structure could be branched or networked.

Termination of the polymer chain can occur in one of the three ways. The active site can react with the initiator or with some other impurity that bonds and has no more open sites for continued bonding. Two active sites (perhaps of two different chains) can bond together, or two active sites can come into contact with one giving up an atom (usually hydrogen) to the other, terminating both chains without combining.

4.4 Material Preparation

4.4.1 Possible Silicone Combinations

At any point in the development of polymer science, the technical appreciation and understanding of the silicone chemistry is essential and important. There are thousands of silicones in the current commercial markets, and there are many curing mechanisms for silicone polymerization, such as air/moisture, thermal, UV light and platinum catalyst. The design goal of this project is to find two different curing polymerization methods to polymerize both the polymer matrix and macromer. The materials contain two polymer components. Initially, a polymer matrix is formed by addition cure (platinum cure) method. This silicone is a matrix material with a network structure. Macromer is the second silicone component and is polymerized by UV light. Polymerized macromer has a branched or cross-linked structure that extends homogeneously throughout the matrix.

There are many possible combinations of using any two silicones with different curing polymerization mechanisms. In this research, silicones for matrix and macromer

are prepared and tested. The material information for matrix and photo sensitive macromers is shown in Table 4.1.

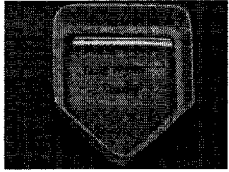



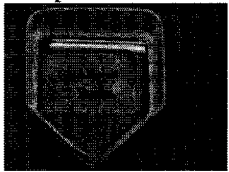

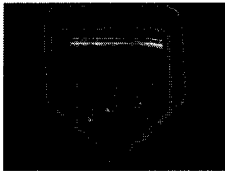
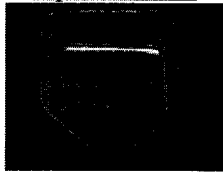
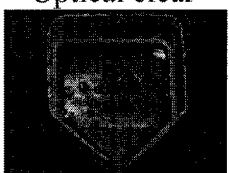






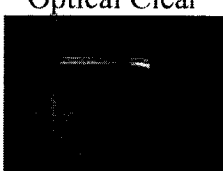







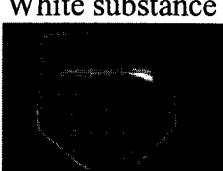
Table 4.1 Basic material information for matrix and macromers

Function	Material Name	Viscosity cSt	Molecular Weight g/mol	Refractive Index n_D^{20}
Matrix	MED-6233	50,000	36,000	1.410
	PDV-0325	500	15,500	1.420
	SYLGARD 184	3900	$\geq 5,500$	1.430
	PDV-0525	500	14,000	1.430
	PDV-1625	500	9,500	1.465
	PMV-9925	300~600	2000~3000	1.533
Macromer	DBE-R12	80~120	1500~1600	1.450
	DMS-U22	180~250	1000~1200	1.436
	SIB 1400.0	14~18	683	1.432
	SIB 1402.0	1~2	386	1.449

Table 4.2 shows the change on the physical appearance of mixture after matrix and macromer are blended. There are some interesting phenomena when two different silicones are blended together. Due to the difference of refractive index and some chemical structure, some mixtures become white opaque gels. According to polymer chemistry, two different silicone polymers with a significant difference in refractive index and incompatible chemical composition may cause the white appearance after blending. A mixture of two different materials with incompatible chemical composition may generate many small phase separations which are uniformly distributed within the mixture solution. The light cannot go through the mixture directly and be bended randomly. This characteristic is the reason for the white color and opacity appearing in some mixtures. The mixture of matrix and macromer cannot phase separate, so light transmission by the optical element should be unaffected. Mixing oil and water is a notable example. Both oil and water before mixing are transparent. When they are mixed together and stirred in a certain speed, their mixture becomes opaque with very poor

transparency. The phase separation is generated while mixing two incompatible materials and causes the mixture becoming opaque.

Table 4.2 Physical appearance after mixing macromer and matrix

		Photo-Sensitive Macromers			
		SIB 1400.0 RI: 1.432	DMS-U22 RI: 1.436	DBE-R12 RI: 1.450	SIB 1402.0 RI: 1.450
Matrix Materials	MED-6233 RI: 1.41	White 	Slight white 	White substance 	White substance 
	PDV-0325 RI: 1.42	Optical clear 	Optical clear 	White substance 	Optical clear 
	SYLGARD 184 RI: 1.430	Optical clear 	Slight white 	White substance 	White substance 
	PDV-0525 RI: 1.430	Optical Clear 	Optical Clear 	Slight White 	Optical Clear 
	PDV-1625 RI: 1.465	Optical Clear 	Slight White 	White substance 	White 
	PMV-9925 RI: 1.533	White substance 	White substance 	White substance 	White substance 

It is necessary to find which silicones are incompatible and which are compatible before making GRIN lenses. Several observations in this experiment have indicated the results on the compatibility of two mixed silicones. This data is very important for selecting proper silicones for matrix and macromer. The composition of the mixture which contains matrix and macromer is 7 parts of matrix and 3 parts of macromer. All mixtures are blended well to ensure two silicones are mixed completely. All samples are placed in a dark room for 24 hours. In Table 4.2, the observed results have been summarized.

At the preliminary design stage for a diverging GRIN lens, Gelest Inc's PDV-0325 and SIB 1402.0 are chosen as matrix and macromer, respectively. The difference in the refractive index is about 0.03. In the following sections, the details on material information and the reason for choosing them as lens materials are discussed.

There are two different combinations for diverge and converge GRIN lenses. By selecting the proper silicones for matrix and macromer, diverging and converging GRIN lens can be fabricated. If the matrix has a lower refractive index than macromer, the higher refractive index macromer can diffuse into the lens from periphery toward the lens center. The refractive distribution is a parabolic profile in which the refractive index is highest on the lens periphery and decreases toward the center with the square of the radial distance from the optical axis. This refractive distribution induces a diverging GRIN lens. On the other hand, if the macromer's refractive index is lower than the matrix's, the refractive distribution can be changed to the higher refractive index on the lens axis, and it decreases toward the periphery. Thus, this kind of lens is a converging GRIN lens.

For material design for diverging lens, the matrix is Gelest PDV-0325 Silicone Elastomer, a pourable, optically clear silicone. The diffusant is 1,3-BIS(3-Methacryloxypropyl) Tetramethyldisloxane Gelest SiB1402.0. Their refractive indices are given in Table 4.3.

Table 4.3 Molecular weight and refractive index of matrix and macromer

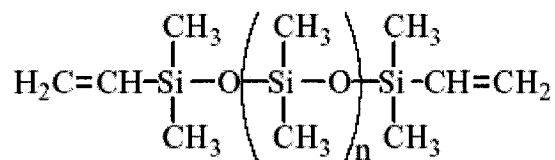
GRIN Type	Diverging Lens		Converging Lens	
Silicone Function	Matrix	Macromer	Matrix	Macromer
Silicone Name	PDV-0325	SIB 1402.0	PDV-1625	SIB 1400.0
Molecular Weight (g/mol)	15,500	386.64	9,500	683
Refractive Index (n)	1.420	1.450	1.465	1.432
Δn	0.030		0.033	

Large differences in molecular weight between matrix and macromer afford large diffusion depths, with a refractive index change (Δn) of near 0.03. For converging lens, the materials for matrix and macromer are PDV-1625 and SIB 1400.0, respectively. PDV-1625 also provides a large molecular weight. The refractive index change is about 0.033.

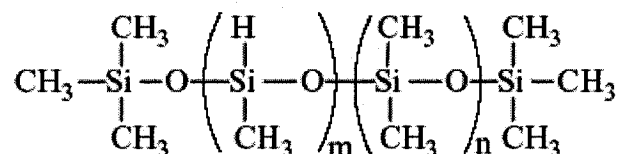
4.4.2 Polymer Matrix

In this research, a vinyl-terminated diphenylsiloxane-dimethylsiloxane (PDV-0325 and PDV-1625 from Gelest Inc.) is used as the matrix. In general, the polymer matrix comprises at least one monomer that upon polymerization will form the polymer matrix. The curing system for the polymer matrix is designed to use addition cure system (platinum Pt cure). The advantage of using addition cure chemistry is that it can provide an extremely flexible basis for formulating silicone elastomers. An important feature of the cure system is that no byproducts are formed, allowing fabrication of parts with good dimensional stability.

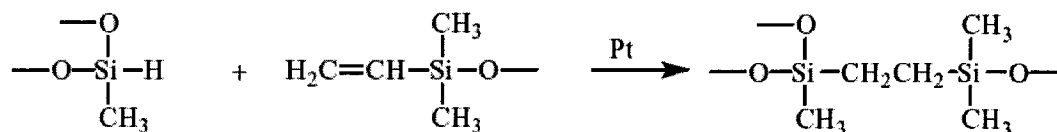
Both PDV-0325 and PDV-1625 are copolymer silicone which has a long molecular string. Its molecular structure is



The long molecular string is terminated by Vinyl group (CH_2) on both ends. By using CH_2 to terminate the string, it can control the molecular weight between two ends of Vinyl group (CH_2). In the molecular structure, larger value of n indicates a longer string and higher molecular weight. According to Gelest, the molecular weight can range from 9,500 up to 78,000 g/mole. In order to achieve the crosslinking it is necessary to add a crosslinker HMS-301 (or some hydride fluid) in the mixture. Without it, the vinyl terminated silicones will not have anything to react with the Pt catalyzed reaction. The molecular structure for the crosslinker HMS-301 is:



Vinyl terminated polymers are employed in addition cure systems. The bond forming chemistry is the platinum catalyzed hydrosilylation reaction which proceeds according to the following equation:



Both optical and mechanical properties for the polymer matrix are very important. The refractive indexes of the matrix are 1.42 for PDV-0325 and 1.465 for PDV-1625. The cured silicone matrix is an optically clear elastomer. According to Gelest Inc.'s product catalog, the tensile strength is 500 psi with a large elongation of 400~450%. Both tensile strength and elongation are two critical factors to influence the deformability of "Electro-Active Polymer" (EAP) actuation system. Moreover, the molecular weight of the matrix is 15,500 g/mol which must be larger than macromer (~386 g/mol). The ratio of molecular weight of matrix and macromer is about 40. The larger molecular weight ensures that macromer can freely move within the matrix structure.

4.4.3 Photo-Sensitive Macromer

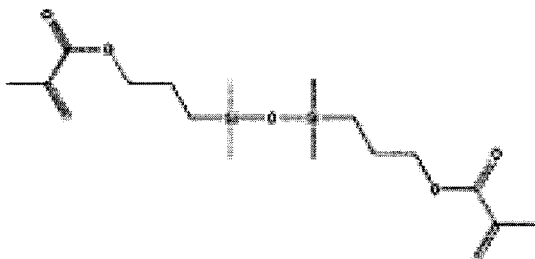
The polymer matrix is polymerized and cross-linked in the presence of the macromer. Under this scenario, the macromer must be compatible and not appreciably interfere with the formation of the polymer matrix. Similarly, the formation of the second polymer matrix should also be compatible with the existing first polymer matrix. The first polymer matrix and the second polymer matrix should not phase separate and light transmission by the optical element should be unaffected.

As described previously, the macromer may be a single component or multiple components so long as:

1. It is compatible with the formation of the first polymer matrix;
2. It remains capable of photo-polymerization after the formation of the first polymer matrix; and
3. It is freely diffusible within the first polymer matrix.

In preferred embodiments, the photo-induced polymerization is designed. In general, the same type of monomers that is used to form the first polymer matrix may be used as a component of the macromer. However, because of the requirement that the macromer must be diffusible within the first polymer matrix, the macromer generally tends to be smaller (i.e., have lower molecular weights) than the monomers which form the first polymer matrix. The macromer must be blended with other components such as initiators and crosslinkers that facilitate the formation of the second polymer matrix.

To fulfill all three requirements, UV curable silicones are studied in this case. There are many types of UV curable silicones, all providing high transparency and refractive index control. They can be classified into two categories: Methacrylate and Acrylate Functional Siloxanes. Methacrylate and Acrylate functional siloxanes undergo the same reactions generally associated with methacrylates and acrylates, the most conspicuous being radical induced polymerization, such as UV light. In this research, 1,3-BIS(3-Methacryloxypropyl) Tetramethyldisloxane (Gelest SIB 1400.0 and SIB1402.0) is used as the diffusible macromer. Its refractive indexes are 1.432 and 1.4488, respectively and molecular weights are 683 and 386.64 g/mol, respectively. The low molecular weight makes SIB 1400.0 and SIB 1402.0 very attractive as the diffusible macromer. Its chemical structure is:



The viscosity of this UV curable macromer is about 1~18 cSt, which is contingent on the molecular weight. Due to low viscosity, this UV curable macromer exhibits properties of liquid form.

4.5 Fabrication Procedures

4.5.1 Silicone Compositions

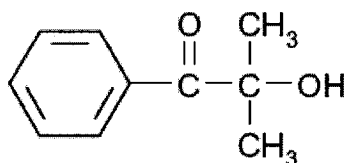
Materials comprising various amount of (a) poly-dimethylsiloxane (PDMS) (Vinyl-addition silicone) as matrix, (b) Methacryloxypropyl Terminated PolyDimethylsiloxanes as photo-sensitive macromer, (c) a UV photoinitiator, 2-Hydroxy-2-methyl-1-phenyl-1-propanone (Ciba Darocur 1173), (d) a crosslinker (Gelest HMS-301), and (e) a Pt initiator for Vinyl-addition silicone cure (SIP6830.3), are made and tested. The first four components (a, b, c & d) are blended together initially. PDMS with the crosslinker HMS-301 is polymerized by addition of platinum catalyst as an initiator. PDMS formed is the polymeric matrix, and macromer and Darocur 1173 together are as photo-sensitive macromer composition. Table 4.4 shows that samples' preparation and testing.

Table 4.4 Material composition for making GRIN lenses

Test No.	Diverging GRIN Lens		Converging GRIN Lens		Crosslinker	Photoinitiator	Initiator	Results
	Matrix	Macromer	Matrix	Macromer				
	PDV-0325 (wt %) RI:1.420	SIB 1402.0 (wt %) RI:1.450	PDV-1625 (wt %) RI:1.465	SIB 1400.0 (wt %) RI:1.432	HMS-301 (wt %) <i>Respect to Matrix</i>	Darocur 1173 (wt %) <i>Respect to Macromer</i>	Platinum Catalyst (wt %) <i>Respect to macromer</i>	
1	90	10	-	-	10	1.5	0.15	No Diffusion
2	80	20	-	-	10	1.5	0.15	No Diffusion
3	70	30	-	-	10	1.5	0.15	Good Diffusion
4	60	40	-	-	10	1.5	0.15	Good Diffusion
5	-	-	90	10	10	1.5	0.15	No Diffusion
6	-	-	80	20	10	1.5	0.15	Little Diffusion
7	-	-	70	30	10	1.5	0.15	Good Diffusion
8	-	-	60	40	10	1.5	0.15	Good Diffusion

Appropriate amounts of matrix, macromer, Darocur 1173, and HMS-301 are weighed together in a plastic pan, then manually stirred at room temperature until all materials are well-mixed. These initial mixtures are stirred mechanically for 20 minutes before a platinum catalyst is added. Then 0.15% of platinum catalyst with respect to matrix is added into this mixture, and stirred manually. During stirring the mixture, many bubbles are generated due to the platinum catalyzed reaction. The mixture is not disturbed and allowed to rest at room temperature for 5 minutes. All bubbles move toward the surface of the mixture surface, and disappear when they reach the surface. Due to the fast curing rate of this polymerization process, the reaction is about 10 minutes after a platinum catalyst is added into the mixture. The material handling is very critical after platinum catalyst has been added. The resulting silicone composition is poured into a mold which is made by transparent poly(methyl methacrylate) (PMMA). The mold is a small flat sample holder. The mold is a square container with 4 side walls. The base area is $105 \times 105 \text{ mm}^2$ and the depth is 1.4 mm.

The amount of photo initiator (1.5 wt. %) is based on the data provided from the company (Ciba Specialty Corporation). Darocur 1173 is a versatile highly efficient liquid photoinitiator, used to initiate the photopolymerisation of chemically prepolymers. Darocur 1173 is 2-Hydroxy-2-methyl-1-phenyl-propan-1-one. Its chemical structure is with a molecular weight of 164.2 g/mol:



According to the data analysis of absorption spectrum from Ciba in Figure 4.5, 1.5 wt. % of Darocur 1173 is suggested to add to the samples to initiate the polymerization chain reaction for a better polymer.

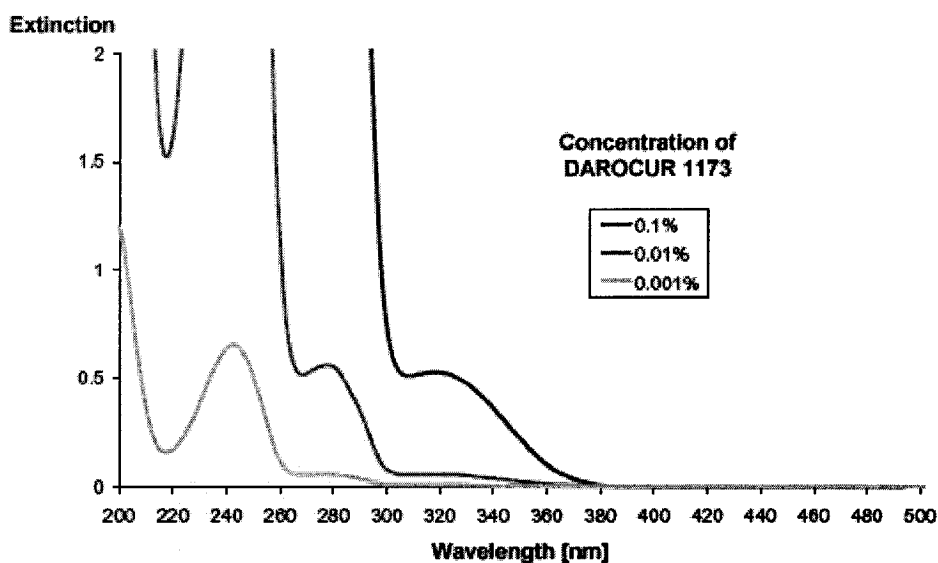


Figure 4.5 Absorption spectrum for various concentration of Darocur 1173

The cure time for the first matrix to be formed takes about 30 minutes after platinum (Pt) catalyst is added. The matrix with unpolymerized macromer composition in the mold is moisture cured and stored in the dark at room temperature for a period of 30 minutes to ensure that the resulting first matrix is non-sticky, clear, and transparent.

4.5.2 Lithography Exposure Steps

The exposure procedures are similar to the conventional lithography. A mask is prepared and made the same size as the mold with several through holes. The diameter of the holes is 2.00 mm. Figure 4.6 shows the photograph of the mask. The mask is placed on top of the sample with a gap about 100~200 μ m. The sample with a mask on top of it is exposed to UV radiation under atmosphere in a clean room, using Electronic Vision Mask

Aligner's UV lamps exhibiting a wavelength $\lambda=365\text{nm}$ and an intensity $I_0=7\text{ mW/mm}^2$ for 120 seconds.

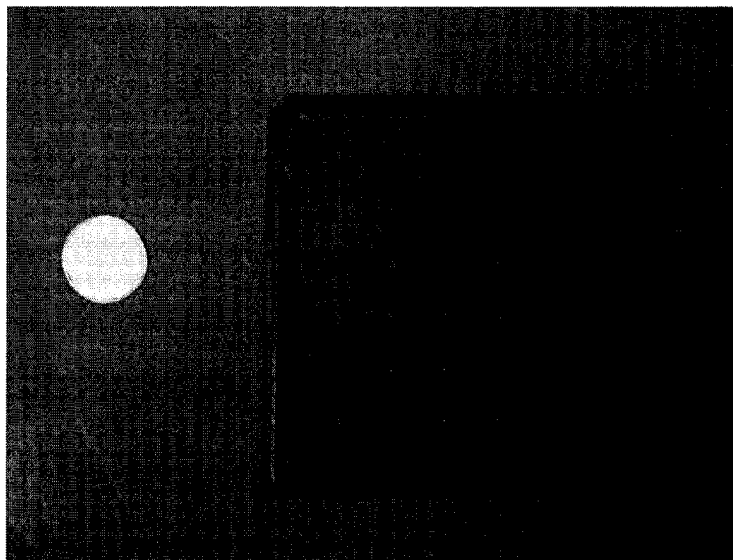


Figure 4.6 Photography of mask

The irradiated sample is then placed in the dark room for 24 hours to permit polymerization and macromer diffusion. After the diffusion step, the sample is photo-polymerized to lock all non-polymerized macromer in position by continuously exposing the entire for 5 minutes. The exposure time is set to 5 intervals. Each exposure interval is fixed to 60 seconds. Each interval has 60 seconds breaking time, so the total exposure process takes 10 minutes.

After complete polymerization, a good symmetric and bubble-free GRIN lens was fabricated. Experiments have been performed to show the images with no distortion. These images can be observed through the GRIN lenses prepared by 2-Step copolymerization. In Chapter 6, a complete experimental result of GRIN lenses on the optical properties is described. The optical results for both converging and diverging GRIN lens are shown, and the imaging measurement setup is established and the detail of instrument setup is discussed.

CHAPTER 5

SMART MATERIALS: ELECTRO-ACTIVE

POLYMER (EAP)

5.1 Introduction to EAP

With the drive towards smaller and more efficient mechanical systems, there is a growing demand for powerful and lightweight actuators. Smart materials are being investigated as a technology to fulfill this need. Smart materials can alter their physical properties in response to an external influence, such as temperature, pH levels, current or magnetic fields. As a result of this characteristic, powerful smart material actuators are being considered as an alternative actuator in an increasing number of applications. However, these smart materials behave in a highly non-linear fashion, and there exists hysteresis in the actuator response, both responses which make achieving an effective control algorithm difficult [36]. Some examples of smart materials are Shape Memory Alloys (SMA), piezoelectric ceramics and electro-active polymers (EAPs).

Electro-active polymers offer the promise of performance, physical and operational characteristics that are not found in other transducer technologies. Originally developed as muscle-like actuators for small robots, dielectric elastomers, sometimes called “electroelastomers”, in particular, are a type of electroactive polymer that has

demonstrated large strains, fast response, high efficiency, and other characteristics that suggest that it may have wide industrial and commercial applicability [37].

This chapter focuses specifically on the dielectric elastomer type of EAP. Perhaps as a result of the rapid advancement of polymer materials in the latter part of the 20th century, many of the new actuator materials have been polymers, specifically electroactive polymers. One new polymer actuator approach with good overall performance is dielectric elastomers (DEs), which consist of a polymer material sandwiched between two compliant electrodes. The electrodes can be made of a variety of compliant conductive materials such as colloidal carbon in a polymer binder. When a voltage difference is applied between the electrodes, the electrostatic forces resulting from the free charges squeeze and stretch the polymer. Polymer film compresses in thickness and expands in area when a voltage is applied across the film. Figure 5.1 shows the functionality of EAP actuator before and after a voltage is applied [37]. This well-known phenomenon, Maxwell stress, occurs with all insulators subject to an electric field from deposited electrodes [38]. However, in the past, Maxwell stress has generally been regarded as a “nuisance” effect in polymers—too weak to provide good actuation by itself. With the development of soft polymer thin films with high dielectric breakdown strengths, this view is changing, and several materials with exceptional overall performance have been identified. The actuator performance of dielectric elastomers can be quite high, particularly with respect to strain and energy density.

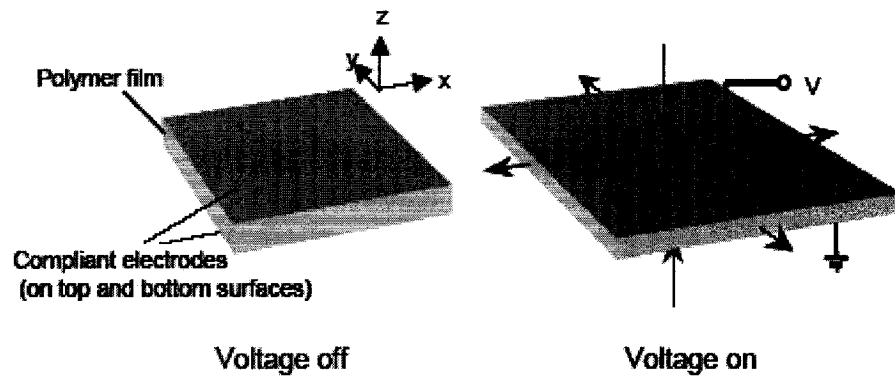


Figure 5.1 Functional element of dielectric elastomers

Successful applications for dielectric elastomer EAPs will be those in which these unique characteristics best satisfy the demand of the particular application. In this research, dielectric elastomer EAPs may simply offer a higher-performance or lower-cost alternative to conventional transducer technologies. Based on the principle of satisfying demand, compressing a polymeric film in thickness and expanding the film in area can be carefully evaluated to integrate with GRIN lens in order to change the lens shape and the optical properties such as focal length. By changing the physical appearance of flexible polymeric GRIN lens in thickness and area, the dimension of GRIN lens is changed and the focal length of GRIN lens can be controlled. The reason for studying EAP actuation as a tunable focal lens mechanism is clear: EAP actuation converts electric energy to mechanical deformation. This effect draws attention to control the focal length of a flexible polymeric lens precisely by adjusting the applied voltage.

In Chapter 3, variable focusing microlens with microfluidic chip was demonstrated. This microfluidic approach requires a high power external pump to control the pressure of a liquid filled lens. There are some drawbacks of using fluidic pressure driven mechanism, such as slow response time, complicated packaging process, and low reliability. Consequently, EAP actuation can achieve much faster response time and

simple assembly than previous variable focal length liquid filled lens with an external pump. Further, its benefits include electrically modulated focal lengths as well as non-optical distortion, as the electrodes are not located within the lens structure. EAP driven actuation is an innovative design, advantageous as a micro optical actuator for its fast response time, easy production, low cost, and accurate control ability on actuation.

In this research, EAP is first to be introduced by integrating with GRIN lens. The unique properties of EAPs can enable the development of fundamentally optical devices, but the promise of such new devices presents challenges associated with the design and practical implementation of EAP-driven devices. This chapter describes the design and fabrication of EAP actuator.

5.2 Actuation Principle

The EAP actuator based on dielectric elastomer technology operates on a simple principle. Basically a capacitor with two compliant electrodes, the Dielectric EAP actuator consists of incompressible yet highly deformable elastomeric material. As for a capacitor, when an electric field is applied to the electrodes, positive charges appear on one electrode, and negative charges on the other. These opposite charges give rise to Coulomb forces between two electrodes, generating a pressure, known as the Maxwell Stress [39]. When a voltage is applied across the compliant electrodes to generate Coulomb forces between the electrodes, the polymer shrinks in thickness and expands in area. In this research, exploiting this principle involves materials design and processing as well as design of actuator geometries for dynamically controlling the focal length of a polymeric GRIN lens.

As described above, dielectric elastomer is composed of small molecular dipoles, and they become polarized when exposed to an electric field. The polarized molecular dipoles can convert electrostatic energy to mechanical energy (strain, stress) through the Maxwell stress. In the following sections, the electronic properties are presented.

5.2.1 Dielectric Properties

In practice, most dielectric materials are solid. Examples include porcelain (ceramic), mica, glass, plastics, and the oxides of various metals. Some liquids and gases can serve as good dielectric materials. Dry air is an excellent dielectric and is used in variable capacitors and some types of transmission lines. Distilled water is a fair dielectric. A vacuum is an exceptionally efficient dielectric. Figure 5.2(a) shows the situation in which a constant voltage is applied to a set of capacitor electrodes. Electric field lines may only begin on free positive charges and end on free negative charges. Thus, surface charge concentration builds up on the capacitor electrodes. The charge build up continues until the voltage drop over the capacitor plates matches that of the voltage source. The relation between the amount of free charge, Q and the voltage drop, V is

$$Q = C \cdot V \quad (5.1)$$

where C is the capacitance of the capacitor,

$$C = \frac{\epsilon_0 \cdot A}{t} \quad (5.2)$$

where A is the area of the electrode plates, and t is the distance between electrodes. ϵ_0 is the vacuum permittivity, $\epsilon_0 = 8.854 \times 10^{-12}$ F/m. The density of the field lines is known as the electric flux density, or flux density. It is given by

$$D = \epsilon_0 E \quad (5.3)$$

where E is the electric field between the capacitor plates.

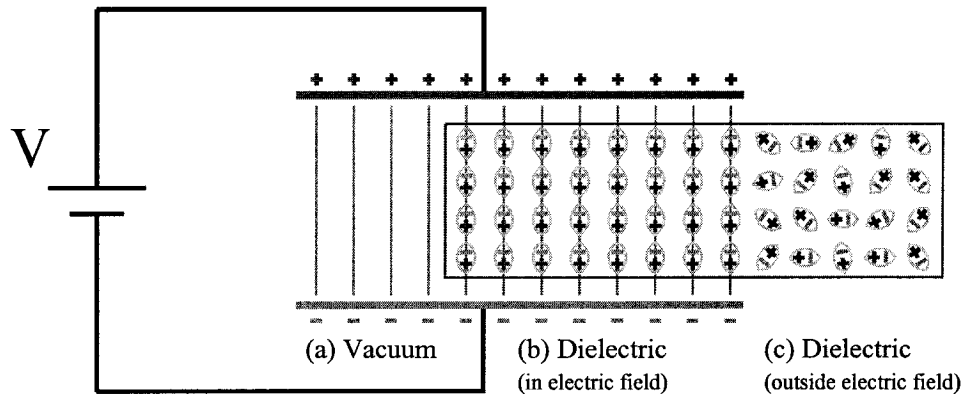


Figure 5.2 Sketch for electric field in (a) vacuum, the dipole orientations for dielectric material (b) between two electrodes, and (c) outside the electrodes

EAP elastomer is also an insulating, non-conductive material. This insulating material composes small dipoles, which are electrically neutral, but positive and negative electric charges are separated when an electric field is applied. Figure 5.2(b) depicts the orientation of the dipoles which are exposed in an electric field. Comparing Figure 5.2(c) with Figure 5.2(b), the dipoles have random orientation without an electric field is applied. When exposed to an external electric field, the tendency of a single dipole is to align itself with the direction of electric field, such that the positive end points toward lower potential, and the negative end points toward the higher potential. When all the dipoles align in this way to an applied electric field, the material is known as a dielectric.

The flux density for dielectric material can be obtained by

$$D = \epsilon E \quad (5.4)$$

where ϵ is the dielectric constant of the material. The relative dielectric ϵ_r constant is defined as the ratio between the flux density in vacuum and in the dielectric:

$$\epsilon_r = \frac{\epsilon}{\epsilon_0} \quad (5.5)$$

Therefore, the flux density and capacitance for dielectric material can be re-written as

$$D = \epsilon_r \epsilon_0 E \quad (5.6)$$

$$C = \frac{\epsilon_r \cdot \epsilon_0 \cdot A}{t} \quad (5.7)$$

5.2.2 Maxwell Stress

Coulomb charge attraction induces mechanical driving force in the EAP actuator. When EAP film, as a capacitor, is charged by an electric field, positive charges reside on one electrode, and equal amount of negative charges accumulate on the other electrode. The compliance of the elastomer allows the charges to move closer by reducing the film thickness and moving two electrodes together. Due to volume conservation, EAP is a significant elastomer that can expand transversely to the electric field. This expansion tends to increase the area of the electrodes. This increasing area lets charges on one electrode move further apart, lowering the internal energy of the charges.

Suppose that the charge $\pm Q$ on each plate is built up gradually by transferring small amounts of charge from one plate to another. If the instantaneous charge on the plates is $\pm q$ and an infinitesimal amount of positive charge dq is transferred from the negatively charged plate to the positively charge plate then the work done is

$$dW = Vdq = q \frac{dq}{C} \quad (5.8)$$

Note that the voltage difference is such that it opposes any increase in the charge on either plate. The total work done in charging the capacitor is

$$W = \frac{1}{C} \int_0^Q q \cdot dq = \frac{Q^2}{2 \cdot C} = \frac{1}{2} \cdot C \cdot V^2 \quad (5.9)$$

W is the energy stored in a capacitor.

The force (F) between the electrodes can be found from

$$F = -\frac{dW}{dt} \quad (5.10)$$

The differential of the energy is

$$dW = d\left(\frac{1}{2} \cdot \frac{\epsilon_r \cdot \epsilon_0 \cdot A}{t} \cdot V^2\right) = \frac{1}{2} \cdot \epsilon_r \cdot \epsilon_0 \cdot V^2 \cdot d\left(\frac{A}{t}\right) = \frac{\epsilon_r \cdot \epsilon_0 \cdot V^2}{2} \cdot \left(\frac{1}{t} dA - \frac{A}{t^2} dt\right) \quad (5.11)$$

when the voltage is constant. The differential of $\frac{A}{t}$ is found by noting that the volume is

constant during deformations,

$$\begin{aligned} d(At) &= t \cdot dA + A \cdot dt = 0 \\ \frac{dA}{A} &= -\frac{dt}{t} \end{aligned} \quad (5.12)$$

which is inserted in the above to yield

$$\begin{aligned} dW &= -\frac{\epsilon_r \cdot \epsilon_0 \cdot V^2}{2} \cdot 2 \frac{A}{t^2} dt = \epsilon_r \cdot \epsilon_0 \cdot AE^2 dt \\ F &= -\frac{dW}{dt} = \epsilon_r \cdot \epsilon_0 AE^2 \end{aligned} \quad (5.13)$$

Using this simple electrostatic model, we can derive the effective stress produced by the electrodes on the film as a function of the applied voltage. This stress, σ is

$$\sigma = \frac{F}{A} = \epsilon_r \cdot \epsilon_0 \cdot E^2 = \epsilon_r \cdot \epsilon_0 \cdot \left(\frac{V}{t}\right)^2 \quad (5.14)$$

where ϵ_r and ϵ_0 are the permittivity of free space and the relative permittivity (dielectric constant) of the polymer, respectively; E is the applied electric field; V is the applied

voltage; and t is the film thickness. The response of the polymer is functionally similar to that of electrostrictive polymers, in that the response is directly related to the square of the applied electric field.

The stress depends upon the applied electric field to second order. In writing the electric field as $E=V/t$, it is seen that the thickness of the insulating elastic film does enter, and in fact, the stress is inversely proportional to the square of the thickness. This characteristic opens two ways of increasing the stress: either by thinning the elastomer, or by increasing the voltage. The elastomer thickness in this research was limited downwards to about 20 μm ; the thickness could probably be lowered, but that is not necessary for a proof of principle, since the voltage amplifier provides up to 5 kV. The voltage is limited upwards by the dielectric breakdown strength, a material specific constant. The dielectric breakdown strength depends upon material structure, the temperature, and on the presence of impurities.

5.3 Variety of Compliant Electrodes

The term “compliant” is defined as the ability of a thin, conducting electrode to follow the strain of EAP actuator, without generating opposing stress or losing any conductivity. In this research, only electrodes made from the general system “polymer-graphite” are put to use. Moreover, compliant electrodes play an important role which can influence the performance of EAP actuation dramatically. In the following sections, various types of conducting materials for compliant electrodes are introduced.

5.3.1 Carbon Black Dust Electrodes

At the primary stage, an actuator made from 3M VHB 4910 tape was fabricated by following SRI International's approach. 3M VHB 4910 is a very compliant; it stretches at least 200% before snapping. It is a class of dielectric EAP tapes used in many studies. The tape has two different thicknesses: 0.5 mm and 1.0 mm.

The VHB film is easily stretched on a frame, up to 2 times in two directions. After this stretch, the film is still sticky. Everything sticks to the film, including carbon black powders. A carbon black, obtained from a laser printer's cartridge, is a powder when supplied. This duct can be transferred to the VHB film using a small hairbrush. These electrodes provide with poor electrical conductivity. Moreover, this kind of electrode is only possible to apply to films that are sticky.

5.3.2 Grease Electrodes

Carbon conductive grease is a high purity silicone oil loaded with branched carbon to produce a highly conductive substance. In general, this carbon grease is used as lubricant to improve the electrical and thermal connections between sliding surfaces, while providing protection from moisture and corrosion. It is excellent for use on switches and EMI shielding applications. In this research, carbon grease is used as compliant electrodes. This carbon grease consists of 10~30% carbon black, and 65%~90% of poly(dimethylpolysiloxane), PDMS. It is in paste form and can be applied on EAP film by using a small brush. The density of carbon grease is $\rho=2.7$ g/mL. As a grease electrode, it provides excellent electrical conductivity. The conductivity of the conductive grease is measured with a multi-meter. The resistivity is 1000 ohms-cm.

As a compliant electrode, the conducting grease is very good. With actuator strains below 50%, there is no significant migration of the electrode materials. The drawbacks of a grease electrode are that it is messy to handle and difficult to pattern.

5.3.3 Conducting Silicone Rubber Electrodes

To make electrodes more stable, the PDMS oil should be cross-linked for easy handling. A commercial electrical conductive RTV silicone is used. This silicone is a two-part, black, electrically conductive RTV silicone. NuSil Technology's R-2631 is based on a methyl silicone polymer with a service temperature range of -65°C to 200°C (-85°F to 400°F). R-2631 may be used as RF shielding and EMI shielding for industrial applications. In addition to protection from humidity, radiation, thermal, and mechanical stresses, R-2631 is well suited to formed-in-place conductive gaskets. In this research, R-2631 is the best material for patterning compliant electrodes on EAP films.

R-2631 Part A and Part B are mixed in a convenient 1:1 mix ratio with a 8-hour working time. R-2631 may be cured while exposed to air or completely sealed at temperatures ranging from 25°C to 150°C (77°F to 300°F). After 48 hours at 25°C (77°F), cure is sufficient for handling; however, optimum properties will be achieved after seven days. R-2631 conductive elastomer silicone fulfills all the requirements for compliant electrodes. The tensile strength of R-2631 is 800 psi (~ 5.5 MPa), and elongation is about 350%. R-2631 can be made as a flexible and thin film. The volume resistivity of cured silicone is 84 ohm-cm.

5.4 Actuator Fabrication

The theoretical dielectric elastomer actuator consists of an insulating elastomer film with compliant electrodes on both sides. This structure is the basic structure for fabricating a dielectric EAP actuator. In the previous sections, possible compliant conducting materials for electrodes are described in detail. In this section, fabrication process of EAP actuators with a patterned electrode is demonstrated. The EAP actuator is made by Dow Corning Sylgard 184. Both conventional lithography and casting method are used to pattern an electrode on one side of the dielectric elastomer film. The fabrication processes can be summarized into three parts: electrode mold, silicone film spinning, and compliant electrode casting, and it is a new method to pattern an electrode on the dielectric film.

5.4.1 SU-8 Electrode Pattern Design

The first step in manufacturing the SU-8 master is to draw a sketch of the desired pattern in AutoCAD. Three different patterns were made for different diameters of lens. Figure 5.3 shows the mask layout of electrode for 4" wafer and the detail dimensions for all three sizes of electrodes. The compliant electrode design consists of circular pattern and has an empty hole inside. The outer diameter of the circular electrode is 6000 μm . The lens is designed to be placed in the center of the electrode, so the Coulomb force, generated between two compliant electrodes, can cause the deformation of lens. There are three lens sizes. The diameters for inner circle are 2000, 3000, and 4000 μm . Moreover, there is a lead for each circular electrode. The lead is designed to connect to external wire from the power source.

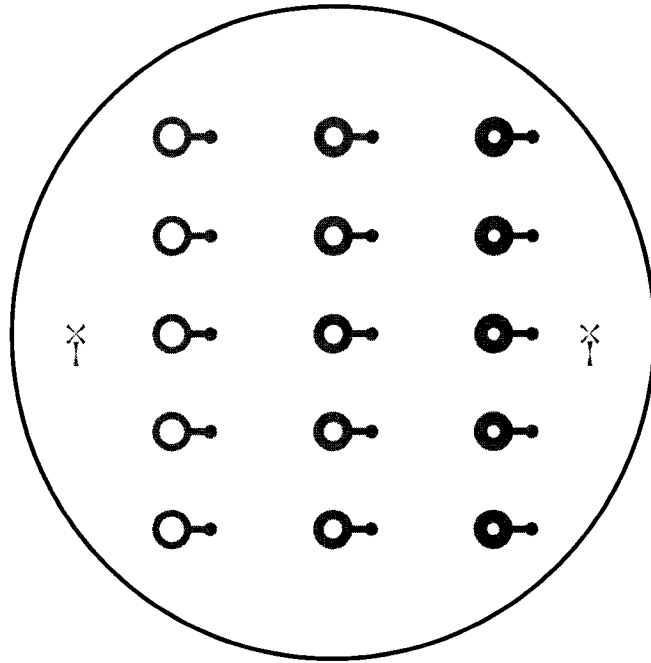
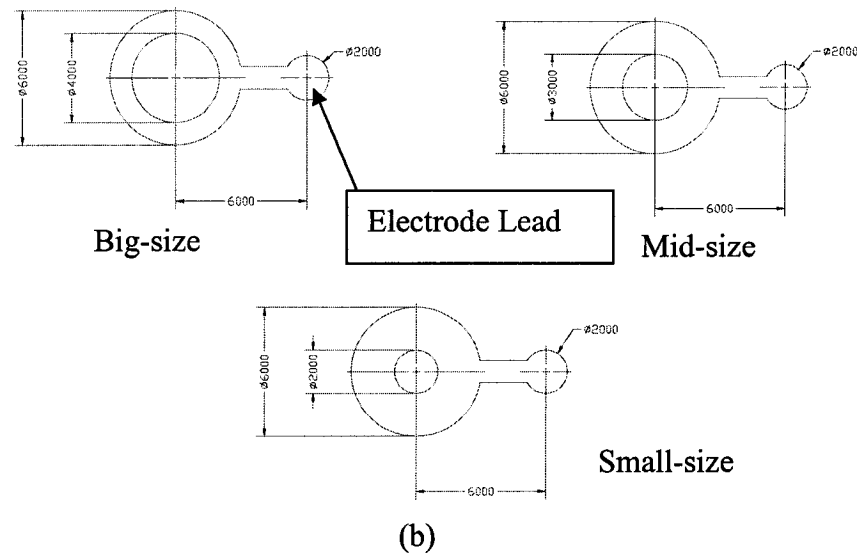


Figure 5.3 (a) the mask layout of 4" wafer



(b)
Figure 5.3 (b) Three sizes of the electrodes

5.4.2 SU-8 Electrode Master

The following steps were taken to make the SU-8 master. All work to produce the SU-8 master was done in a clean room.

1. A 4-inch silicon wafer was cleaned and blown dry in nitrogen.
2. The wafer was baked on a hot plate at 200°C for 20 minutes to dehydrate the

surface. The wafer was naturally cooled down to ambient temperature after 20-minute baking.

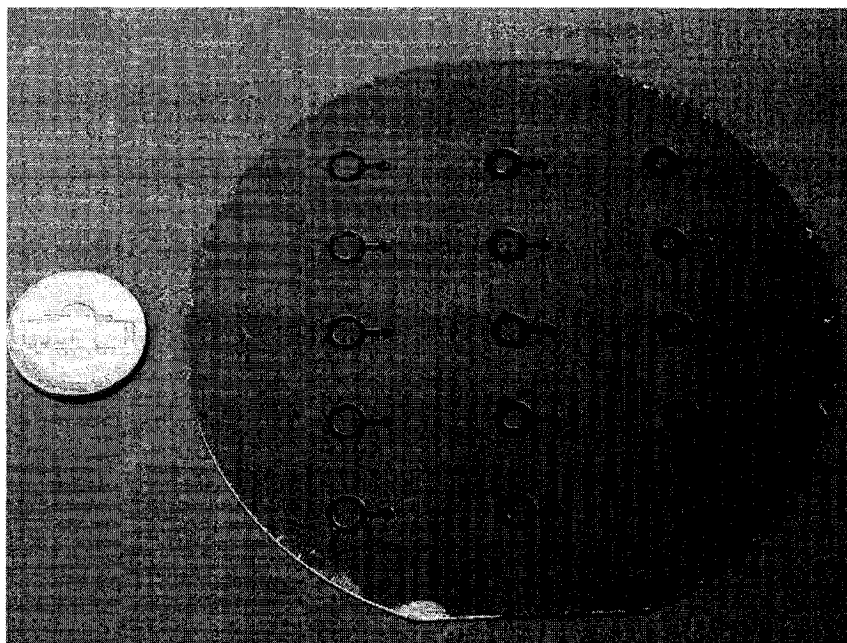
3. A good amount of SU-8 50 resist was introduced at the center of the wafer without causing any bubbles.
4. The wafer was spun at 500 rpm with an acceleration of 100rpm/sec for 15 seconds to spread the resist. To get the desired thickness, the wafer was further spun again at a higher rotational speed. The following table (Table 5.1) shows the corresponding rotational speed with the structure thicknesses.

Table 5.1 Relationship for thickness and spin speed for SU-8 50

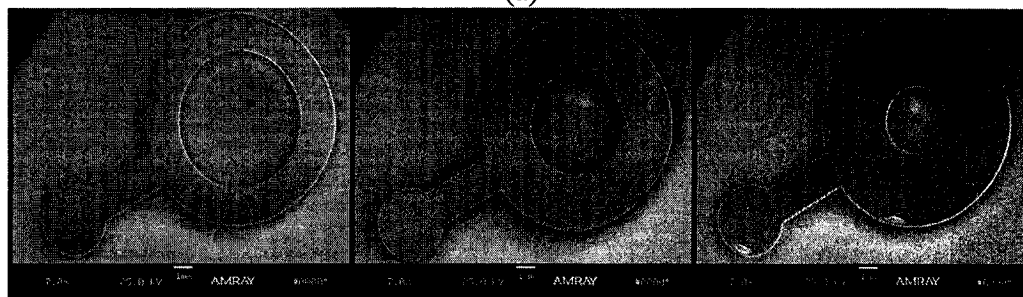
Second Spin Speed (rpm)	4000	2000	1500
Acceleration Rate(rpm/sec)	300	300	300
Duration Time (sec)	45	45	45
Final Thickness (μm)	40	72	100

5. The resist was prebaked at 65°C for 5 minutes, then 95°C for 10 minutes on a hot plate.
6. The wafer was adjusted to the mask in a contact mask aligner and exposed to UV of 7 mW/mm²) for 300 seconds, which should be enough to penetrate 100 μm of SU-8.
7. The resist was post-exposure baked (PEB) at 65°C for 2 minutes, then 95°C for 10 minutes on a hot plate. Following exposure, a post exposure bake must be performed to selectively cross-link the exposed portions of the film.
8. Following development for 5 minutes in SU-8 developer (developer has to be handled in a fume cupboard) and subsequent rinsing with 2-propanol and water, then drying in nitrogen.

9. The resist was postbaked on a hot plate at 120°C for 10 minutes. Figure 5.4 shows the SU-8 electrode patterns on a 4-inch wafer. All three electrode sizes have been made on one single wafer.



(a)



Big-size

Mid-size

Small-size

(b)

Figure 5.4 (a) Photography for three electrode sizes made by SU-8 photoresist, and (b) SEM micrograph for three sizes of electrode mold

5.4.3 Silicone Film Spinning

After three SU-8 master molds have been made with varying structure thickness, these master molds are used to duplicate elastic silicone films by using spin coating method. Before pouring the uncured elastomer onto the SU-8 master mold, a releasing agent is needed to coat on the surface of the SU-8 master mold. Since the thickness of

silicone film is the most critical factor to affect the performance of EAP actuation, the thickness of the silicone film has to be minimized. However, it is difficult to peel off elastomeric film from the master mold, if the silicone film is too thin. It is necessary to have a releasing coat on the master surface for easy peeling off the silicone film from the master mold. Dow Corning 20 Release Coating provides a durable parting film which effectively releases plastics, adhesives, and other elastomeric silicone film that are sometimes difficult to release from mold surfaces. For easier application and finer control of the amount applied to mold surfaces, Dow Corning 20 Release Coating should be diluted to one part coating to 5-10 parts solvent: 10 parts of Dow Corning 20 Release Coating with 80 parts isopropanol (99%). After dilution, Dow Corning 20 Release Coating can be applied by spin coating method. Mold surfaces should be cleaned prior to application. The best parting characteristics are obtained when this product is applied in a very thin film.

A solution of DC Sylgard 184-base™ and DC Sylgard 184 catalyzer™ is stirred together and degassed for 15 minutes in low vacuum. The mixture is poured onto the center of the SU-8 master. A small pump sucks the substrate to the spinning clutch during spinning. The spinner has options for acceleration and deceleration rates, spinner speed up to several thousand rpm, and spinning time. Typical spinning time is 60 seconds, and a typical spinning velocity is 500 rpm. The resulting films have a thickness of 100~120 μm .

After spinning, the SU-8 master with un-cured silicone is placed in an oven, at 70°C. In the oven, crossing-linking is finished in 2 hours. Each film is inspected visually for

dust specks and streaks. The result of the PDMS electrode pattern, transferred from SU-8 master, is shown in Figure 5.5.

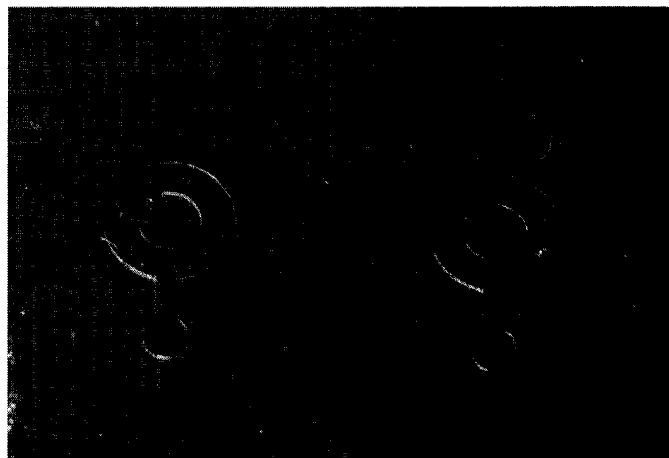


Figure 5.5 Photograph of PDMS electrode patterns on PDMS after peeling-off from the SU-8 master mold.

5.4.4 Conducting Film Squeegee-Coating Processing

The electrode pattern has been transferred from SU-8 mast mold to PDMS film after the PDMS film is peeled off from the SU-8 mold. The electrode areas on PDMS film are sunken. The depth of these hollows is depended on the height of SU-8 electrode structures. Three different heights of SU-8 electrode structure have been prepared, and the fabrication process has been discussed in the pervious two sections. They are 40 μm , 72 μm , and 100 μm in height. Compliant conducting materials, such as conducting grease or electrical conductive RTV silicone, can be used to fill in the sunken by a squeegee-coating process. The squeegee-coating process uses a piece of glass with a very flat smooth edge to scrape across the PDMS top surface. Figure 5.6 illustrates the squeegee-coating process. The extra conducting material is removed and a very flat layer of the thin conducting film is filled in the sunken as compliant electrodes. Figure 5.7 shows the photograph of a complaint electrode.

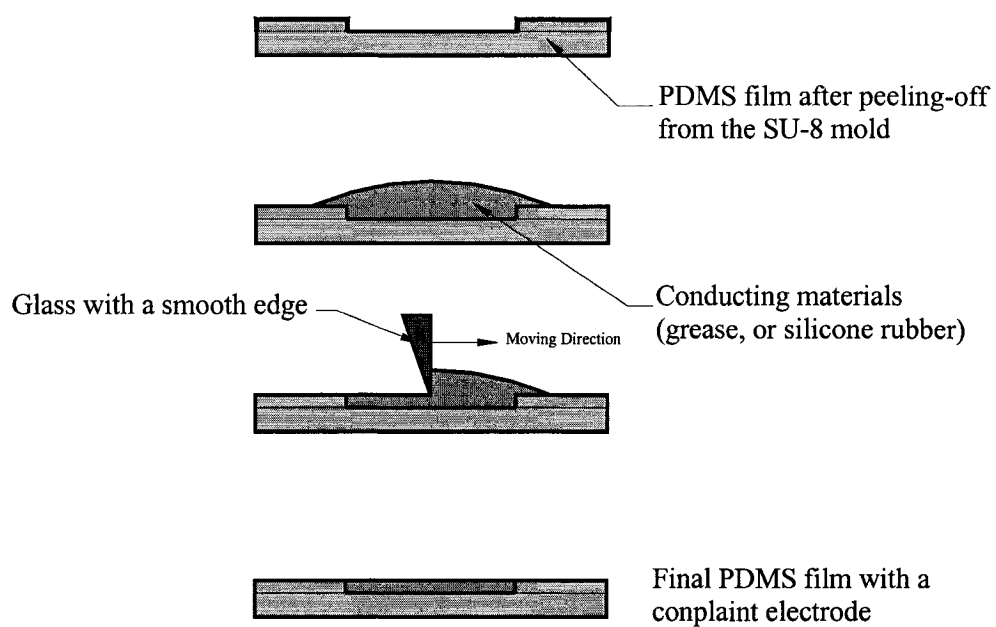


Figure 5.6 Schematic illustration of the squeegee-coating process.



Figure 5.7 Photograph of compliant electrode

CHAPTER 6

RESULTS AND DISCUSSION

This chapter is devoted to descriptions of experimental results, including measurement set-ups and experimental procedures, for 3D microfluidic lens, GRIN lenses and EAP actuators. The principles behind the optical and actuation set-up are outlined.

6.1 3D Microfluidic PDMS Lens

The back focus length has been characterized by Contact-Angle Measurement System (Data Physics, Future Digital Scientific Corp.). Figure 6.1 shows the contact angle experiment set up.

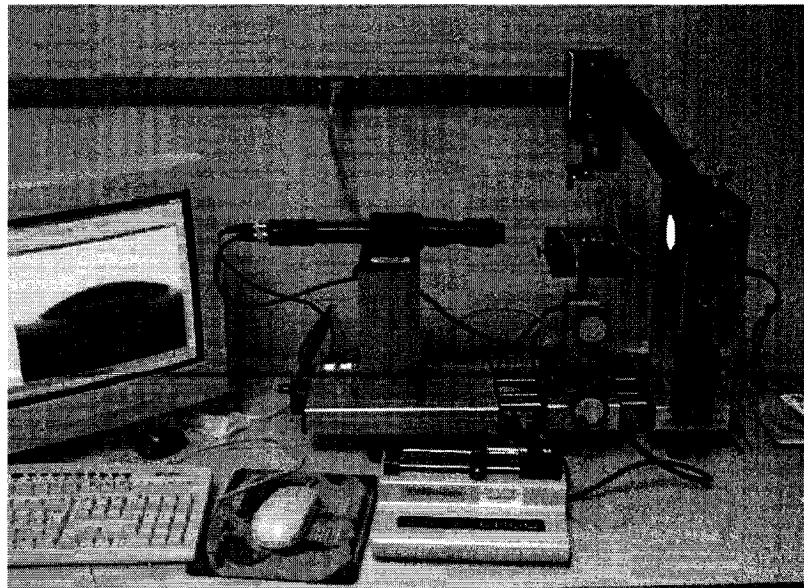


Figure 6.1 Experimental setup for contact angle measurement

The different pressure of pumped-in fluid changes the lens's curvature, shown in Figure 6.2. As the fluid volume increases, the contact angle is also increasing. Each contact angle for different pumped liquid volume is measured carefully for further lens' optical property calculations, such as curvature, and back focal length. The curvature (R) can be obtained by the following equation [28]:

$$R = \left[\frac{3V}{\pi(2 + \cos\theta)(1 - \cos\theta)^2} \right]^{\frac{1}{3}} \quad (6.1)$$

where V is equal to lens' volume and θ is contact angle.

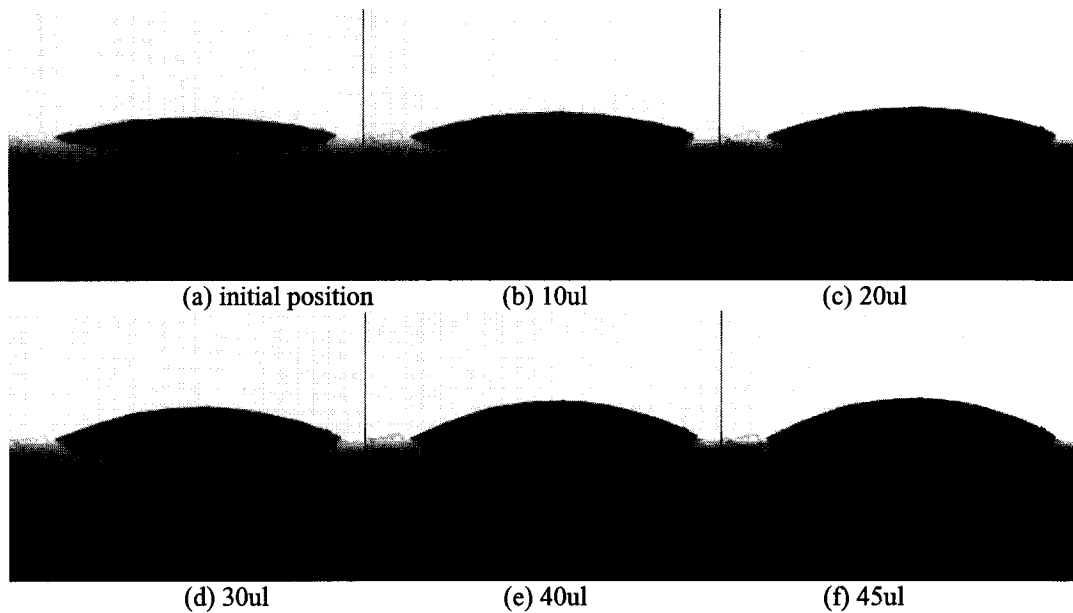


Figure 6.2 Photo for the curvature changes of PDMS film lens with different volume of pumped-in fluid

The curvature changes of the lens cause the focal plane shift. Figure 6.3(a) and Figure 6.3(b) show the relationship of pumped-in volume, contact angle, and curvature. The back focal lengths with different pumped-in volume are calculated. A microlens on microfluidic channel is considered as a plane convex refractive lens assuming that the lens profile is spherical.

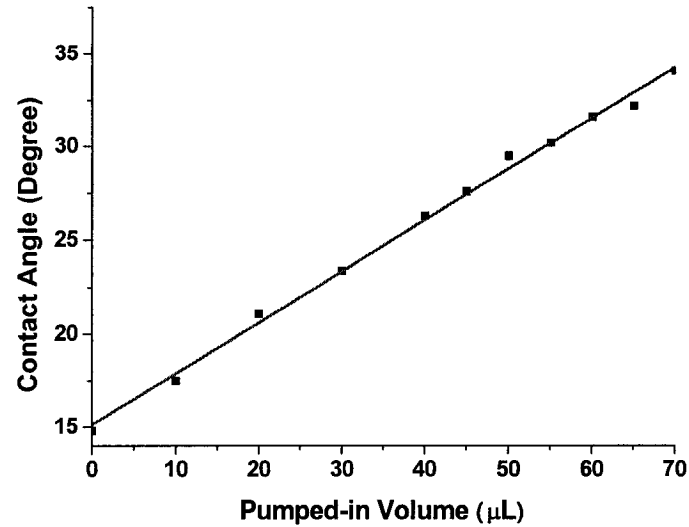


Figure 6.3(a): Linear relationship between pumped-in volume and contact angle

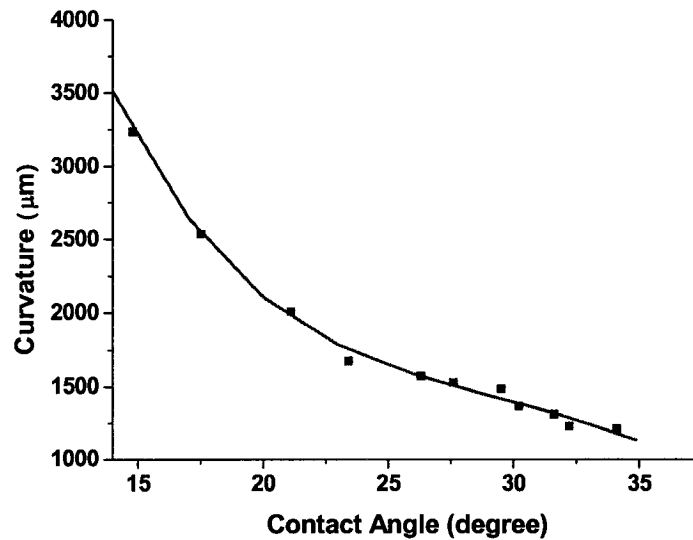


Figure 6.3(b) Relationship between contact angle and curvature

The back focal length (f_B) can be obtained by the following equations [28]:

$$f_B = n_2 \frac{1 + (n_1 - 1) \cos \theta}{n_1 (n_1 - 1)} R \quad (6.2)$$

Where n_1 , and n_2 are the refractive index for PDMS microlens and water respectively ($n_1=1.401$ and $n_2=1.33$). The range of back focal length is from 3.82 mm to 10.64 mm.

Figure 6.4 shows the relationships between pumped-in volume and back focal length. In addition, numerical aperture can be calculated by the following equation:

$$NA = n_2 \left\{ \frac{n_2^2 [1 + (n_1 - 1) \cdot \cos \theta]^2}{n_1^2 \cdot (n_1 - 1)^2 \cdot \sin^2 \theta} + 1 \right\}^{-\frac{1}{2}} \quad (6.3)$$

The numerical apertures with various focal lengths have been determined and listed in Table 6.1. The numerical aperture can be tunable between 0.087~0.24. Table 6.1 presents a detailed summary of the optical properties of a variable focal microlens. The detail of mathematic calculation for curvatures, back focal lengths, and numerical apertures with different pump-in volume is list in Appendix A.

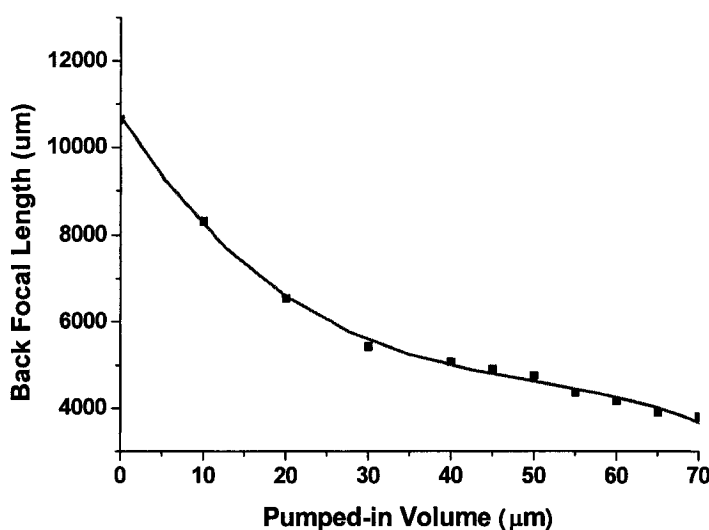
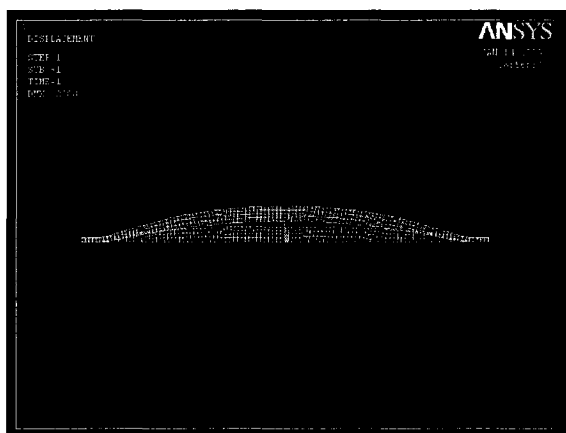


Figure 6.4 Relationship between back focal length and pumped-in volume

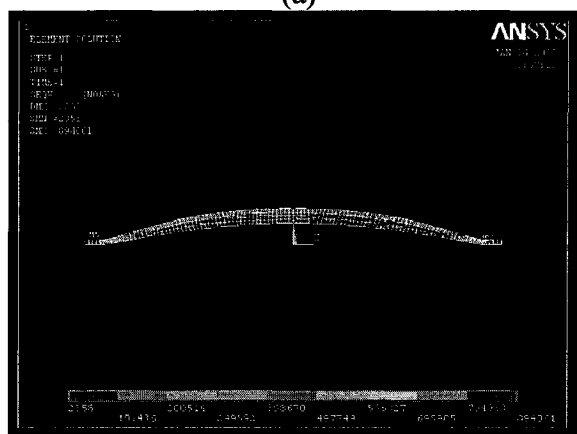
Table 6.1 Optical properties of a 1400μm diameter of microlens with different pumped-in volume

Photos						
Pumped-in volume (μL)	0.0	10.0	30.0	50.0	60	70.0
Chamber Pressure (psi)	0.71	1.06	2.12	2.83	3.54	4.24
Contact Angle (°)	14.8	17.5	23.4	29.5	31.6	34.1
Curvature (μm)	3238	2538	1677	1488	1312	1210
Back Focal Length (μm)	10640	8307	5430	4751	4167	3815
Numerical Aperture (NA)	0.09	0.11	0.17	0.19	0.22	0.24

A comprehensive finite element analysis for PDMS microlens under various internal pressures has been performed. Figure 6.5 shows the lens deformation and stress distribution on the cross-section of microlens. Furthermore, a 3D model has been created to provide more accurate results shown in Figure 6.6. The maximum stress occurs on the most outer ring of the lens' bottom surface. The thickness on outer ring of lens's body is thinner than one on the center of lens. By applying a uniform pressure on the bottom surface, the stress on the outer ring will increase more than the other area of the lens. The results for curvature changes due to the pressure applied agree with the experimental results.

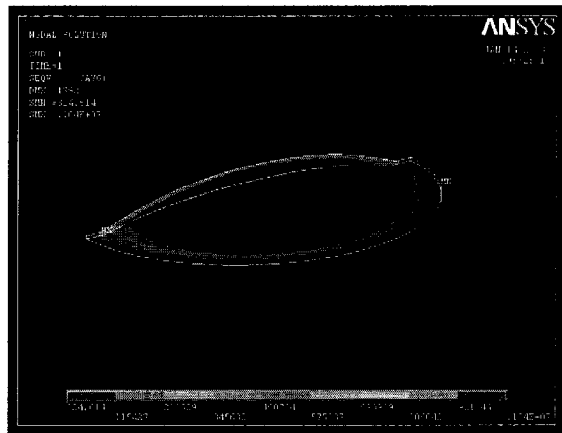


(a)

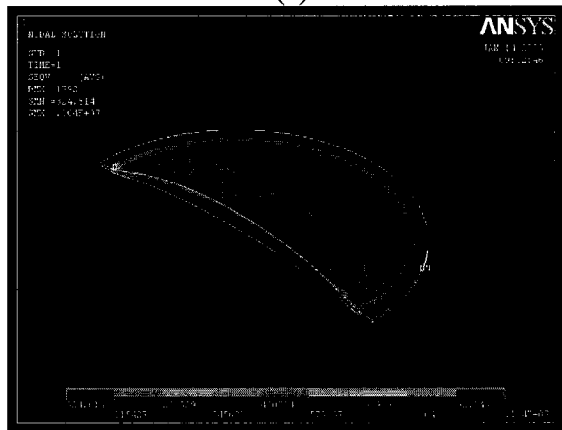


(b)

Figure 6.5 2D ANSYS simulation of microlens (a) for deformation, (b) for stress distribution



(a)



(b)

Figure 6.6 3D ANSYS simulation of microlens (a) for stress on bottom surface (b) for stress on top surface

6.2 Silicone-Based GRIN Lens

Two experimental setups have been established for diverging and converging GRIN lenses. Figure 6.7 and Figure 6.8 show the configurations for each testing system for diverging GRIN lens and converging GRIN lens, respectively. From Figure 6.7, d_1 is the distance between CCD camera and a double-side convex lens, and d_2 is the double-side convex lens to the GRIN lens. The distance d_3 is the space between object to the GRIN lens. From Figure 6.8, d_4 is the distance between CCD camera and a converging GRIN lens. The distance d_5 is the space between object to the GRIN lens.

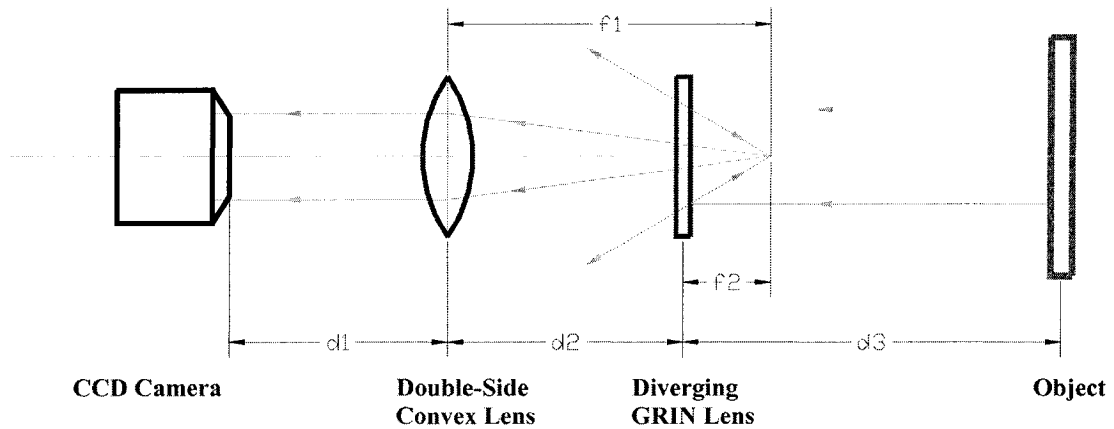


Figure 6.7 Optical setup for diverging GRIN lens

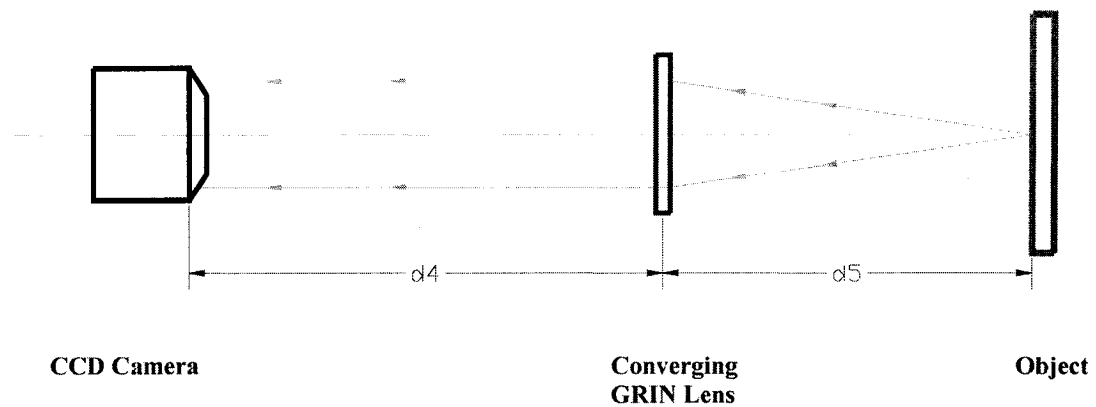


Figure 6.8 Optical setup for converging GRIN lens

In Figure 6.9, the optical results show that the objective images are reduced through the diverging GRIN lens. A diverging GRIN lens with 2.0mm in diameter is demonstrated in the experiment. The diverging GRIN lens reduces the objective's image and provides very good optical quality. However, the experimental testing results for a converging GRIN lens are not as satisfying as the ones for a diverging GRIN lens. Figure 6.10 shows the image through the converging GRIN lens. These images do show that the image of the object is magnified, but the image is not very clear. A further research on material design, and fabrication techniques is needed to improve the imaging quality of the converging GRIN lens.

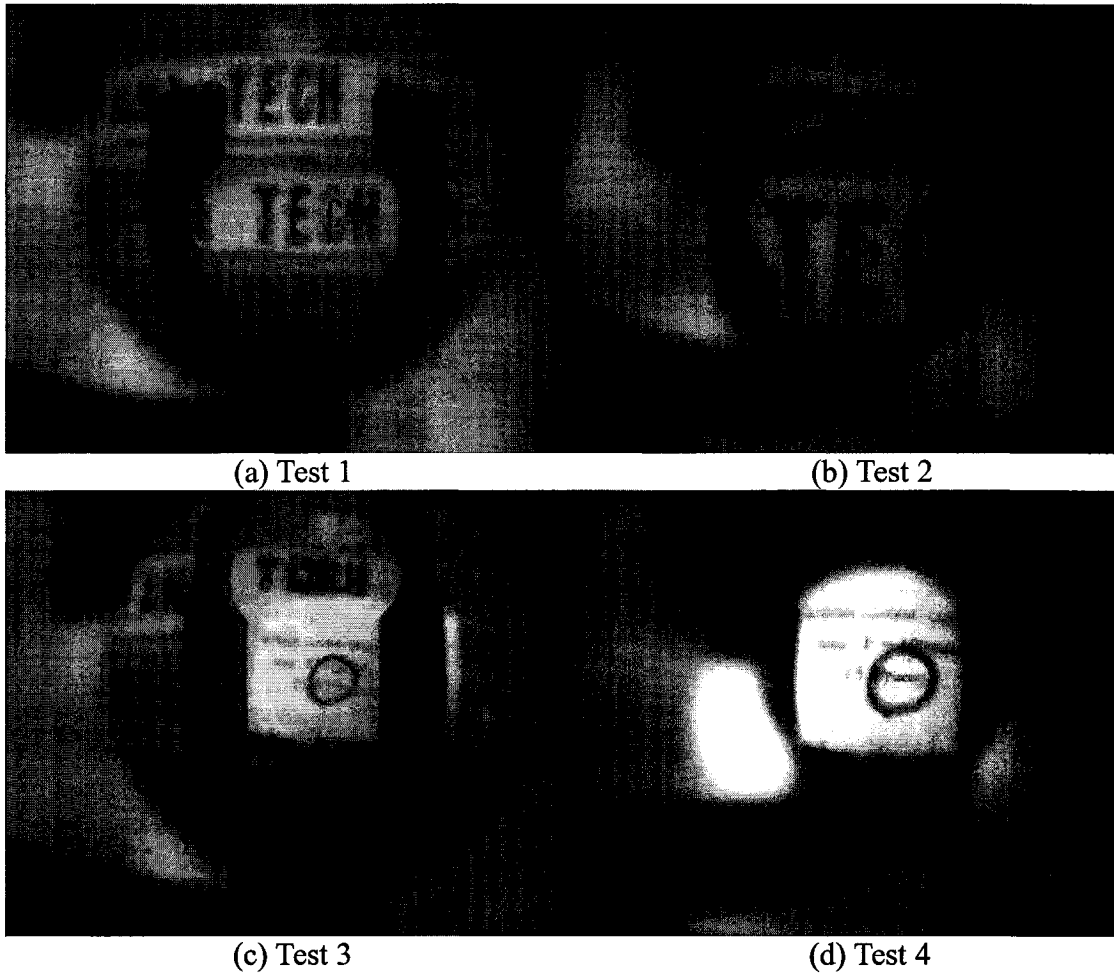


Figure 6.9 Images obtained from CCD camera through a diverging GRIN lens

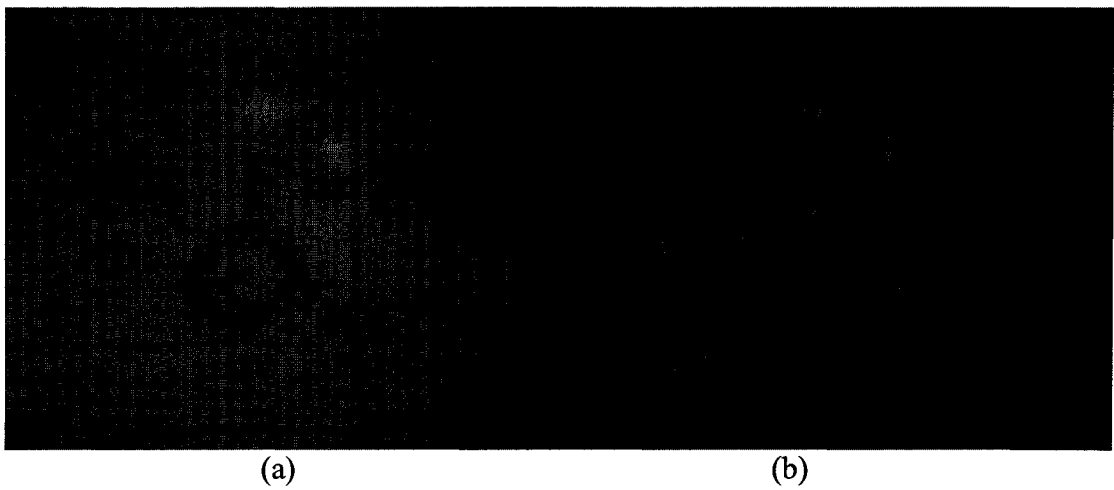


Figure 6.10 Images obtained from CCD camera through a converging GRIN lens

6.3 Silicone EAP Actuator

Silicone actuators are manufactured by the procedure described in Chapter 5. One compliant electrode is patterned on one side of silicone film. On the other side of the film, the other electrode is made with conducting carbon grease. Conducting carbon grease is transferred to the film using a small hairbrush. This electrode is as conducting as the electrode made earlier, and it is stable. The final thickness of the silicone film is $\sim 120\mu\text{m}$, after spin coating and peeling-off from the SU-8 mold. Because the different heights of SU-8 mold structures, they are $40\mu\text{m}$, $72\mu\text{m}$, and $100\mu\text{m}$, the thicknesses of the PDMS film between two electrodes are $80\mu\text{m}$, $48\mu\text{m}$, and $20\mu\text{m}$. A simple sketch illustrates the thickness for SU-8 microstructure and PDMS film, shown in Figure 6.11.

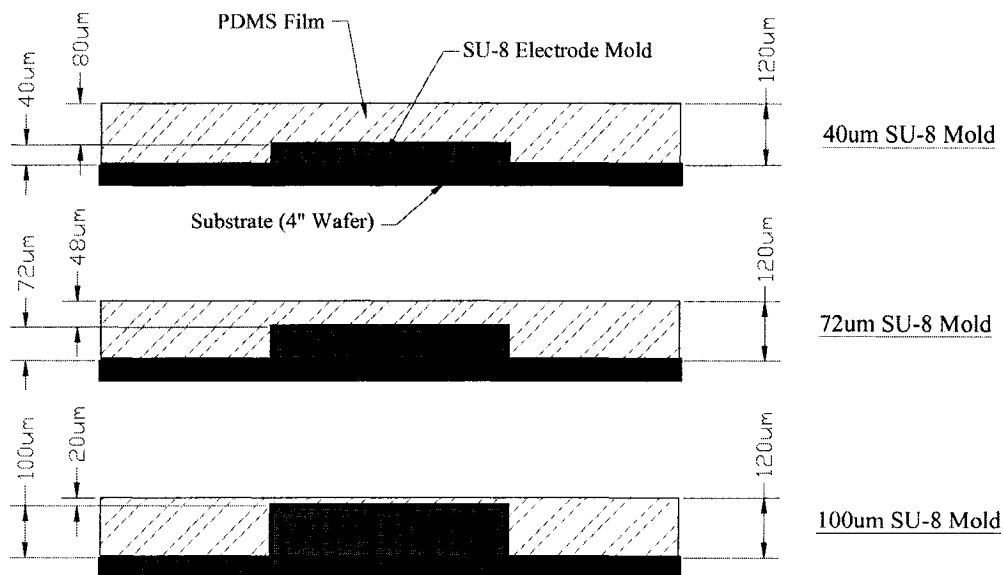


Figure 6.11 Sketch for three different heights of SU-8 electrode molds with a same thickness of PDMS

6.3.1 Deflection Testing Setup

The actuator was mounted in the actuator test bench, and was measured using the experimental setup shown in Figure 6.12. A visible light impinges perpendicular to the center transparent portion. Upon changing the voltage difference between two electrodes, the membrane deforms, focusing the collimated light. The EAP actuator sits on a XYZ micromanipulator. XYZ micromanipulator is a stage which can be moved in X-, Y-, Z-directions. The focal spot image is visualized with a CCD camera by adjusting the vertical distance between the EAP actuator and the microscope objective. A RC circuit is used to control the applied voltage between two compliant electrodes. The RC circuit and other electrical setup for transferring low DC voltage to high DC voltage are described in the next sections.

The focal length was measured from the center point of the un-deformed PDMS membrane. The center point on the top surface corresponds to the zero reference point of the XYZ micromanipulator. By vertically adjusting the XYZ stage, the focal plane of the EAP actuator is brought into focus, and the corresponding distance is recorded by Nikon digital height gage (MF-501+MFC-101). The positioning precision of the XYZ micromanipulator is less than $0.5\mu\text{m}$, and the accuracy of Nikon digital height gauge is $1.0\mu\text{m}$. Therefore, the accuracy of the measurement is limited by observer's ability to visually identify the smaller and more intense focused spot while observing it real time through the CCD camera.

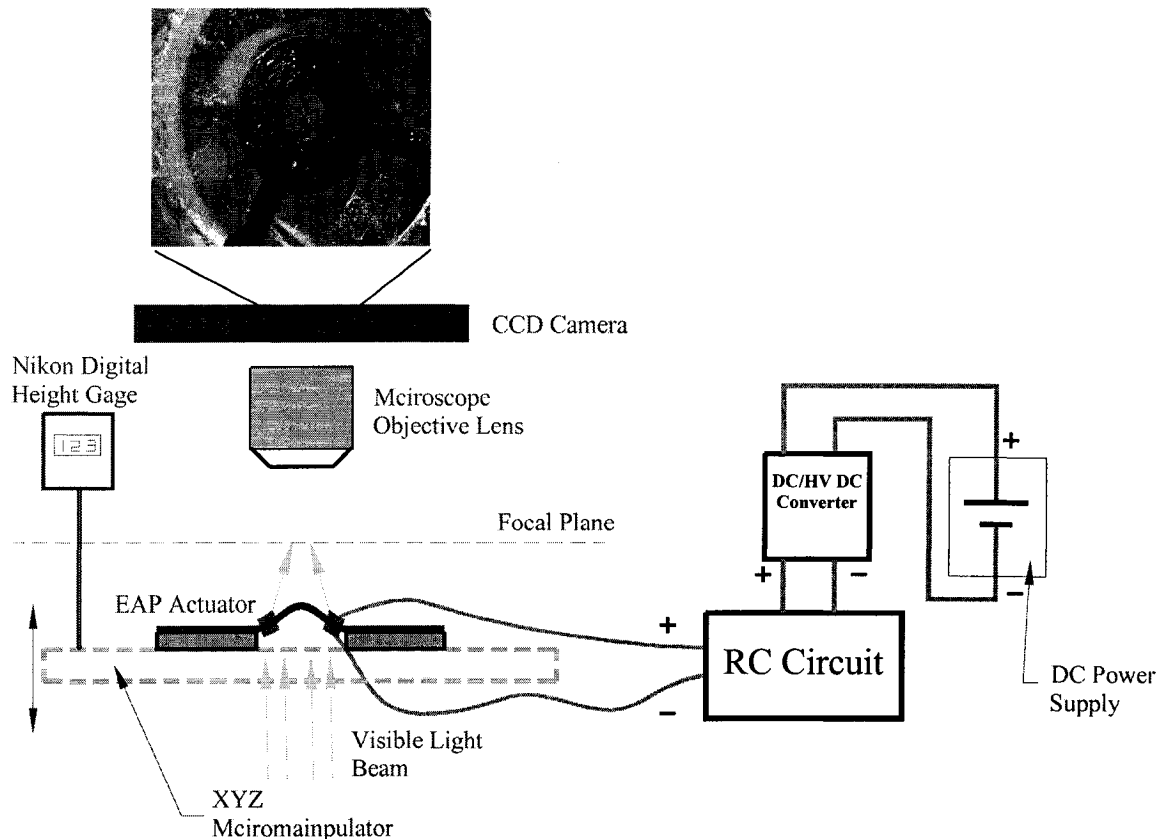


Figure 6.12 Experimental setup for measuring the deflection of EAP actuator.

6.3.2 RC Circuit and a DC-to-HV DC Converter Setup

Capacitors and resistors are often found together in a circuit, called an RC circuit. There are two situations: charging and discharging. In the charging mode (switch S is on), current begins to flow through the circuit, shown in Figure 6.13(a). Electrons will flow out of the negative terminal of the power supply, through the resistor R, and accumulate on the upper plate of the capacitor, and electrons will flow into the positive terminal of the power supply leaving a positive charge on the other plate of the capacitor. As the charges accumulate on the capacitor, the current is reduced until eventually the voltage across the capacitor equals the voltage of power supply, and no further current flows. The potential difference across the capacitor, which is proportional to the charge on the

capacitor ($V=Q/C$) thus increases gradually. The product of the value of the resistance times that of the capacitor is called the time constant τ of the circuit: $\tau =RC$; it is a measure of how quickly the capacitor becomes charged. Specifically, it can be shown that the product RC gives the time required for the capacitor to reach 63 percent of full voltage.

The other mode is called the discharging circuit. When a capacitor is already charged, it is allowed to discharge through a resistance R . In this case, the switch S is turned off, and there is no power supply, shown in Figure 6.13(b). When the switch is closed, charge begins to flow through resistor R from one side of the capacitor toward the other side, until it is fully discharged. The voltage falls 63 percent of the way to zero in a time $\tau =RC$.

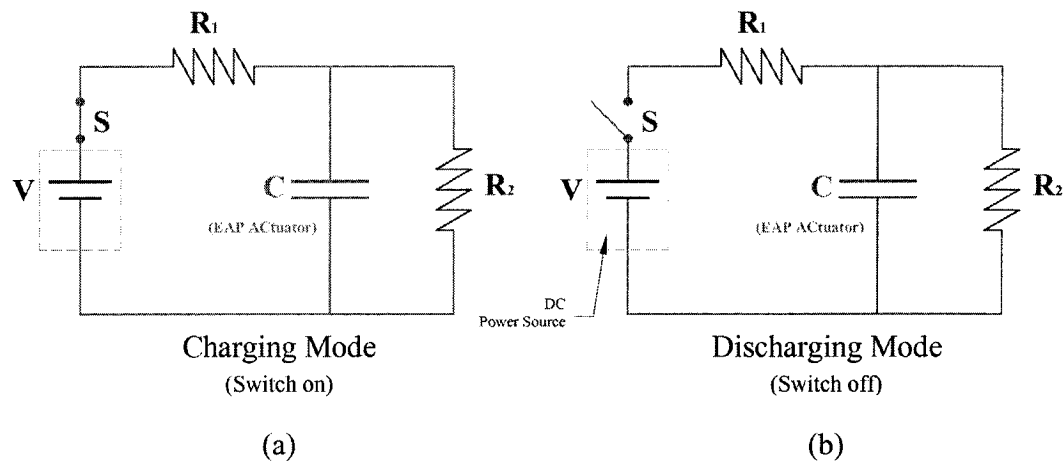


Figure 6.13 RC circuits in (a) charging mode, and (b) discharging mode.

In this RC circuit design, the capacitor is replaced by the EAP actuator. The DC power source consists of two components; DC power supply and “DC to HV DC” converter. Since the EAP actuator needs a high DC voltage, a converter is used to transfer the DC voltage from the power supply (0~13 Volts) to high DC voltage (≥ 5000 Volts). A “DC to HV DC” converter, from EMCO G50, is a small device which its isolated output

voltage is directly linear proportional to the input voltage. The relationship between input voltage and output voltage is shown in Figure 6.14. The resistivity of R_1 and R_2 are $5M\Omega$ and $10M\Omega$, respectively. Both R_1 and R_2 are large to decrease the current flow for safety reasons under a high voltage condition. Moreover, the value of R_2 is much larger than R_1 , and the discharging current must be minimized for safety, so the discharge is much slower than the charging process. The EAP actuator can be repeatedly charged and discharged.

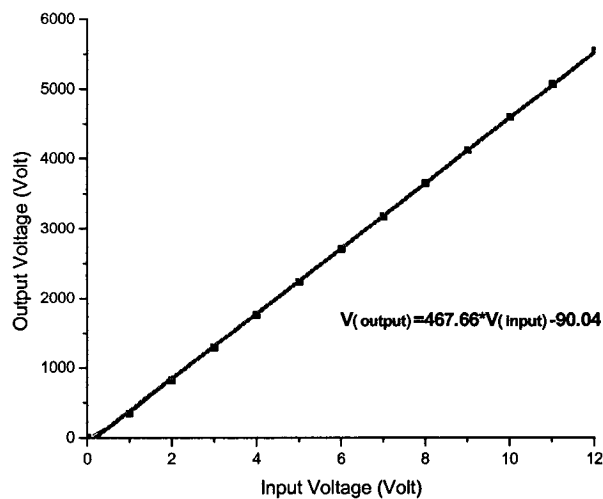


Figure 6.14 Linear relationship between input and output voltages from a DC-DC converter

6.3.3 Deflection Results of EAP Actuator

In this EAP deflection testing setup, there are three design parameters: thickness of PDMS film, electrode material, and electrode size. Samples were prepared with 20, 48, 80 μ m in thickness, three different sizes of electrodes, and carbon grease and conducting silicone rubber as electrode materials.

The actuator was mounted in the actuator test bench described above. The voltage was applied from 0V to 13V in steps of 1.0V. The deflection in the center of PDMS film

was measured and recorded. Table 6.2 shows the comparison of maximum deflection in the center of the film with different electrode materials.

Table 6.2 (a) Comparison of EAP thickness and electrode size at an applied voltage of 13V and carbon grease was used as the electrode material

EAP thickness \ Electrode Size	Ø4000µm (Big)	Ø3000µm (Mid)	Ø2000µm (Small)
20µm	0.240 mm	0.281 mm	0.380 mm
48µm	0.228 mm	0.242 mm	0.344 mm
80µm	0.222 mm	0.240 mm	0.317 mm

Table 6.2 (b) Comparison of EAP thickness and electrode size at an applied voltage of 13V and conducting silicone rubber was used as the electrode material.

EAP thickness \ Electrode Size	Ø4000µm (Big)	Ø3000µm (Mid)	Ø2000µm (Small)
20µm	0.237 mm	0.429 mm	0.523 mm
48µm	0.223 mm	0.276 mm	0.398 mm
80µm	0.234 mm	0.264 mm	0.292 mm

From the experimental results on maximum deflection in Table 6.2(a) and Table 6.2(b), there is more deflection when the electrode size decreases with the same EAP thickness. Under the same size of electrode, the thinner EAP film can produce more deflection. In addition, it shows that there are no significant changes on the maximum deflection between EAP thickness of 48µm and 80µm. As expected, the thinner PDMS film with small electrode size can produce the most deflection. The main reasons for this effect were due to the larger actuation area and the thickness of PDMS film. From Equation 5.14 in Chapter 5,

$$\sigma = \frac{F}{A} = \epsilon_r \cdot \epsilon_0 \cdot E^2 = \epsilon_r \cdot \epsilon_0 \cdot \left(\frac{V}{t}\right)^2 \propto \left(\frac{1}{t}\right)^2 \quad (6.4)$$

The stress depends upon the applied electric field to second order. Writing the electric field as $E=V/t$, it is seen that the thickness of the insulating elastic film does enter, and in fact the stress is inversely proportional to the square of the thickness. Thinning the PDMS

film causes to increase the stress; thus producing the largest deformation. The experimental results match with theoretical principle.

Under the same PDMS thickness and electrode material, the deflections versus applied voltage with the same PDMS thickness are shown in Figure 6.15 for carbon grease as electrode material, and Figure 6.16 for conducting silicone rubber as electrode material. All plots show that the curves do not retrace themselves on the same path; this phenomenon is called hysteresis. The data serves as evidence of the statement made in a recent paper about the hysteresis behavior of the EAP actuators [36]. Moreover, the deformation shows nonlinear properties from the experimental results. Nonlinearity and hysteresis behaviors have become the difficulties in characterizing EAP actuators. To support the need for reliable data, a characterization technique is developed to quantify the electroactive responses and makes sure all other parameters are same except the controlling parameter. Figures 6.15 and 6.16 show that the dimension of the electrode does affect the performance of deflection. The larger actuation area can produce higher deformation. Therefore, the smallest hollow hole in the center of the electrode can produce the maximum deformation. In general, the deflection performances of mid-size and big-size electrodes have very similar deflection paths when the applied voltage is increased in charging and discharging modes. Comparing the maximum deflection at 13V of input voltage, the smallest electrode size has the highest deflection, and the biggest electrode has the lowest one. As seen in Figure 6.15, and Figure 6.16, they show deflection measurements obtained on the same thickness of PDMS film and two different compliant materials for electrodes with three different electrode sizes: big, mid, and small. These plots include all the measurements of charging and discharging condition.

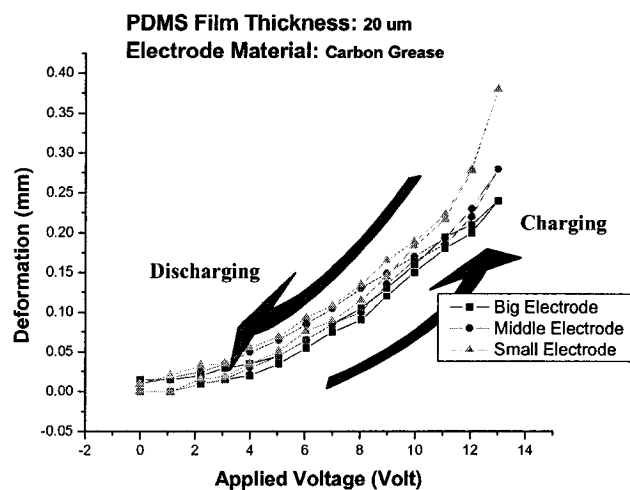
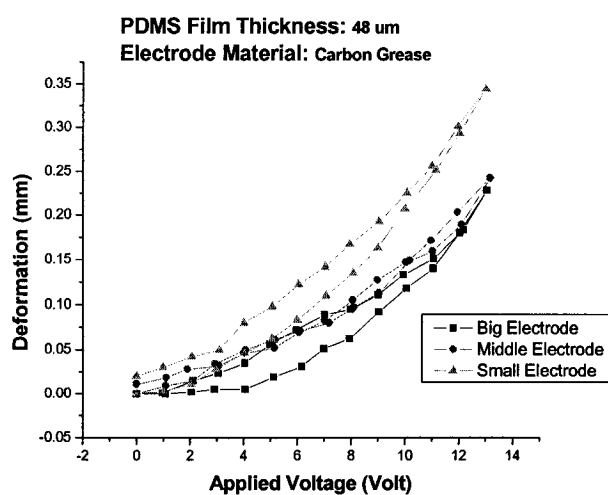
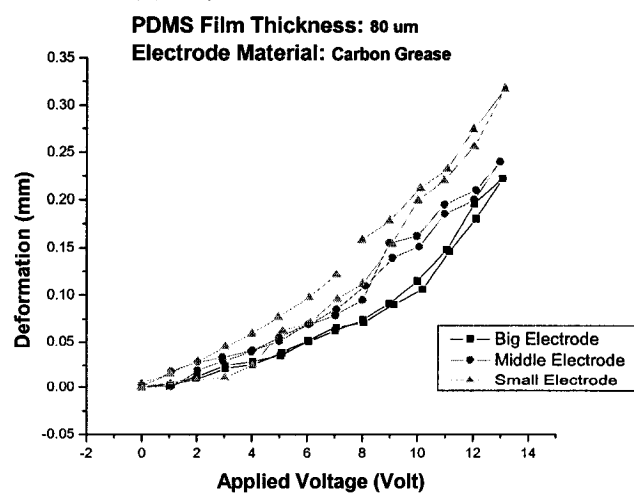
(a) 20 μm thick of PDMS Film(b) 48 μm thick of PDMS Film(c) 80 μm thick of PDMS Film

Figure 6.15 Deflection measurements with different EAP thicknesses
(carbon grease)

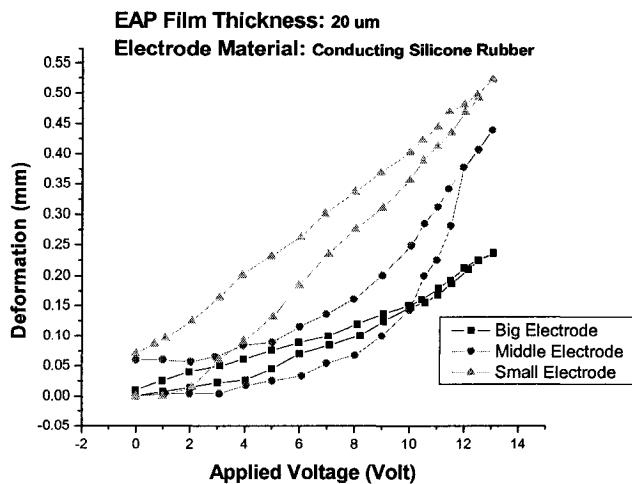
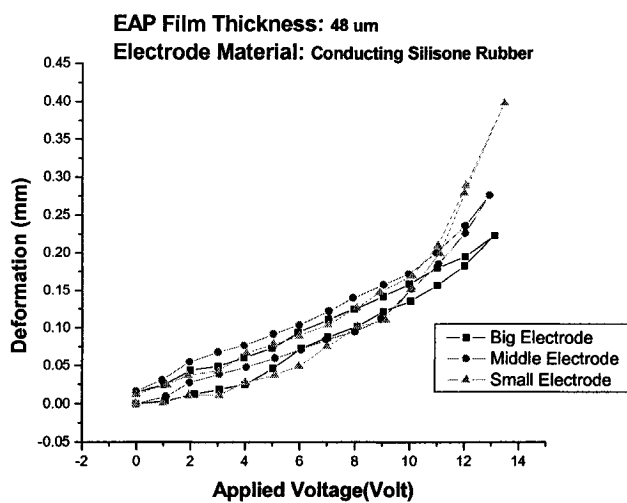
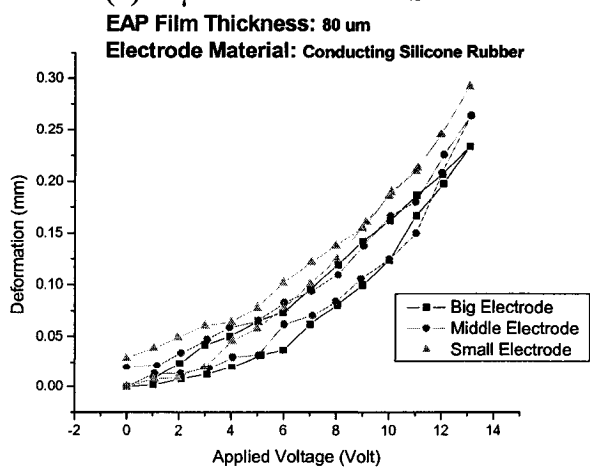
(a) 20 μm thick of PDMS Film(b) 48 μm thick of PDMS Film(c) 80 μm thick of PDMS Film

Figure 6.16 Deflection measurements with different EAP thicknesses (conducting silicone rubber)

Figure 6.16 shows deflection measurements obtained on the same thickness of PDMS film and conducting silicone rubber, as the electrode material with three different electrode sizes: big, medium, and small. These plots include all the measurements of charging and discharging condition.

From the results in Figure 6.15 and Figure 6.16, it can be concluded that the smallest size of electrode in all possible conditions produces the largest deformation. In Figure 6.15 and Figure 6.16, they indicate the comparison of the EAP deflection with same PDMS film thickness and electrode material. However, the other factor, which can affect the EAP performance, is the thickness of the PDMS film. In Figure 6.17, the thinner PDMS film has higher deformation. Conducting silicone rubber, as electrode material, together with 20 μ m thick PDMS film can produce the largest deflection. 20 μ m thick PDMS with small-size carbon grease electrodes is the optimum configuration for maximum deflection. Despite the maximum deflection at a high voltage, the deflection path for different electrode materials should also be taken into account in the design considerations.

Figure 6.18 indicates the deflection path for charging and discharging modes for two different electrode materials. In particular, it shows that conducting silicone rubber used as the electrode material can produce a higher deformation comparing with carbon grease with different applied voltage. Note should also be taken of the charging and discharging paths. The charging and discharging paths for carbon grease are much closer than the ones for conducting silicone rubber. Therefore, the carbon grease EAP actuator can provide with more stable and controllable deflection than conducting silicone rubber.

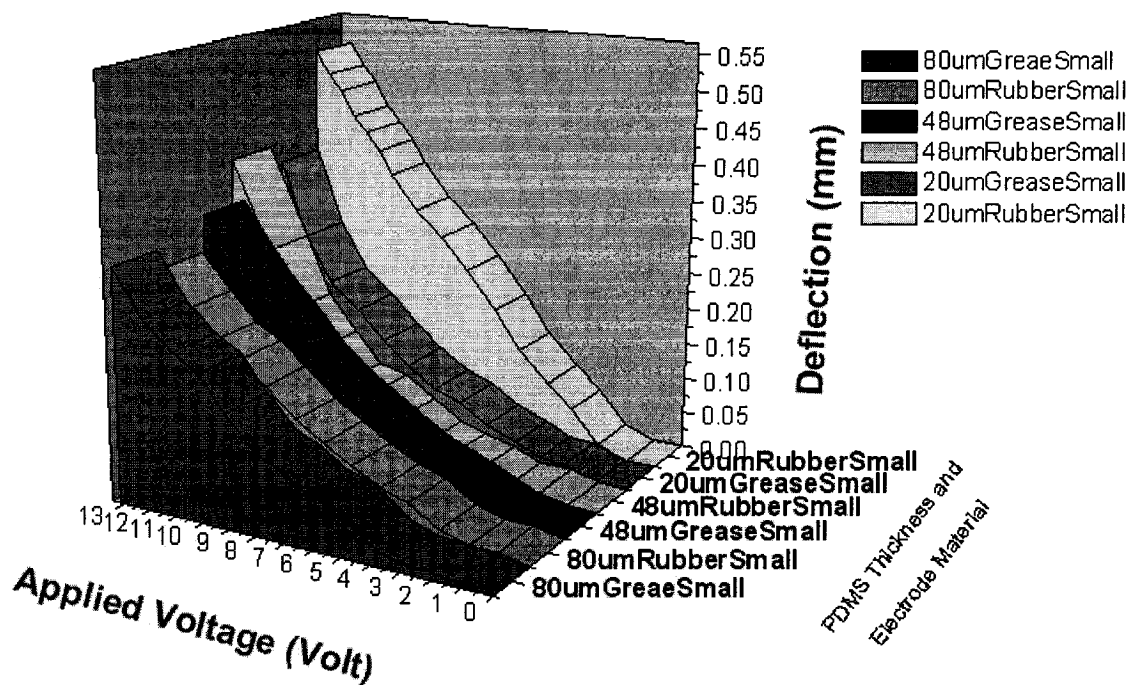


Figure 6.17 Deflection measurements obtained on the same electrode size (small) with different thicknesses and electrode materials. This plot is for charging mode.

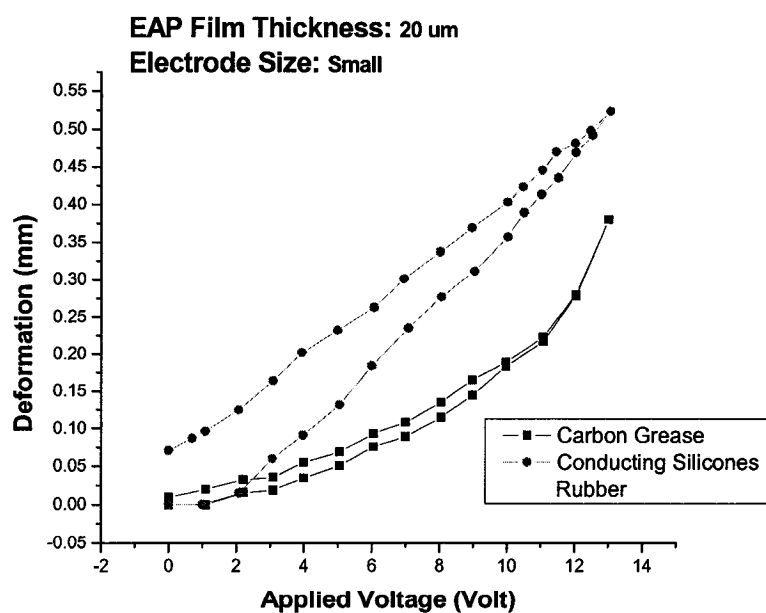


Figure 6.18 Deflection measurements for 20µm thick PDMS and small-size electrode with two different electrode materials.

CHAPTER 7

CONCLUSIONS AND FUTURE WORK

7.1 Conclusions

A 3D flexible PDMS microlens and a controllable focusing module are successfully fabricated and characterized. Furthermore, a novel PDMS casting process with PDMS mold to fabricate PDMS microlens film is developed. This fabrication technique provides high optical properties, high dimensional accuracy, and low cost for mass production. Micro lenses with a diameter of 600~1400 μm are fabricated using this fabrication technique, and the optical and mechanical properties of this prototype device are characterized. The surface roughness of the PDMS lens was 18 nm. The curvature changes of the microlens were from 1210 μm to 3238 μm . With this wide range of curvature changes, we can control the back focal length from 3.82 mm to 10.64 mm, and numerical aperture between 0.09 to 0.24. The numerical aperture of this optical device can reach 0.24 which is about 4 times that of a conventional planar diaphragm (NA=0.05). These results prove the possibility of using the present lens's model for many optical applications. Its benefits are applicable not only to various optical MEMS applications such as tunable range wavefront sensors, beam spanning control for free space optical actuation, but also to biomedical applications.

A second method to fabricate a dynamic tunable focusing length lens has been introduced by coupling polymeric GRIN lens with an EAP actuator. GRIN lenses are developed using lithographic and diffusion techniques to make flexible polymeric lens. A new two-step polymerization has been designed for fabricating silicone-based GRIN lenses. This fabricating technique uses two different silicone materials with different curing systems, addition cure and UV cure. The characteristics of these silicone-based GRIN lenses are that they are deformable under an applied force, dielectric in the electric field, and these lenses have a gradient refractive index distribution with an Δn of nearly 0.03. Many silicones systems have been examined to fabricate GRIN lenses. Converging and diverging lenses have been developed by changing the matrix and diffusant materials. The optical properties for diverging lenses have a very high quality images; however, the objective image goes through the converging lenses and becomes blurred. A large improvement is still needed to modify the silicone system for a better converging GRIN lens.

EAP actuation is another method developed to control the focal length of a polymeric lens. By compressing a polymeric film in thickness and expanding the film in area, it can be carefully evaluated to integrate with GRIN lens in order to change the lens' shape and the optical properties such as focal length. By changing the physical appearance of flexible polymeric GRIN lens in thickness and area, the dimension of GRIN lens is changed and the focal length of GRIN lens can be controlled. The reason for studying EAP actuation as a tunable focal lens mechanism is not hard to see: EAP actuator converts electric energy to mechanical deformation. This understanding draws attention to control the focal length of a flexible polymeric lens preciously by adjusting

the applied voltage. The operating setup of EAP actuator is much simpler than microfluidic actuation system also presented in this dissertation. As a matter of fact, there are some drawbacks of using fluidic pressure driven mechanism such as slow response time, complicated packaging process, and low reliability. Consequently, EAP actuation can achieve much faster response time and simple assembly than variable focal length liquid filled lens with an external pump.

Procedures for manufacturing of EAP actuator with different size of electrodes are presented. Silicone actuators are made from spun elastomer films. Electrode structures are also patterned on the elastomer film. Experimental results on deflection were observed with different electrode sizes, electrode materials and EAP film thicknesses. The maximum deflection is $523\mu\text{m}$ in the center of a $20\mu\text{m}$ thick EAP film with a small-size, conducting silicone rubber electrode. However, $20\mu\text{m}$ thick EAP film with a small-size, carbon grease electrode can produce more stable deflection curves in charging and discharging modes. Different configurations of EAP actuators have been observed with various input voltages, all share one common drawback: the driving voltage is high. Typical driving voltages lie in the range between 1kV to 5.5kV, depending on the polymer breakdown field and thickness of the polymer film.

At current stage, the GRIN lens is not yet coupled with EAP actuator. Therefore, the complete optical measurements can not be presented in this dissertation. Comparison with microfluidic lens and EAP GRIN lens is also not included. The final development related to the integration of silicone-based GRIN lens with EAP actuator is expected to evolve as the field is advanced and the fully-package of GRIN lens driving with EAP actuation is future research work.

7.2 Future Work

In continuation of this research work, there is room for improving in areas such as the optical measurements of microfluidic lens, and the integration of GRIN into EAP actuation system. With the optical measurements, 3D PDMS lens with microfluidic chip can have a complete device with fabrication process and testing data. This information is very important for studying on microfluidics system.

For silicone-based GRIN lens, different silicones and curing systems should also be examined. Some systems may provide Δn value greater than 0.03, but it is unknown if these index gradients can be created over large distances. Additionally, a diffusion model of these large distance remains to be developed in many cases.

The final stage will be to integrate an elastic GRIN lens into EAP actuator for a complete optical microlens system with dynamically variable focal length.

REFERENCES

- [1] Nikolas Chronis, et al, "Tunable liquid-filled microlens array integrated with microfluidic network," *Optics Express*. Vol. 11, No. 19 (September 2003)
- [2] L. G. Commander, et al, "Variable focal length microlenses," *Opt. Commun.* 177, 157 (2000)
- [3] S. Kwon, and L. P. Lee, "Focal length control by microfabricated planar electrodes-based liquid lens (μ PELL)," 11th International conference on solid-state sensors and actuators: Transducers'01, Munich, Germany, June 10-14, 2001.
- [4] T. Krupenkin, S. Yang, and P. Mach, "Tunable liquid microlens," *Appl. Phys. Lett.* 82, 316 (2003).
- [5] <http://www.research.philips.com/InformationCenter/Global/FNewPressRelease.asp?>
- [6] T. Krupenkin, S. Yang, and P. Mach, "Tunable liquid microlens," *Applied Physics Letters* Volume 82, Issue 3, pp. 316-318
- [7] O'Neill F T and Sheridan J T, "Photoresist reflow method of microlens production: I. Background and experiments," *Optik* 113 391–404
- [8] Severi M and Mottier P, "Etching selectivity control during resist pattern transfer into silica for the fabrication of microlenses with reduced spherical aberration," *Opt. Eng.* 38 146–50
- [9] Iga I, Kokubun Y and Oikawa M, "*Fundamentals of Microoptics*," (London: Academic) 1984
- [10] Kufner M and Kufner S, "Fabrication of monolithic integrated fiber-lens connector arrays by deep proton irradiation," *Microsyst. Technol.* 2 114–8 1996
- [11] Fu Y Q and Bryan N K A, "Novel one-step method of microlens mold array fabrication" *Opt. Eng.* 40 1433–4 2001
- [12] Daly D J, "The fabrication and measurement of melted photoresist microlenses," *Doctoral Thesis* Kings College London, UK 1998

- [13] Hutley, MC, "Optical techniques for the generation of microlens array," *J. Mod. Opt.* 37 253-265 1990
- [14] Popovic Z D, Sprague R A and Connell GAN, "Technique for monolithic fabrication of microlens arrays," *Appl. Opt.* 27 1281-8 1988
- [15] S. Exner, "The Retinal Image of Insect Eyes," *Sb. Akad. Wiis Wien* 98, 13 (1889).
- [16] Arthur G. Bennett and Ronald B. Rabbetts, *Clinical Visual Optics*, 1 ed. (Butterworths, London, 1984).
- [17] Photonics Spectra September 1999
- [18] Duncan T. Moore, "Gradient-index optics: a review," *Applied Optics* 19 (7), 1035-1038 (1980).
- [19] <http://www.ophthalmologytimes.com/ophthalmologytimes/article/articleDetail.jsp?id=57616&pageID=1>
- [20] Roy Kornbluh, et al, "High-filied electrostriction of elastomeric polymer dielectrics for actuation," *Proc. SPIE Smart Structure and Materials 1999: Electroactive Polymer Actuators and Devices*, Y. Bar-Cohen, ed., 3669, pp. 149-161, 1999.
- [21] Kaneko T, Ohmi T, Ohya N, Kawahara N and Hattori T, "A new, compact and quick-response dynamic focusing lens," *Transducers '97: Proc. 9th Int. Conf. on Solid State Sensors and Actuators* pp 63-6 (1997)
- [22] Sato M, Shimokawa F, Makihara M and Nishida Y, "Two types of thermo-capillary optical switches," *Tech. Digest MOEMS97* pp 238-42 (1997)
- [23] Commander L G, Day S E, Chia C H and Selviah D R, "Microlenses immersed in nomadic liquid crystal with electrically controllable focal length," *EOS Topical Digest Meetings Microlens Arrays* vol 5, pp 72-6 (1995)
- [24] Sato S, "Application of liquid crystals to variable-focusing lenses," *Opt. Rev.* 6 471-85 (1999)
- [25] Berge B and Peseux J, "Variable focal lens controlled by an external voltage: an application of electrowetting," *Eur. Phys. J. E* 3 159-63 (2000)
- [26] Ahn S-H and Kim Y-K, "Proposal of human eye's crystalline lens-like variable focusing lens," *Sensors Actuators A* 78 48-53 (1999)
- [27] D. A. Fletcher, K. B. Crozier, K. W. Guarini, S. C. Minne, G. S. Kino, C. F. Quate, and K. E. Goodson, "Microfabricated silicon solid immersion lens," *J. Microelectromechanical Systems*, vol. 10, no. 3, pp. 450-459, (2001)

- [28] Jeong K H and Lee L P A new method of increasing numerical aperture of microlens for biophotonic MEMS *2nd Ann. Int. IEEE-EMBS Special Topic Conf. on Microtechnologies in Medicine & Biology (Madison, WI, USA, 2-4 May 2002)* pp 380-3 (2002)
- [29] Jui-Hsiang Liu, Hung-Tsai Liu, "Gradient refractive-index optical rod prepared from methacrylate derivatives," *Optics Letters*, Volume 22, Issue 10, 668-670 May 1997
- [30] Y. Ohtsuka and Y. Terao, *J. Appl. Polym. Sci.*, 26, 2907 (1981)
- [31] Y. Ohtsuka and T. Sugaho, *Appl. Opt.*, 22, 413, 1983
- [32] B. C. Ho, J. H. Chen, W. C. Chen, and Y. H. Chang, *Polym. J.*, 27, 310, 1995
- [33] Y. Koike, Y. Kimoto, and Y. Ohtsuka, *Appl. Opt.*, 21, 1057, 1982
- [34] J. H. Liu and M. H. Chu, *Angew. Makromol. Chem.*, 174, 1, 1989
- [35] D. J. Fischer, C. J. Harkrider, D. T. Moore, "Design and Manufacture of a Gradient-Index Axicon," *Applied Optics* 39 (16) pp. 2687-94, 2000
- [36] Bar-Cohen, Yoseph, Sherrit, Stewart, Lih, Shyh-Shiuh, "Characterization of the electromechanical properties of EAP materials," *Proc. SPIE Vol. 4329*, p. 319-327, *Smart Structures and Materials*, 2001
- [37] Ron Pelrine, et al, "Applications of Dielectric Elastomer Actuators," *Proc. SPIE Vol. 4329*, p. 335-349, *Smart Structures and Materials*, 2001
- [38] R. Pelrin, R. Kornbluh, and G. Kofod, "High-Strain Actuator Materials Based on Dielectric Elastomers," *Advanced Materials* 2000 12:16, pp. 1223-1225, 2000
- [39] Sommer-Larsen, Peter, et al, "Response of dielectric elastomer actuators," *Proc. SPIE Vol. 4329*, p. 157-163, *Smart Structures and Materials*, 2001

Appendix A

Mathematic Calculations for Back Focal Length and Number Apertures

Calculation of Back Focal Length and Numerical Apertures for Microfluidic Lens

Radius of microlens (r_0):

$$r_0 := 700 \text{ } \mu\text{m}$$

The maximum height (h) in the center of convex microlens was measured from the CCD images. Because the radius of the microlens is known, the maximum height in the center of the convex microlens was calculated by scaling the height to the radius of the microlens. The corresponding pump-in volume (Vol) is listed:

$$Vol := \begin{pmatrix} 0 \\ 10 \\ 20 \\ 30 \\ 40 \\ 50 \\ 55 \\ 60 \\ 65 \\ 70 \\ 75 \\ 80 \end{pmatrix} \mu\text{L} \quad h := \begin{pmatrix} 65.625 \\ 76.5625 \\ 98.4375 \\ 125.7813 \\ 153.125 \\ 164.0625 \\ 169.5313 \\ 175 \\ 192.5 \\ 202.3438 \\ 218.75 \\ 223.125 \end{pmatrix} \mu\text{m}$$

The curvature of the microlens can be calculated by the following equation:

$$i := 0..11$$

$$R_{i,0} := \frac{(h_{i,0})^2 + r_0^2}{2 \cdot h_{i,0}}$$

	0	
0	3766.15	μm
1	3238.28	
2	2538.11	
3	2010.72	
4	1676.56	
5	1575.36	
6	1529.93	
7	1487.5	
8	1368.98	
9	1311.98	
10	1229.38	
11	1209.6	

The contact angle (θ) was obtained by using a contact-angle measurement system (Data Physics, Future Digital Scientific Corp.).

$$\theta := \begin{pmatrix} 13.4 \\ 14.8 \\ 17.5 \\ 21.1 \\ 23.4 \\ 26.3 \\ 27.6 \\ 29.5 \\ 30.2 \\ 31.6 \\ 32.2 \\ 34.1 \end{pmatrix} \text{ degree}$$

The backfocal length (f_B) can be calculated by the following equation:

$$n_w := 1.33 \quad \text{Refractive index for water}$$

$$n_d := 1.401 \quad \text{Refractive index for PDMS}$$

$$f_{B_{i,0}} := n_w \cdot \frac{\left[1 + (n_d - 1) \cdot \cos\left(3.14 \cdot \frac{\theta_{i,0}}{180}\right) \right]}{n_d \cdot (n_d - 1)} \cdot R_{i,0}$$

	0	
0	12394	
1	10638.5	
2	8306.8	
3	6541.1	
4	5429.9	
5	5070.4	μm
6	4909.2	
7	4750.7	
8	4364.3	
9	4167	
10	3898.2	
11	3814.7	

The numerical aperture of a lens system is defined to be the sine of the angle, θ_1 , that the marginal ray (the ray that exits the lens system at its outer edge) makes with the optical axis multiplied by the index of refraction (n) of the medium. The numerical aperture can be defined for any ray as the sine of the angle made by that ray with the optical axis multiplied by the index of refraction: $NA = n \sin \theta$.

- Curvature of a lenslet

$$R = \left[\frac{3V}{\pi(2 + \cos \theta_c)(1 - \cos \theta_c)^2} \right]^{\frac{1}{3}}$$

- Back focal length

$$f_B = n_2 \frac{1 + (n_2 - 1) \cos \theta_c}{n_1(n_2 - 1)} R$$

- Numerical aperture

$$NA = n_2 \sin \varphi = n_2 \left\{ \frac{n_2^2 [1 + \cos \theta_c (n_2 - 1)]}{n_1^2 [n_2 - 1 + \sin^2 \theta_c]} + 1 \right\}^{-\frac{1}{2}}$$

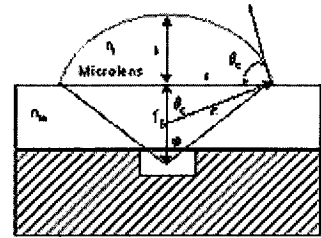


Fig.2 Plano convex microlens formed by UV curable polymer on micro fluidic channel

$$NA_{i,0} := n_w \cdot \frac{r_0}{\sqrt{r_0^2 + (f_{B_{i,0}})^2}}$$

	0
0	0.075
1	0.087
2	0.112
3	0.142
4	0.17
5	0.182
6	0.188
7	0.194
8	0.211
9	0.22
10	0.235
11	0.24

NA =

Appendix B

Published Papers

Variable-focusing microlens with microfluidic chip

Jackie Chen, Weisong Wang, Ji Fang and Kody Varahramyan

Institute for Micromanufacturing, Louisiana Tech University, Ruston, LA, USA

E-mail: jfang@coes.latech.edu

Received 14 November 2003

Published 17 March 2004

Online at stacks.iop.org/JMM/14/675 (DOI: 10.1088/0960-1317/14/5/003)

Abstract

A new polymer microlens with variable focusing properties is designed and fabricated. The microlens consists of a thin diaphragm with 3D convex lens, chamber and microchannel, which are made of polydimethyl-siloxane (PDMS). A novel fabrication approach has been developed to cast the PDMS microlens film using a PDMS mold. The elastomeric PDMS microlens film acts as a diaphragm. The flexible PDMS microlens and diaphragm are integrated on a microfluidic chip. By varying the pressure in the microfluidic chamber, which produces a shift in the microlens' focal plane, this can change the back focal length of lens. The new fabrication method provides easy fabrication, low-cost production and precise dimension control. Measurement with an atomic force microscope reveals that the surface roughness of the lens is 18.6 nm, and real-time contact-angle measurements show the back focus length tuning range is from 3.8 mm to 10.6 mm. The variable focal length of the microlens is critical to increase the efficiency of the light detection in optical or biophotonic applications. In this paper, the fabrication processing, mechanical and optical property testing, and simulation results are presented in detail.

(Some figures in this article are in colour only in the electronic version)

1. Introduction

The study of variable focusing microlenses has been an area of activity for many years. Variable focal length is a necessary attribute in many optical applications if the object being imaged is not in a fixed position. Several recent publications have recognized the potential for the variable microlens to impact significantly on the field of optical applications [1, 2]. The variation of focal length can be provided by a focalizing mechanism that causes the focal plane to shift. Different approaches using liquid crystal [3, 4] and the electrowetting method [5, 6] have been investigated by some researchers, but the liquid crystal lens is limited to small lenses and the electrowetting liquid concept lens requires a high voltage source. Both methods require electrodes, which are immersed in the electrolyte solution, causing severe optical distortion. A variable focusing liquid-filled lens with a pressure-driven mechanism was also demonstrated [7]. However, the numerical aperture of this lens is limited because the lens was made by a planar glass diaphragm.

A new concept has been developed to fabricate a flexible polydimethyl-siloxane (PDMS) microlens with a microfluidic chip. The microlens is a 3D convex polymer lens on a thin diaphragm. The diaphragm is integrated on a microfluidic chamber to simultaneously control the focal length of microlens. The microchamber on the microfluidic chip is filled with working fluid. By changing the fluid pressure, it causes a change of curvature of the polymer lens and this induces focal plane shift. Together with the deflection of the PDMS diaphragm, a microlens, which is attached to the diaphragm, can provide much higher numerical aperture than a planar glass or polymeric membrane. Moreover, the 3D convex lens provides a focal point when the diaphragm is at an initial position. This design of microlens, working as the human eye's crystalline lens, provides more flexibility on back focal length and higher numerical aperture than previous research on liquid-filled variable focal lenses. The numerical aperture of the new PDMS microlens can reach 0.24 which is about four times that of a conventional planar glass diaphragm ($NA \approx 0.05$) [7]. The higher numerical aperture

microlens integrated on a microfluidic chip will perform high resolution and high signal-to-noise detection in optical MEMS applications. The high numerical aperture of a microlens is critical to increase the efficiency of the detection ability. This design has the advantages that it can be used as a microoptical component with high numerical aperture, variable focal length and low optical distortion. They make this design attractive for the optical pickup in many applications, such as optical switches, cameras, microscopes and optical signal processing.

In addition, a novel batch process for making polymer lens arrays has been developed. It is a cast method to fabricate convex PDMS microlenses on a thin diaphragm by using a cured PDMS concave microlens master mold. This method can produce high dimensional accuracy, high optical quality, and high production rate with low cost. The design, simulation, fabrication and characterization are presented in the following sections.

2. Fabrication

A conventional lens has a fixed focal length. However, a variable focus lens should work like a human eye's crystalline lens that can be deformed by muscles. A variable focal length microlens was successfully designed and fabricated and includes two parts: microlens diaphragm and microfluidic chip. The PDMS thin film with convex lens is a passive diaphragm while the microfluidic chip acts as the actuating part. PDMS is selected as the lens material, because it features good optical properties with large elongation and biocompatibility.

2.1. Microlens film fabrication

New design and fabrication technology of microstructures for optical elements are strongly demanded with the diversification of optical devices and systems. One of the key processes is 3D microlens fabrication. Several fabrication processes for microlenses have been reported, such as reactive ion etching (RIE) [8], ion diffusion [9], deep proton irradiation [10], and physical methods such as hot embossing [11], injection molding micromachining [12] and photoresist reflow [13]. The microlens materials are varied depending on the fabrication methods, which include polymethyl methacrylate (PMMA), photosensitive glass, photopolymers and UV curable resins [14]. However, each microlens, which is produced from the above methods, has a rigid structure with a unique focal length. Most of their fabrication processes are complicated and require specific facilities for producing microlenses.

A novel PDMS casting fabrication process has been developed. The processing schematic is shown in figure 1. To fabricate the microlens by molding, a mother lens of the same shape as the final PDMS lens is needed. The photoresist reflow method is used to make the mother lens. The first step is to generate a photoresist pattern by conventional photolithography. Secondly, the photoresist pattern is thermally treated for reflowing into a lens shape. The photoresist reflow method, suggested by Prpovic in 1988, is to melt photoresist structures to form small lens shapes due to the surface tension of the liquid resist [14]. SEM photographs

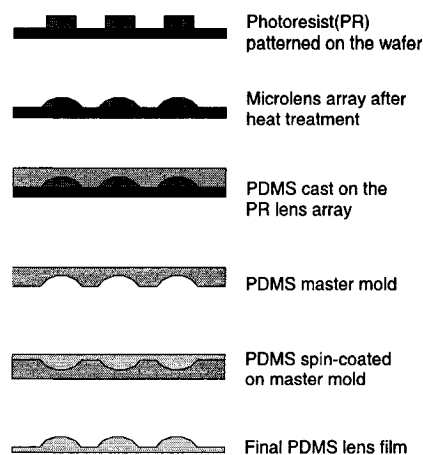


Figure 1. Fabrication sequence for an array of polymer microlenses.

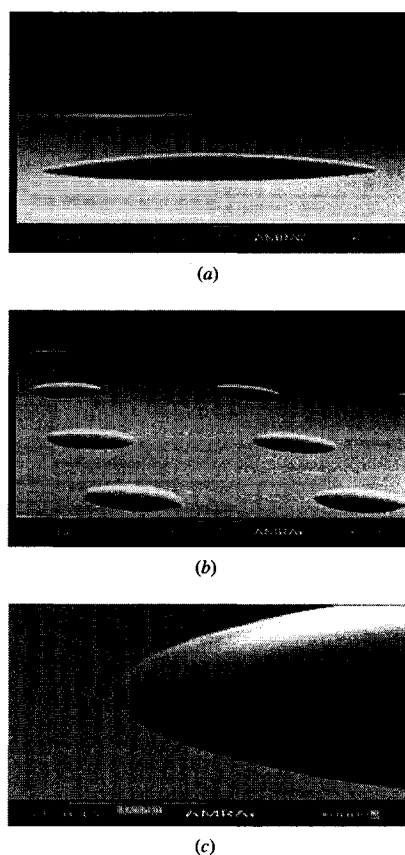


Figure 2. SEM images of 1400 μm diameter photoresist microlenses: (a) single spherical lens, (b) an array of microlenses and (c) closer view of the edge of a photoresist microlens.

of a photoresist microlens with a diameter of 1400 μm and an array after the thermal reflow process are shown in figure 2. The photoresist we used is AZ 100XT. The photoresist patterns are thermally treated on a hot plate, and the reflow temperature is 120 $^{\circ}\text{C}$, and the reflow time is 60 s.

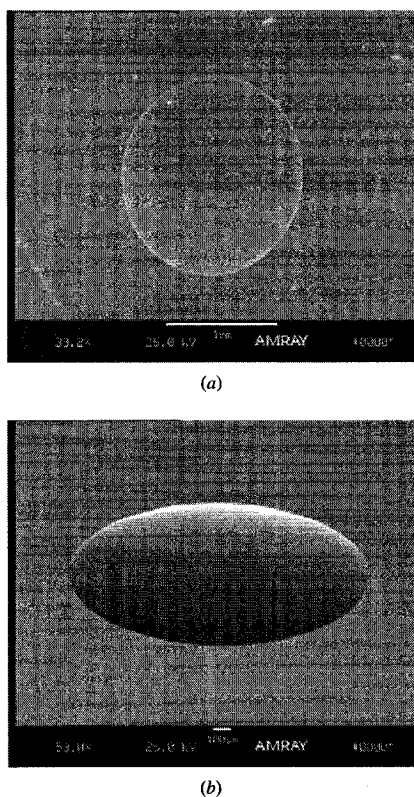


Figure 3. SEM photographs for (a) PDMS concave master and (b) final PDMS film with convex lens.

After completing the photoresist mother lens, the next step is the transfer of the photoresist microstructure to a PDMS master by a casting method. PDMS is chosen as a master material because it provides high-dimensional accuracy, and easy fabrication. Dupont Sylgard 186 silicone is used as the master material. After the PDMS master is cured in a vacuum oven for 2 h at 5 mTorr of pressure at 75 °C, the mold is peeled off from the mother lens wafer. The PDMS master consists of a concave microlens array. Figure 3(a) shows the SEM images of the master. The diameter of the concave surface is 1400 μm .

The final step is spin-coating PDMS on the PDMS master. Depending on the spinning speed, a thick or thin film with a unique dimension of microlens can be obtained. Then, PDMS film is cured for 2 h at 5 mTorr of pressure at 75 °C. Finally the lens film was peeled off the PDMS master. Since the new PDMS layer does not crosslink with the cured PDMS master mold at the interface during curing process, it is easy to peel off the film from the master mold. The SEM pictures in figure 3 show a PDMS mold and PDMS microlens film with a microlens (1400 μm at diameter and 85 μm height at the center of lens).

2.2. Microfluidic chip fabrication

The microfluidic chip includes a silicon chamber, and a PDMS chamber block with an inlet channel. Figure 4(a) shows a cross-section view of the microfluidic chip structure. It

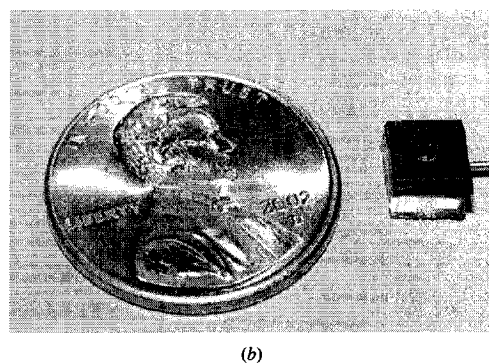
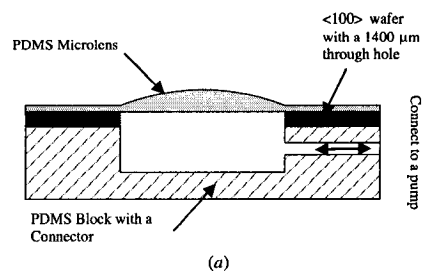


Figure 4. (a) Schematic cross section for microfluidic chip structure and (b) a prototype of variable focal lens with microfluidic chip.

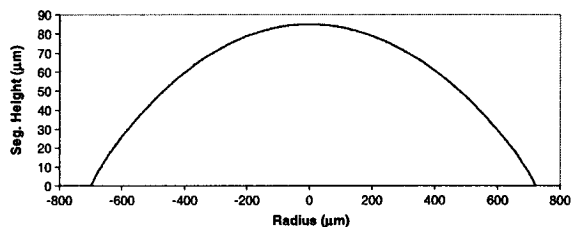


Figure 5. Surface profile for the photoresist microlens.

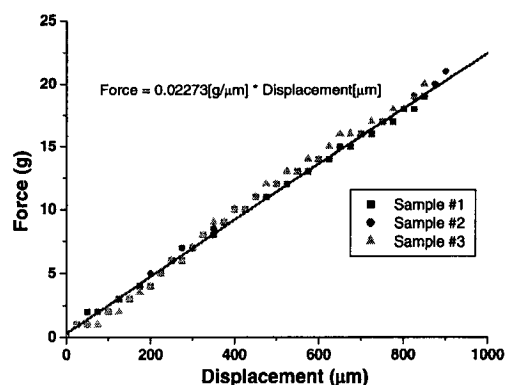
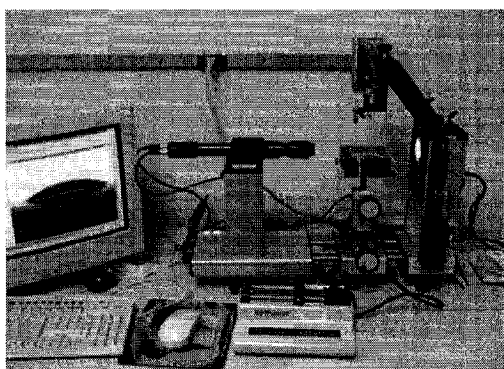


Figure 6. The plot for force versus displacement.

is necessary to have a silicon wafer between the PDMS microlens film and PDMS chamber block. The silicon wafer provides a smooth and rigid surface for bonding with both the PDMS microlens film and PDMS chamber block. A through hole on the silicon wafer with a diameter of 1400 μm is formed

Table 1. Comparison of surface roughness for the photoresist microlens, the PDMS master and the final PDMS microlens.

	Photoresist microlens	PDMS master	Final PDMS microlens
Average roughness (nm)	8.61	17.2	18.6

**Figure 7.** Experimental setup for contact-angle measurement.

by inductively coupled plasma (ICP) dry etching. A chamber mold is designed and built to create a circular chamber with an inlet channel. PDMS prepolymer mixture is then cast to form the body of a 1400 μm chamber and a channel. The PDMS mixture is subsequently cured in an oven for 2 h at 75 $^{\circ}\text{C}$. The cured PDMS chamber is peeled off from the mold.

Finally both the lens film and PDMS chamber block are bonded to the silicon substrate by using a high strength epoxy to avoid any leakage (Devcon All Purpose Epoxy). The overall dimension of the prototype, as shown in figure 4(b), is about 5 mm \times 4.5 mm \times 2.5 mm ($L \times W \times H$).

3. Experimental results

PDMS microlenses, diameter range from 600 μm to 1400 μm , are successfully fabricated. In this paper, a microlens with 1400 μm diameter is used for characterization. The surface profile, mechanical and optical properties of the PDMS microlenses have been characterized. In addition, a simulation with finite element analysis (FEA) has been performed.

The surface profile of the melted photoresist microlens is measured using a Tencor Alpha Step 500 System. This equipment uses a stylus with a 2 μm chisel head as a probe and scans the sample surface. Figure 5 shows the surface

profile of a photoresist lens. The height of the photoresist mother lens is 85 μm at the center point and the diameter is 1400 μm (figure 5).

The surface roughness of the mother lens and PDMS master mold are the very important parameters, which may affect the optical properties of final lens. An atomic force microscope (Quesant Instruments scanning probe microscope, AFM) is used to examine the surface roughness. AFM provides true 3D topographic images, which also yield surface roughness data on the nanometer scale. The analysis results of the photoresist microlens, PDMS master and final PDMS lens film are shown in the table 1. The results indicate that surface roughness is changed after each processing step of the PDMS coating and peel-off process. However, the surface roughness of the PDMS master and the final PDMS microlens film do not have a significant change. The roughness for both the master mold and final PDMS microlens film is about 17–18.6 nm, which is still in an acceptable range for optical lens requirements.

The mechanical properties of the PDMS film were examined by applying a load at the center of the PDMS film. The corresponding deflections with various loadings are measured. Figure 6 shows a linear relationship between applied load and deformation at the center of the film. The maximum loading force for 100 μm thick PDMS film is about 20 g. The PDMS film can be ruptured if the force is larger than this value.

The back focus length has been characterized using a contact-angle measurement system (Data Physics, Future Digital Scientific Corp.). Figure 7 shows the contact-angle experiment setup. The different pressure of pumped-in fluid changes the lens curvature, as shown in figure 8. As the fluid volume increases, the contact angle also increases. Each contact angle for a different pumped liquid volume is measured carefully for further lens optical property calculations, such as curvature and back focal length. The curvature (R) can be obtained by the following equation [15]:

$$R = \left[\frac{3V}{\pi(2 + \cos \theta)(1 - \cos \theta)^2} \right]^{\frac{1}{3}}$$

where V is lens volume and θ is the contact angle.

The curvature changes of the lens cause the focal plane to shift. Figures 9(a) and (b) show the relationship of the pumped-in volume, contact angle and curvature. The back focal lengths with different pumped-in volume are calculated. A microlens on a microfluidic channel is considered as a plane convex refractive lens assuming that the lens profile is spherical. The back focal length (f_B) can be obtained by the

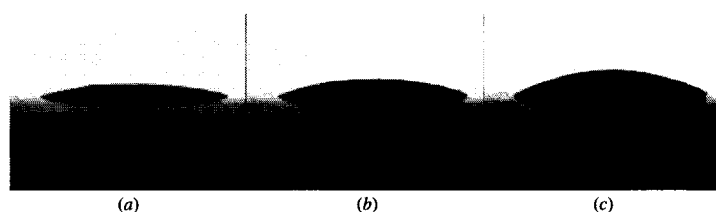






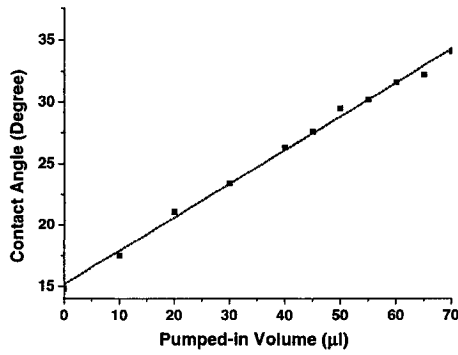
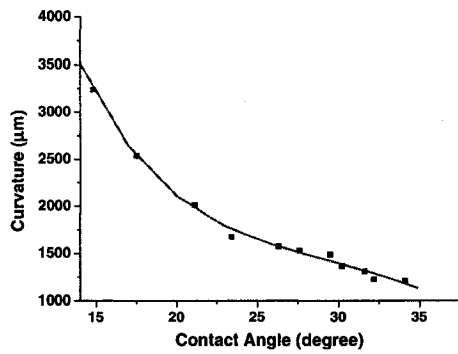
**Figure 8.** Photos for the curvature changes of the PDMS film lens with different volumes of pumped-in fluid: (a) initial position, (b) 20 μl and (c) 45 μl .

Table 2. Optical properties of a 1400 μm diameter microlens with different pumped-in volumes.

Photos						
Pumped-in volume (μl)	0.0	10.0	30.0	50.0	60	70.0
Chamber pressure (psi)	0.71	1.06	2.12	2.83	3.54	4.24
Contact angle (°)	14.8	17.5	23.4	29.5	31.6	34.1
Curvature (μm)	3238	2538	1677	1488	1312	1210
Back focal length (μm)	10 640	8307	5430	4751	4167	3815
Numerical aperture (NA)	0.09	0.11	0.17	0.19	0.22	0.24



(a)



(b)

Figure 9. (a) Linear relationship between pumped-in volume and contact angle. (b) Relationship between contact angle and curvature.

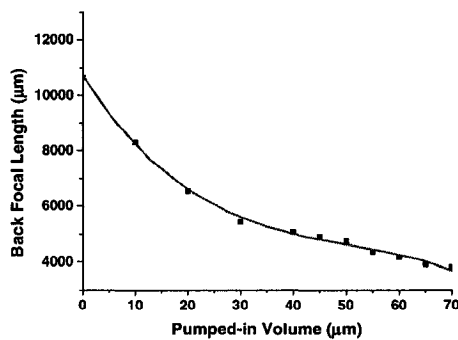
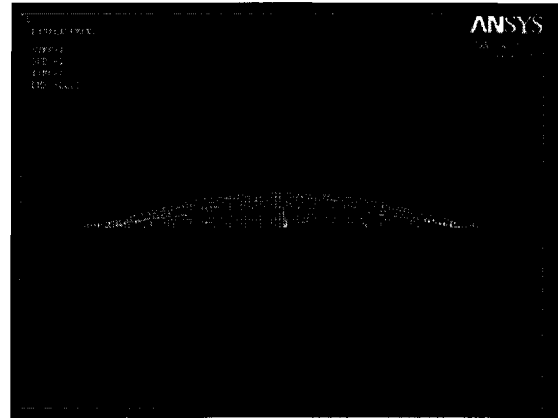


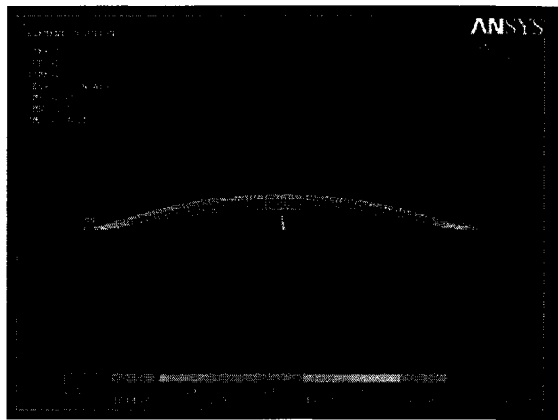
Figure 10. Relationship between back focal length and pumped-in volume.

following equation [15]:

$$f_B = n_2 \frac{1 + (n_1 - 1) \cos \theta}{n_1 (n_1 - 1)} R.$$



(a)



(b)

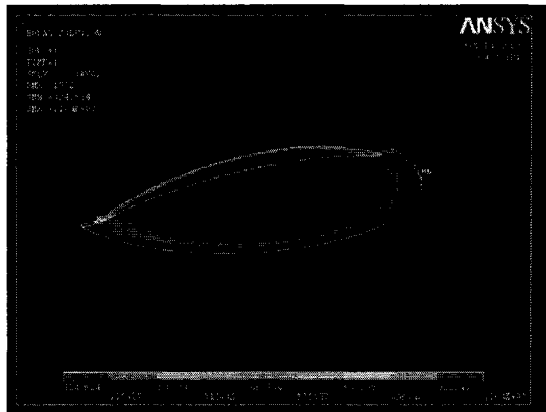
Figure 11. 2D ANSYS simulation of microlens (a) for deformation and (b) for stress distribution.

Where n_1 and n_2 are the refractive indexes for the PDMS microlens and water, respectively ($n_1 = 1.401$ and $n_2 = 1.33$). The range of back focal length is from 3.82 mm to 10.64 mm. Figure 10 shows the relationship between pumped-in volume and back focal length.

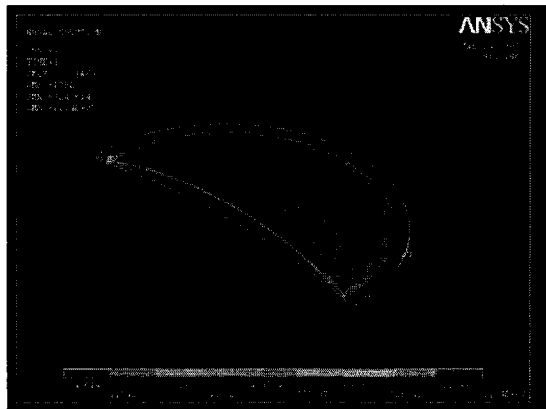
In addition, numerical aperture can be calculated by the following equation:

$$NA = n_2 \left\{ \frac{n_2^2 [1 + (n_1 - 1) \cos \theta]^2}{n_1^2 (n_1 - 1)^2 \sin^2 \theta} + 1 \right\}^{-\frac{1}{2}}.$$

The numerical apertures with various focal lengths have been determined and listed in table 2. The numerical aperture can be tuned between 0.09 and 0.24. Table 2 presents a



(a)



(b)

Figure 12. 3D ANSYS simulation of microlens (a) for stress on bottom surface and (b) for stress on top surface.

detailed summary of the optical properties of a variable focus microlens.

A comprehensive finite element analysis for a PDMS microlens under various internal pressures has been performed. In figure 11, it shows the lens deformation and stress distribution on a cross section of the microlens. Furthermore, a 3D model has been created to provide more accurate results in figure 12. The maximum stress occurs on the outer most ring of the lens' bottom surface. An outer ring of the lens's body is thinner than one at the center of lens. By applying a uniform pressure on the bottom surface, the stress on the outer ring will increase more than the other areas of the lens. The results for curvature changes due to the pressure applied agree with the experimental results.

4. Discussions and conclusions

A new flexible PDMS microlens and a controllable focus module are successfully fabricated and characterized. A novel PDMS casting process with a PDMS mold to fabricate the microlens film is developed. This fabrication process provides good optical properties, high dimensional accuracy and low cost for mass production. Microlenses with a diameter of 600–1400 μm are fabricated using this fabrication technique.

The optical and mechanical properties of a prototype are characterized. The surface roughness of the lens was 18 nm. The curvature changes of the microlens were from 1210 μm to 3238 μm . With this wide range of curvature changes, we can control the back focal length from 3.82 mm to 10.64 mm, and numerical aperture between 0.09 and 0.24. These results prove the possibility of using the present lens model for many optical applications. Its benefits are applicable not only to various optical MEMS applications such as tunable range wavefront sensors, beam spanning control for free-space optical actuation, but also to biomedical applications.

Acknowledgment

This work was funded by the DARPA (Defense Advanced Research Projects Agency) (contract no. BAA 01-42 no. 427).

References

- [1] Kaneko T, Ohmi T, Ohya N, Kawahara N and Hattori T 1997 A new, compact and quick-response dynamic focusing lens *Transducers '97: Proc. 9th Int. Conf. on Solid State Sensors and Actuators* pp 63–6
- [2] Sato M, Shimokawa F, Makihara M and Nishida Y 1997 Two types of thermo-capillary optical switches *Tech. Digest MOEMS97* pp 238–42
- [3] Commander L G, Day S E, Chia C H and Selviah D R 1995 Microlenses immersed in nematic liquid crystal with electrically controllable focal length *EOS Topical Digest Meetings Microlens Arrays* vol 5, pp 72–6
- [4] Sato S 1999 Application of liquid crystals to variable-focusing lenses *Opt. Rev.* 6 471–85
- [5] Kwon S and Lee L P 2001 Focal length by microfabricated planar electrodes-based liquid lens (μPELL) *11th Int. Conf. on Solid-State Sensors and Actuators (Munich, Germany, 10–14 June 2001)*
- [6] Berge B and Peseux J 2000 Variable focal lens controlled by an external voltage: an application of electrowetting *Eur. Phys. J. E* 3 159–63
- [7] Ahn S-H and Kim Y-K 1999 Proposal of human eye's crystalline lens-like variable focusing lens *Sensors Actuators A* 78 48–53
- [8] Severi M and Mottier P 1999 Etching selectivity control during resist pattern transfer into silica for the fabrication of microlenses with reduced spherical aberration *Opt. Eng.* 38 146–50
- [9] Iga I, Kokubun Y and Oikawa M 1984 *Fundamentals of Microoptics* (London: Academic)
- [10] Kufner M and Kufner S 1996 Fabrication of monolithic integrated fiber-lens connector arrays by deep proton irradiation *Microsyst. Technol.* 2 114–8
- [11] Fu Y Q and Bryan N K A 2001 Novel one-step method of microlens mold array fabrication *Opt. Eng.* 40 1433–4
- [12] Daly D J 1998 The fabrication and measurement of melted photoresist microlenses *Doctoral Thesis* Kings College London, UK
- [13] Popovic Z D, Sprague R A and Connell G A N 1988 Technique for monolithic fabrication of microlens arrays *Appl. Opt.* 27 1281–8
- [14] O'Neill F T and Sheridan J T 2002 Photoresist reflow method of microlens production: I. Background and experiments *Optik* 113 391–404
- [15] Jeong K H and Lee L P 2002 A new method of increasing numerical aperture of microlens for biophotonic MEMS *2nd Ann. Int. IEEE-EMBS Special Topic Conf. on Microtechnologies in Medicine & Biology (Madison, WI, USA, 2–4 May 2002)* pp 380–3

THE NEWSLETTER OF
 TOOLS AND PRODUCTS
 IN MICRO AND
 NANOTECHNOLOGY

NANO

From the Editors of R&D Magazine

- 5 MEMS Briefs
- 11 Patent snapshots
- 15 Fluid lenses change shape
- 15 And another lens changes shape

- 4 Array Technology
- 9 Quantum dots
- 10 Nanospheres separate DNA with speed
- 16 Circular biosensor chip moves DNA
- 18 Biotech Briefs
- 19 Liposomes self-assemble

- 3 Nano Briefs
- 5 Create cooling current
- 8 Nanobridges
- 9 Quantum dots
- 14 Dope molecules one atom at a time
- 16 Gel produces aligned nanotubes
- 19 Nanorings

- 8 FETs reveal hidden behavior
- 14 One-step production of CNT ropes
- 18 Method controls length, orientation, and shape
- 19 Process zaps mutated cells
- 10 Nanocomposites are worth their weight
- 13 How does nano fare in Europe?
- 20 MEMS based startups

- 2 Industry Report
- 12 Show Report
- 21 Coming Events
- 22 Awards & Grants
- 23 Subscription

Emergence of nano-enabled sensors

By Sharon Smith, Lockheed Martin Corp. and David J. Majel, George Washington University

A new generation of sensors is emerging, one that is based on nanotechnology or, even more prevalently, on a combination of micro- and nanotechnologies. The trend toward the micro and nano level is giving rise to sensor capabilities previously unachievable. Lighter weight, lower power requirements, and higher sensitivities and specificities are a few of the characteristics to be exploited in these new sensors. As an example, carbon nanotubes (CNTs) possess unique properties that may help NASA make measurements in deep space, a challenging, and almost impossible goal today¹.

By their very nature, nanotubes are radiation tolerant—sensors based on nanotubes may be very small, sensitive to a wide variety of molecules, and require very low power, all characteristics needed for analyses in deep space

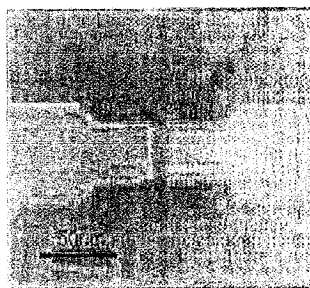


Fig. 1. SWNT chemical Li contacts evaporated on top of SWNT film grown on thermal SiO₂. Source: to describe the conditions are 10 × 20 μm. Si substrate serves as back gate. Source for graphics: *Applied Physics Letters*

missions. Potential applications of nanosensors to medical diagnostics, drug screening, environmental monitoring, and other

Fluidic machine has unique setup

Microfluidic machines that self-assemble and yet are reconfigurable have been developed by Bartosz Grzybowski, Northwestern Univ., Evanston, Ill., and colleagues from Harvard Univ. and ProChimia Poland. The machines consist of patterns of rotors that perform many tasks in a liquid environment (sort floating particles; mix reagents). The rotors are made in molds and then freed onto a liquid-air interface. Their positions at the interface are controlled by localized magnetic fields (Fig. 1) produced by an array of electromagnets immersed in the liquid. The unique feature is that the axes of rotation of the rotors are not permanently fixed, and can be changed by

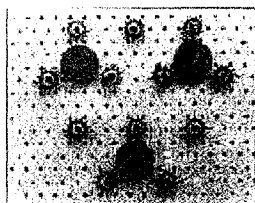


Fig. 1. Self-assembly of 2 rotors above array of electromagnets. Source: *Northwestern Univ., Evanston, Ill.*

modifying the magnetic fields produced by the electromagnets. The rotors, therefore, can move across the interface by activating different electromagnets. Because the fluid motion linked with the rotation of the rotors gives rise to hydrodynamic repulsions between them, no two rotors can stay above the same electromagnet. Thus, for a given configuration of active electromagnets, the rotors always self-assemble into a unique structure, and the configuration of the machine and its function is uniquely determined. The work is described in the March 8, 2004 issue of *Applied Physics Letters*.

For information, contact Bartosz Grzybowski at grzyb@northwestern.edu.

Ness Display Co. Ltd. (www.nessdisplay.com), South Korea, will build a \$40-\$60 million organic light emitting diode (OLED) plant in Singapore to produce 15-20 million display panels/year by 2006.

Pasadena, Calif.-based Arrowhead Research Corp. (<http://arrowres.com>) will form a subsidiary to produce an ultrathin crystal nanofilm technology developed by Harry Atwater from the California Institute of Technology.

World's first databank for all living systems (microbes to DNA sequencing) will be at Bridging the Rift (BTR) Center (<http://ip.cals.cornell.edu/btr>), 50 miles south of the Dead Sea, and led by Cornell and Stanford Univ.

Bothell, Wash.-based Microvision (www.microvision.com) has a \$1.0 million contract with an Asian manufacturer of printers/office equipment to develop a MEMS-based scanning engine for high-speed laser printers.

Fujitsu (www.fujitsu.com), Tokyo, will build a \$1.5 billion-dollar quakeproof plant to produce chips for cell phones, DVD recorders, and hi-tech gadgets. Monthly chip turnout will be ~13,000 Si wafers by 2006. Next-generation circuits to be produced will be 65 nm wide.

Fluid lenses change shape

A novel variable-focus lens system that has no mechanical moving parts has been developed by lead project leader Stein Kuiper and colleagues at Philips Research in Eindhoven, the Netherlands. Called the FluidFocus system, it mimics the action of the human eye using a fluid lens that alters its focal length by changing shape. The lens, which lends itself to high volume manufacturing, overcomes the fixed focus disadvantages of many of the low-cost imaging systems.

The lens consists of two immiscible (non-mixing) fluids of different refractive index

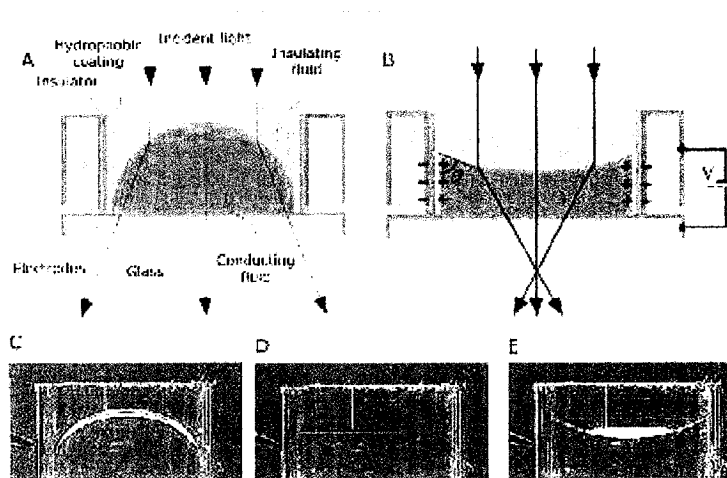


Fig. 1. A) FluidFocus lens principle. B) When voltage is applied, charges accumulate in glass wall electrodes and opposite charges collect near solid/liquid interface in conducting fluid. Resulting electrostatic force covers solid/liquid interface, lens on end contact angle θ . (C-E) Lens shape for imaging at different focal lengths. *Science*, Phillips, Eindhoven, the Netherlands.

one an electrically conducting aqueous solution and the other an electrically non-conducting oil, both contained in a short tube with transparent end caps. The internal surfaces of the tube wall and one

of its end caps are coated with a hydrophobic coating that causes the aqueous solution to form itself into a hemispherical mass at the opposite end of the tube where it acts as a spherically curved lens.

The shape of the lens is adjusted by using the electrowetting process across the hydrophobic coating so that it becomes less hydrophobic. As the surface tension changes, the aqueous solution begins to wet the sidewalls of the tube, altering the radius of curvature of the meniscus between the two fluids, and therefore, the focal length of the lens. By increasing the applied electric field, the surface of the initially convex lens can be made completely flat or concave—the lenses can transition smoothly from being convergent to divergent and back again.

The lens has a 3-mm dia and is 2.2 mm in length. The focal range extends from 5 cm to infinity—switching occurs in <10 ms. Controlled by a DC voltage and presenting a capacitive load, the lens consumes virtually zero power. The durability of the lens is also very high, having been tested in >1 million focusing operations without loss of optical performance.

And another lens changes shape

A new polymer microlens with variable focusing properties that is integrated in a microfluidic chip has been developed by Jackie Chen, Weisong Wang, Ji Fang, and Kody Varshamyan at the Louisiana Tech Univ., Ruston, La. A cast method is used to fabricate convex PDMS (polydimethyl-siloxane) microlenses (600–1400 μm) on a thin diaphragm by using a cured PDMS concave master mold, which produces accuracy, high optical quality, and low-cost mass production.

The microlens consists of a thin diaphragm with a 3-D convex lens, chamber, and microchannel. The diaphragm is integrated on a microfluidic chamber to simultaneously control the focal length of the microlens. The microchamber on the microfluidic chip is filled with working fluid. By changing the fluid pressure, it causes a change of curvature of the polymer lens and this induces focal plane shift. Together with the deflection of the PDMS diaphragm, the microlens can provide much higher numerical aperture than a planar glass or polymeric membrane—at present, 4x more.

The surface roughness of the lens is 18.6 nm with the

curvature changes of the microlens being from 1210–3230 μm . With this wide range of curvature changes, the back focal length can be controlled from 3.82–10.64 mm, and numerical aperture between 0.09–0.24. The variable focal length of the microlens is critical to increase the efficiency of the light detection in optical or biophotonic applications.

The maximum stress occurs on the outer most ring of the lens' bottom surface. An outer ring of the lens' body is thinner than one at the

center of the lens. By applying a uniform pressure on the bottom surface, the stress on the outer ring will increase more than the other areas of the lens. The results for curvature changes due to the pressure applied agree with the experimental results.

Potential applications for use are in various optical MEMS devices like tunable range wavefront sensors, beam spanning control for free-space optical actuation, and biomedical. The work is described in the March 17, 2004 issue of the *Journal of Micromechanics and Microengineering*.

For information, contact Ji Fang at fang@coex.inteltech.edu.

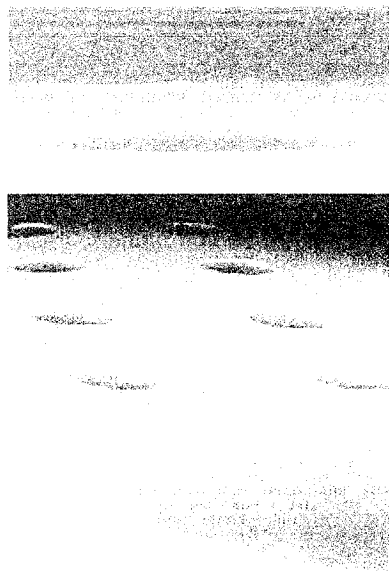


Fig. 1. Photoresist microlens has 1400- μm dia. A) Single spherical lens. B) Array of microlenses. C) Edge microlenses. *Sensors*, Journal of Micromechanics and Microengineering.

Did you know . . .

The US microfluidics market was ~\$128 million in 2002 and is expected to grow to ~\$710 million by 2008.

Source: *Logic of Frost & Sullivan*, New York City, NY